# 28th Spencer J. Buchanan Lecture

Friday, November 6, 2020 at 1 PM Central Time

Virtually Via Zoom

https://briaud.engr.tamu.edu/buchanan.lecture/

## Soil Characterisation for Advanced Geotechnical Design: Parameter Derivation

The 2020 Spencer J. Buchanan Lecture

By Dr. Lidija Zdravkovic

## Response of Soil Sites During Earthquakes, A 60-Year Perspective

The 2019 Terzaghi Lecture

By Dr. Ed Idriss

Sponsored by FUGRO

# Table of Contents

# SPENCER J. BUCHANAN

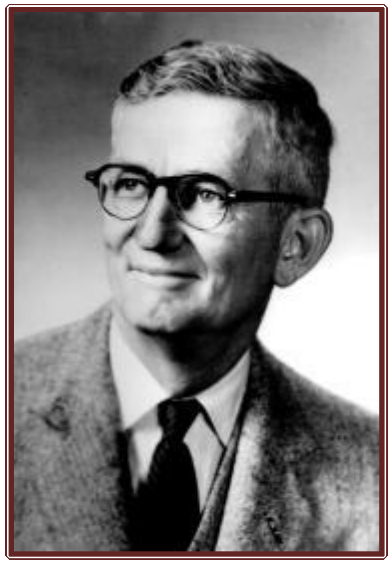

Spencer J. Buchanan, Sr. was born in 1904 in Yoakum, Texas. He graduated from Texas A&M University with a degree in Civil Engineering in 1926, and earned graduate and professional degrees from the Massachusetts Institute of Technology and Texas A&M University.

He held the rank of Brigadier General in the U.S. Army Reserve, (Ret.), and organized the 420th Engineer Brigade in Bryan-College Station, which was the only such unit in the Southwest when it was created. During World War II, he served the U.S. Army Corps of Engineers as an airfield engineer in both the U.S. and throughout the islands of the Pacific Combat Theater. Later, he served as a pavement consultant to the U.S. Air Force and during the Korean War he served in this capacity at numerous forward airfields in the combat zone. He held numerous military decorations including the Silver Star. He was founder and Chief of the Soil Mechanics Division of the U.S. Army Waterways Experiment Station in 1932, and also served as Chief of the Soil Mechanics Branch of the Mississippi River Commission, both being Vicksburg, Mississippi.

Professor Buchanan also founded the Soil Mechanics Division of the Department of Civil Engineering at Texas A&M University in 1946. He held the title of Distinguished Professor of Soil Mechanics and Foundation Engineering in that department. He retired from that position in 1969 and was named professor Emeritus. In 1982, he received the College of Engineering Alumni Honor Award from Texas A&M University.

He was the founder and president of Spencer J. Buchanan & Associates, Inc., Consulting Engineers, and Soil Mechanics Incorporated in Bryan, Texas. These firms were involved in numerous major international projects, including twenty-five RAF-USAF airfields in England. They also conducted Air Force funded evaluation of all U.S. Air Training Command airfields in this country. His firm also did foundation investigations for downtown expressway systems in Milwaukee, Wisconsin, St. Paul, Minnesota; Lake Charles, Louisiana; Dayton, Ohio, and on Interstate Highways across Louisiana. Mr. Buchanan did consulting work for the Exxon Corporation, Dow Chemical Company, Conoco, Monsanto, and others.

Professor Buchanan was active in the Bryan Rotary Club, Sigma Alpha Epsilon Fraternity, Tau Beta Pi, Phi Kappa Phi, Chi Epsilon, served as faculty advisor to the Student Chapter of the American Society of Civil Engineers, and was a Fellow of the Society of American Military Engineers. In 1979 he received the award for Outstanding Service from the American Society of Civil Engineers.

Professor Buchanan was a participant in every International Conference on Soil Mechanics and Foundation Engineering since 1936. He served as a general chairman of the International Research and Engineering Conferences on Expansive Clay Soils at Texas A&M University, which were held in 1965 and 1969.

Spencer J. Buchanan, Sr., was considered a world leader in geotechnical engineering, a Distinguished Texas A&M Professor, and one of the founders of the Bryan Boy's Club. He died on February 4, 1982, at the age of 78, in a Houston hospital after an illness, which lasted several months.

# The Spencer J. Buchanan '26 Chair in Civil Engineering

The College of Engineering and the Department of Civil Engineering gratefully recognize the generosity of the following individuals, corporations, foundations, and organizations for their part in helping to establish the Spencer J. Buchanan '26 Professorship in Civil Engineering. Created in 1992 to honor a world leader in soil mechanics and foundation engineering, as well as a distinguished Texas A&M University professor, the Buchanan Professorship supports a wide range of enriched educational activities in civil and geotechnical engineering. In 2002, this professorship became the Spencer J. Buchanan '26 Chair in Civil Engineering.

## Donors

### Founding Donor

Clarence Darrow Hooper '53

### Sponsor ($30,000 - $100,000)

Fugro

### Benefactors ($5,000 - $29,999)

East Texas Testing Lab, Inc.
ETTL Engineers and Consultants, Inc.
Flatt Partners, Inc.
Douglas E. Flatt '53

### Patrons ($1,000 - $4,999)

Dionel E. Aviles '53
Aviles Engineering Corporation
Rudolph Bonaparte
Mark W. Buchanan
Spencer J. Buchanan Jr. '53
Dow Chemical Foundation
Spencer J. Buchanan Associates
Lyle A. '53 and Marilyn Wolfskill
John C.B. Elliott
ExxonMobil Foundation
Perry G. Hector '54
Allen Marr
Jose M. Roesset
Wayne A. Dunlap '51
Kenneth H. Stokoe II
Robert S. Patton Jr '61

### Fellows ($500-$999)

John R. Birdwell '53
Joe L. Cooper '56
Harvey J. Haas '59
Conrad S. Hinshaw '39
O'Malley & Clay, Inc.
Mr. & Mrs. Peter C. Forster '63
Alton T. Tyler '44
George D. Cozart '74
RR & Shirley Bryan
Donald E. Ray '68
Roy E. Olson

## Members ($100 - $499)

Adams Consulting Engineers
Demetrios A. Armenakis '58
Eli F. Barker '47
Mr. & Mrs. Bert E. Beecroft '51
Fred J. Benson '36
Mr. & Mrs. Willy F. Bohlmann, Jr. '50
Craig C. Brown '75
G.R. Birdwell Construction, LP
Ronald C. Catchings '65
Ralph W. Clement '57
Coastal Bend Engineering Association
Mr. & Mrs. James t. Collins
John W. Cooper III '46
Murray A. Crutcher Jr. '68
William R. Hudson '54
Homer A. Hunter '25
Homer C. Keeter Jr. '47
Mr. & Mrs. Lyllis Lee Hutchin
Mr. & Mrs. Walter J. Hutchin '47
Mr. & Mrs. Shoudong Jiang '01
Mr. & Mrs. John L. Hermon '63
Charles I. McGinnis '49
Charles B. McKerall, Jr. '50
James D. Murff '70
Mr. & Mrs. Frank H. Newnam Jr. '31
Nicholas & Martha Paraska '47
Mr. & Mrs. Daniel E. Pickett '63
Mr. & Mrs. Richard C. Pierce '51
David B. Richardson '76
Walter E. Ruff '46
Charles S. Skillman Jr. '57
Louis L. Stuart Jr. '52
Ronald G. Tolson '60
Mr. & Mrs. Hershel G. Truelove '52
Mr. & Mrs. Thurman Wathen
Williams Gas Pipelines-Transco
James T.P. Yao
Donald D. Dunlap '58
Enterprise Engineers, Inc.
Edmund L. Faust Jr. '47
David T. Finley '82
Charles B. Foster Jr. '38
Benjamin D. Franklin '57
Thomas E. Frazier '77
Donald N. Brown '43
William F. Gibson '59
Anand Govindasamy '09
Cosmo F. Guido '44
Joe G. Hanover '40
George W. Cox '35
William & Mary Holland
Hubert O. Johnson Jr. '41
William T. Johnson Jr. '50
Richard W. Kistner '65
Andrew & Bobbie Laymay
Yangfeng Li '04
Frank L. Lynch '60
Marathon Oil Company
Dodd Geotechnical Engineering
Morrison-Knudsen Co., Inc.
Mr. & Mrs. Nack R. Nickel '68
Northrop Grumman Foundation
Harry & Josephine Coyle
Pickett-Jacobs Consultants, Inc.
Robert J. Province '60
David E. Roberts '61
Weldon Jerrell Sartor '58
Soil Drilling Services
Hadi Suroor '98
Kenneth C. Walker '78
Donald R. Wells '70
Andrew L. Williams, Jr. '50
Jes D. McIver '51
Mr. & Mrs. Donald W. Klinzing

## Associates ($25 - $99)

Mr. & Mrs. John Paul Abbott
Ronald P. Zunker '62
Mr. & Mrs. Charles R. Arnold '55
Bayshore Surveying Instruments Co.
Carl F. Braunig, Jr. '45
Mr. & Mrs. E.E. Brewster
Robert P. Broussard
Mr. & Mrs. Norman J. Brown '49
William K. Zicker '83
Stewart E. Brown
John L. Buxton '55
Caldwell Jewelers
Lawrence & Margaret Cecil
Mr. & Mrs. Howard T. Chang '63
Lucille Hearon Chipley
Caroline R. Compton
Mr. & Mrs. Joseph R. Compton
Robert L. Creel '53
Robert E. Crosser '49
O. Dexter Dabbs
Guy & May Bell Davis
Robert & Stephanie Donaho
Charles A. Drabek
Mr. & Mrs. Stanley A. Duitscher '55
H.T. Youens, Sr.
Mr. & Mrs. Nelson D. Durst
George H. Ewing '46
Virginia & Edmond Faust
First National Bank of Bryan
Mr. & Mrs. Neil F. Fisher '75
Mr. & Mrs. Albert R. Frankson
Guy & Margaret Goddard
John E. Goin '68
Mr. & Mrs. Dick B. Granger
Howard J. Guba '63
Halliburton Foundation, Inc.
James & Doris Hannigan
Congpu Yao '13
Scott W. Holman, III '80
Lee R. Howard '52
Jack Howell
Robert & Carolyn Hughes
Mr. & Mrs. William V. Jacobs '73
Roland S. Jary '65
Richard & Earlene Jones
Stanley R. Kelley '47
Elmer E. Kilgore '54
Alcoa Foundation
Kenneth W. Kindle '57
Tom B. King
Walter A. Klein '60
Kenneth W. Korb '67
Dr. & Mrs. George W. Kunze
Larry K. Laengrich '86
Monroe A. Landry '50
Lawrence & Margaret Laurion
Mr. & Mrs. Charles A. Lawler
John M. Lawrence Jr.
Lockwood, Andrews & Newnam, Inc.
Linwood E. Lufkin '63
Robert & Marilyn Lytton
W.T. McDonald
James & Maria McPhail
Mr. & Mrs. Clifford A. Miller
Minann, Inc.
Jack & Lucille Newby
Leo Odom
Mr. & Mrs. Bookman Peters
Charles W. Pressley, Jr. '47
Mr. & Mrs. D.T. Rainey
Maj. Gen. & Mrs. Andy Rollins
Mr. & Mrs. John M. Rollins

Mr. & Mrs. J.D. Rollins, Jr.
Allen D. Rooke, Jr. '46
Paul D. Rushing '60
Schrickel, Rollins & Assoc., Inc.
William & Mildred Shull
SK Engineering
Milbourn L. Smith '60
Southwestern Laboratories
Mr. & Mrs. Homer Spear
Mr. & Mrs. Robert F. Stiles '79
Mr. & Mrs.Robert L. Thiele, Jr. '63
W.J. & Mary Lea Turnbill
Mr. & Mrs. John P. Tushek
Edward Varela '88
Troy & Marion Wakefield
Constance H. Wakefield
Mr & Mrs. Allister M. Waldrop
Robert R. Werner '57
Mr. & Mrs. William M. Wolf, Jr. '65
Mr. & Mrs. John Yankey, III '66

Every effort was made to ensure the accuracy of this list. If you feel there is an error, please contact the Engineering Development Office at 979-845-5113. A pledge card is enclosed on the last page for potential contributions.

# Clarence Darrow Hooper

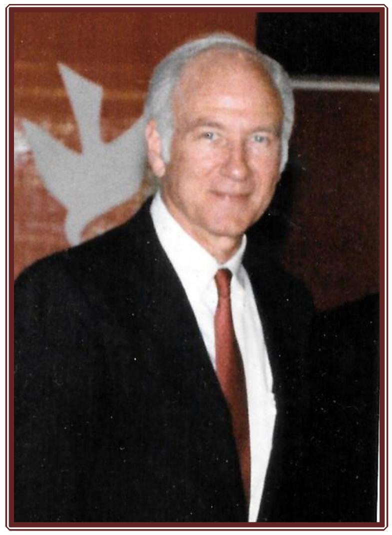


Clarence Darrow Hooper was born on January 30, 1932, in Ft. Worth, TX to Wallace Hooper and Mabel Merritt Hooper. Throughout his long life, he became an accomplished businessman and athlete. Following in his older brother, Wallace's, footsteps, Darrow started college at Texas A&M in 1949. Here, amongst academic success, he developed into a world class athlete. On the football field, he played quarterback, halfback, tight end and place kicker. While his football was very strong, his feats in track and field reached greatness. His career as a shot putter culminated when he represented his country at the 1952 Olympic Games in Helsinki, Finland. The favorite, he was narrowly beaten and won the silver medal, something that he was deeply humbled by and proud of. In 1953, he was drafted by the New York Giants, but chose not to play and instead focused on his career as a civil engineer. Through all of his athletic achievements, Darrow pursued his other goal of becoming a civil engineer and he was an outstanding student.

After graduating from A&M in 1954, he joined the Air Force and became a Second Lieutenant. In his professional career, he worked for Gifford Hill, Texas Testing Laboratories and, in 1977, opened his own company, Hooper Engineering Laboratories. He guided the company with great success for 22 years, until he retired in 1999. He was known as an intelligent, honest and hardworking businessman and garnered much respect in his field.

Darrow's love for his alma mater was evident in the generous gifts he gave to A&M throughout the years. In 1992, he established through a generous gift, the Spencer Buchanan Chair in Civil Engineering to honor his favorite professor. With this endowment, the school was able to appoint Jean-Louis Briaud the professorship, giving prestige to the university's engineering department. Darrow also established a President's Endowed Scholarship in the name of his longtime favorite coach, Colonel Frank Anderson. Darrow was passionate about giving back to the people and places that had helped him in his life; he was a firm believer in paying it forward and loved teaching others the skills he acquired throughout his life. To that end, he was elected as a trustee on the DISD School Board from 1991-1992. Darrow's personal life was as rich as his professional and athletic careers. A proud father of 4, a grandfather to 5 and a devoted husband, he relished in giving his family opportunities to succeed and the freedom to pave their own way in life. He loved to travel, specifically to Estes Park, CO, and Italy, where he enjoyed the solace of the mountains, art, history, and wine. Darrow was respected and loved by many and he will be missed by all who knew him.

Clarence Darrow Hooper, age 86, passed away on August 19, 2018, surrounded by his loving family. Darrow is survived by his wife of 50 years, Mary, children Clarence Darrow Jr., David, James and Elizabeth, grandchildren Caitlin, Sam, Meredith, Ava, and Celia.

# Spencer J. Buchanan Lecture Series

| | | |
|---|---|---|
| 1993 | Ralph B. Peck | "The Coming of Age of Soil Mechanics: 1920 - 1970" |
| 1994 | G. Geoffrey Meyerhof | "Evolution of Safety Factors and Geotechnical Limit State Design" |
| 1995 | James K. Mitchell | "The Role of Soil Mechanics in Environmental Geotechnics" |
| 1996 | Delwyn G. Fredlund | "The Emergence of Unsaturated Soil Mechanics" |
| 1997 | T. William Lambe | "The Selection of Soil Strength for a Stability Analysis" |
| 1998 | John B. Burland | "The Enigma of the Leaning Tower of Pisa" |
| 1999 | J. Michael Duncan | "Factors of Safety and Reliability in Geotechnical Engineering" |
| 2000 | Harry G. Poulos | "Foundation Settlement Analysis – Practice Versus Research" |
| 2001 | Robert D. Holtz | "Geosynthetics for Soil Reinforcement" |
| 2002 | Arnold Aronowitz | "World Trade Center: Construction, Destruction, and Reconstruction" |
| 2003 | Eduardo Alonso | "Exploring the Limits of Unsaturated Soil Mechanics: the Behavior of Coarse Granular Soils and Rockfill" |
| 2004 | Raymond J. Krizek | "Slurries in Geotechnical Engineering" |
| 2005 | Tom D. O'Rourke | "Soil-Structure Interaction Under Extreme Loading Conditions" |
| 2006 | Cylde N. Baker | "In Situ Testing, Soil-Structure Interaction, and Cost Effective Foundation Design" |
| 2007 | Ricardo Dobry | "Pile response to Liquefaction and Lateral Spreading: Field Observations and Current Research" |
| 2008 | Kenneth Stokoe | "The Increasing Role of Seismic Measurements in Geotechnical Engineering" |
| 2009 | Jose M. Roesset | "Some Applications of Soil Dynamics" |
| 2010 | Kenji Ishihara | "Forensic Diagnosis for Site-Specific Ground Conditions in Deep Excavations of Subway Constructions" |
| 2011 | Rudolph Bonaparte | "Cold War Legacy – Design, Construction, and Performance of a Land-Based Radioactive Waste Disposal Facility" |
| 2012 | W. Allen Marr | "Active Risk Management in Geotechnical Engineering" |
| 2013 | Andrew J. Whittle | " Importance of Undrained Behavior in the Analysis of Soil-Structure Interaction" |
| 2014 | Craig H. Benson | "Landfill Covers: Water Balance, Unsaturated Soils, and a Pathway from Theory to Practice" |
| 2015 | William F. Marcuson III | "Katrina in Your Rearview Mirror" |
| 2016 | Edward Kavazanjian | "Bio-Geo-Alchemy: Biogeotechnical Carbonate Precipitation for Hazard Mitigation and Ground Improvement." |
| 2017 | Jonathan D. Bray | "Turning Disaster into Knowledge" |
| 2018 | Paul W. Mayne | "Versatility of Cone Penetration Tests in GeoCharacterization" |
| 2019 | Gregory B. Baecher | "Putting Numbers on Geotechnical Judgement" |
| 2020 | Lidija Zdravkovic | "Soil Characterisation for Advanced Geotechnical Design: Parameter Derivation" |

The texts of the lectures and a video of the presentations are available by contacting:

Dr. Jean-Louis Briaud
Spencer J. Buchanan '26 Chair and Distinguished Professor
Zachry Department of Civil and Environmental Engineering
Texas A&M University
College Station, TX 77843-3136, USA
Tel: 979-845-3795
E-mail: **briaud@tamu.edu**

# Fugro Sponsorship

Texas A&M University and the Zachry Department of Civil Engineering gratefully acknowledge Fugro's sponsorship of the Buchanan Lecture. This Sponsorship, which began in 2013, reinforces the strong ties between the department and Fugro.

-Jean-Louis Briaud

TEXAS A&M UNIVERSITY
Zachry Department of
Civil & Environmental Engineering

# AGENDA

The Twenty-Eighth Spencer J. Buchanan Lecture
Friday, November 6, 2020
Virtually Via Zoom

| | |
|---|---|
| 1:00 p.m. | Introduction by Jean-Louis Briaud |
| 1:15 p.m. | Introduction of Lidija Zdravkovic by Jean-Louis Briaud |
| 1:20 p.m. | "Soil Characterisation for Advanced Geotechnical Design: Parameter Derivation." Professor Lidija Zdravkovic delivers the 2020 Buchanan Lecture |
| 2:20 p.m. | Introduction of Ed Idriss by Jean-Louis Briaud |
| 2:25 p.m. | "Response of Soil Sites During Earthquakes, A 60-Year Perspective." Professor Ed Idriss delivers the 2019 Terzaghi Lecture |
| 3:25 p.m. | Closure with Jean-Louis Briaud |

# Biographies


## Lidija Zdravkovic

Professor of Computational Geomechanics
Imperial College, London, UK
Email: l.zdravkovic@imperial.ac.uk


Lidija Zdravković is Professor of Computational Geomechanic and Head of the Geotechnics division at Imperial College London, UK. She holds MEng and MSc engineering degrees from the University of Belgrade, Serbia, and a PhD from Imperial College London. She joined Imperial College academic staff in 1999 and was promoted to full professor in 2013. Lidija has led and managed several research projects in collaboration with industry and other academic groups, focusing on the development and application of numerical methods in geotechnical design and providing solutions to a wide range of geotechnical problems, including renewable energy, nuclear waste disposal and infrastructure resilience. She is a core member and UK representative on the ISSMGE Technical Committee 103 for numerical analysis. She has authored and co-authored over 200 technical publications and received prizes from the Institution of Civil Engineers (ICE) and the British Geotechnical Association (BGA), UK. She has served as an elected member on the BGA Executive committee (2010-2013) and has consulted for industry on projects involving Heathrow extension tunnels, Crossrail deep excavations, offshore foundations and infrastructure slopes in conjunction with the high speed rail route in the UK.


## Ed Idriss

Professor Emeritus
University of California at Davis
Consulting Geotechnical Engineer
Email: imidriss@aol.com


Dr. Ed Idriss is Professor Emeritus of Civil Engineering at the University of California at Davis (UCD) and an independent consulting geotechnical engineer, currently residing in Santa Fe, New Mexico, USA. His areas of teaching, research and practice are: geotechnical earthquake engineering; soil mechanics and foundation engineering; earthfill and rockfill dam engineering; and numerical modeling. He joined the faculty at UCD in 1989 following 20 years at Woodward-Clyde Consultants in San Francisco, Santa Ana and Oakland where he was a senior Principal. He was a member of the teaching and research staff of the geotechnical engineering group at the University of California at Berkeley from 1967 through 1975. He retired from the faculty position at UCD in July 2004. He has received many awards and honors over the past fifty years, including election to the US National Academy of Engineering in 1989, receipt of the first H. Bolton Seed Medal from ASCE in 1995, the distinguished scholarly public service award from the University of California at Davis in 1999, was elected an honorary member of the Japanese Geotechnical Society in 2005, was elected a Distinguished Member of ASCE in 2008, and is the recipient of the 2010 Ralph Peck Award from ASCE, and the 2010 Casagrande Memorial Lecture from the Boston Society of Civil Engineers. He was elected an Honorary Member of the Earthquake Engineering Research Institute (EERI) in 2012 and the recipient of the George W. Housner Medal from EERI in 2018. He presented the Terzaghi Lecture in 2019.

# *Soil Characterisation for Advanced Geotechnical Design: Parameter Derivation*

The 2020 Spencer J. Buchanan Lecture

By Dr. Lidija Zdravkovic

# Soil characterisation for advanced geotechnical design: parameter derivation

Lidija Zdravković
*Department of Civil and Environmental Engineering, Imperial College London, UK*

**DECLARATION**

The content of this lecture is based in particular on the following published papers:

Zdravković L., Potts D.M. & Taborda D.M.G (2020). Integrating laboratory and field testing into advanced geotechnical design; *Geomechanics for Energy and the Environment*, https://doi.org/10.1016/j.gete.2020.100216

Zdravković L., Jardine R.J., Taborda D.M.G., Abadias D., et al. (2019). Ground characterisation for PISA pile testing and analysis. *Géotechnique*, https://doi.org/10.1680/jgeot.18.pisa.001

Zdravković L., Taborda D.M.G., Potts D.M., Abadias D., et al. (2019). Finite element modelling of laterally loaded piles in stiff glacial clay till at Cowden. *Géotechnique*, https://doi.org/10.1680/jgeot.18.pisa.005

**ABSTRACT**

Contemporary geotechnical design often requires the use of advanced numerical analysis, if it is to take account of the complex nature of many geotechnical problems. One crucial aspect of such analyses is the realistic representation of the facets of soil behaviour that are dominant in any given problem, which in turn requires a careful selection of an appropriate constitutive model and derivation of model parameters from the available, and often disparate, experimental data. This lecture utilises the experience of developing and applying advanced numerical tools in author's research group at Imperial College, to emphasise the importance of close integration of the process involved with interpreting experimental data with the process of selecting and calibrating advanced constitutive models, for successful predictions of the response of geotechnical structures.

## 1. Introduction

The complexities of contemporary geotechnical problems often require application of advanced calculation tools as part of the design process. In effect, developments in congested urban environments, resilience and lifecycle assessment of infrastructure, thermo-hydro-mechanical coupling of soil phases in geothermal energy exploration or in the development of lasting solutions for nuclear waste disposal, are just some of the examples that can be addressed only by application of advanced numerical analysis. In particular, the assessment of serviceability limit states and of the effects that new construction may impose on existing structures and services, have become strongly dependent on the use of numerical analysis, the finite element and the finite difference methods being the main forms employed in engineering practice. This lecture is concerned only with the application of the finite element method (FEM).

In any numerical analysis there are, in principle, three main parts of the geotechnical input that need to be idealised in a realistic manner (Figure 1). One is an idealisation of the problem geometry, which will depend on the ground conditions (different soil layers), dimensions (two-dimensional, 2D, or three-dimensional, 3D) and existence of any structural components (wall, anchor, tunnel lining) and material interfaces that may need to be discretised with appropriate element types. Next is the characterisation of ground conditions and soil behaviour from available field and laboratory investigations, which leads to the selection of appropriate soil constitutive models. The complexity of the employed constitutive model is often determined by the available soil data and the derivation of model parameters has to be consistent with experimental evidence. The final aspect of the numerical idealisation is the application of appropriate boundary conditions, capable of simulating realistically the details of the design brief (e.g. excavation, construction, dewatering, loading). The solution process in the case of the FEM involves a large system of governing equations, from which displacements (and depending on the level of coupling also pore water pressures and temperatures) at element nodes are the primary analysis output, which facilitates the calculation of strains and stresses in the analysed domain. Their interpretation provides predictions of the response of a given boundary value problem idealised in the manner shown in Figure 1. Clearly, the accuracy of predictions will depend on how realistically each of the three elements are idealised.

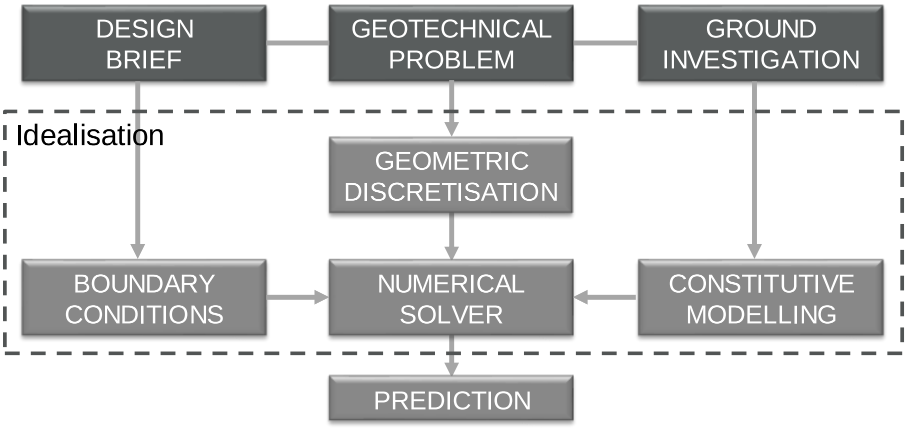


Figure 1: Elements of numerical input to finite element anlaysis

This lecture utilises the experience of advanced numerical analysis, gained over the years in author's research group at Imperial College, to demonstrate, on selected practical geotechnical problems, the process of integrating the numerical input from ground investigation, problem geometry and design requirements. Such a process is necessary for the delivery of accurate numerical predictions and of efficient design solutions for geotechnical structures. Particular focus is placed on the treatment of soil behaviour and the process of integrating laboratory and field experimental evidence to characterise soil behaviour and initial ground conditions. A further focus is on demonstrating the process of selecting an appropriate constitutive model that is consistent with experimental evidence and is capable of reproducing the facets of soil behaviour that are crucial for a given problem. This is an essential step as there is no single constitutive model in existence that can be applied to all soil types and simulate with equal accuracy their mechanical behaviour. The thread of examples discussed in the lecture starts with those that can be analysed as undrained (effective stress-based non-coupled analyses), extending to time-dependent transient problems (requiring hydro-mechanically coupled analyses). The emphasis throughout the lecture is on producing "blind", Class A predictions (Lambe, 1973), as applied in a design scenario, and not on performing back-analyses of given problems. All examples of numerical analyses presented here have been performed with the Imperial College Finite Element Program (ICFEP; Potts & Zdravkovic, 1999; 2001).

## 2. Undrained problems in stiff low-plasticity clays

### 2.1 Background

The selected example considers the design of a large-scale pile testing programme under monotonic lateral loading, in a stiff low-plasticity overconsolidated clay till at Cowden, UK, as part of the PISA

(**PI**le-**S**oil **A**nalysis) Joint Industry Project (JIP). Numerical analyses, ground investigation and in-situ pile testing were integral parts of the PISA project, concerned with the development of new design methods for laterally loaded monopiles, as foundation systems for offshore wind turbines. The existing codified *p-y* methodology (API, 2010; DNV-GL, 2016) was experienced by the relevant industry not to work well for large diameter monopiles with low length to diameter ratios ($L/D$). Central to the new development was academic research, comprising Imperial College London, Oxford University and University College Dublin, with the principal project outcomes featuring in the papers of Zdravkovic et al. (2019a), Burd et al. (2019a), Byrne et al. (2019a), McAdam et al. (2019), Zdravkovic et al. (2019b), Taborda et al. (2019), Byrne et al. (2019b) and Burd et al. (2019b).

Considering the size of wind turbine monopiles, with current diameters of 8 to 10 m, full scale field testing from which to derive a design method, as in the original *p-y* methodology (Reese et al., 1974, 1975), was clearly impractical. Even a reduced scale field testing, as performed at Cowden (Byrne et al., 2019a), was expensive, raising also the question of scale effects. The new design method was therefore envisaged to be developed on the basis of 3D finite element (FE) analyses of monopiles. The key to achieving this successfully and to gaining the confidence of the industry partners and verification bodies on the feasibility of the new design method, was to demonstrate the ability of the finite element modelling to deliver accurate predictions of monopile response in given ground conditions. For this purpose site-specific analyses of medium-scale field tests at Cowden were performed before the field testing took place, and Class A predictions of pile behaviour were compared with subsequent field measurements. The Cowden site was chosen for field testing as its clay till soil is representative of sea-bed conditions in some sectors of the North Sea.

The objective of the PISA project was to establish the backbone of the monotonic load-displacement response of laterally loaded monopiles, as detailed in Zdravković et al. (2019a). For the new design method to be developed, it was deemed essential that the modelling should reproduce accurately the initial part of the backbone curve, corresponding to working loads, and the ultimate capacity of pile at failure. The former is the serviceability limit state which depends on the small strain behaviour of the soil, while the latter is the ultimate limit state which depends on the soil strength. Consequently, interpretations of the Cowden till's small strain stiffness and strength were key design requirements for the monopile field testing programme.

## 2.2 Interpretation of ground conditions at Cowden

Considering that the Cowden site was a test site of the British Research Establishment (BRE) for a number of years, the initial information on ground conditions and on soil behaviour comprised a number of pre-1990s studies, summarised in Powell & Butcher (2003). Additional laboratory and field tests were conducted as part of the PISA project, the former through the PhD research of Ushev (2018) at Imperial College. Detailed integration and interpretation of all experimental data can be found in Zdravkovic et al. (2019a).

### *2.2.1 Ground profile and ground water*

The first insight into ground conditions, provided by the historic evidence in Powell & Butcher (2003), revealed a 40 m deep deposit of glacial clay underlain by chalk, with a bulk unit weight of $21.19\ \mathrm{kN/m^3}$, an average plasticity index $PI{\sim}18$ and clay content of 32%, indicating a low-plasticity clay. These properties were confirmed by index testing on new samples collected for PISA. The cone penetration profiles from new CPT tests conducted across the PISA test site at Cowden (Figure 2) showed a reasonably consistent ground profile in the top 12m, with little local variability. The frequent spikes resulted from the presence of stones in the clay matrix, and the concentrated high resistance between 12 and 14m depth confirmed the existence of a sand layer, previously identified in Powell

& Butcher (2003). These field results limited the maximum embedded length of the test piles to 10.5m, in order for the whole pile to be embedded in a single material type.

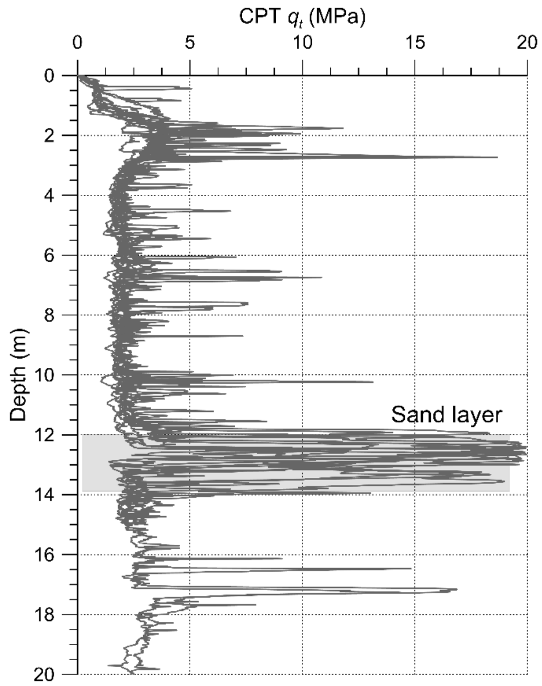


Figure 2: CPT cone penetration traces at PISA Cowden test site

The ground water table was found at 1 m depth and the piezometeric measurements of pore pressure revealed an under-drained pore water pressure profile (i.e. less than hydrostatic) in the top 10 m of the deposit (Figure 3(a)). Such a profile is possible in the field if the permeability reduces with depth and if there is a deeper aquifer with a phreatic surface that is lower than the ground water table. Both conditions exist at Cowden, the permeability in particular reducing from about $k \sim 0.05\ \mathrm{m/year}$ in the top weathered part of the clay till, to about $k \sim 0.007$ to $0.0005\ \mathrm{m/year}$ in the unweathered deposit below (Figure 3(b)). Assessing these values of permeability with respect to the rate of loading that would result from wind and wave actions on the support structure of a wind turbine, it was considered appropriate to perform FE analyses of laterally loaded monopiles under undrained conditions.

### *2.2.2 Initial stresses*

The vertical effective stress is readily established from the bulk unit weight of the soil and the pore water pressure shown in Figure 3(a). The horizontal effective stresses are usually significantly more challenging to assess. The early historic studies at the Cowden site made use of total stress spade cells (Tedd et al., 1989) and pressuremeter tests (Powell et all., 1983), applying various correction factors to estimate horizontal stresses. Further estimates were also made from pre-consolidation stresses derived from oedometer tests, using different relationships between the overconsolidation ratio, $OCR$, and at rest earth pressure coefficient, $K_0$. These estimates are plotted in Figure 4a, indicating $K_0$ values of up to 3 in the top 5 m. Considering that the soil was fissured and affected by glaciation, the one-dimensional oedometer swelling was thought unrepresentative of the processes the ground was subjected to in its geological history. Hence a value of $K_0$ nearing the passive earth pressure coefficient was considered unrealistic. Supported by recent studies on overconsolidated stiff marine clays that have experienced weathering and glaciation (Brosse et al., 2017), which showed that $K_0$ cannot be higher than 1.5 to 1.8 at shallow depths, the $K_0$ value for the Cowden site was limited to 1.5 in the top 5 m, with the remaining profile at depth following the available measurements.

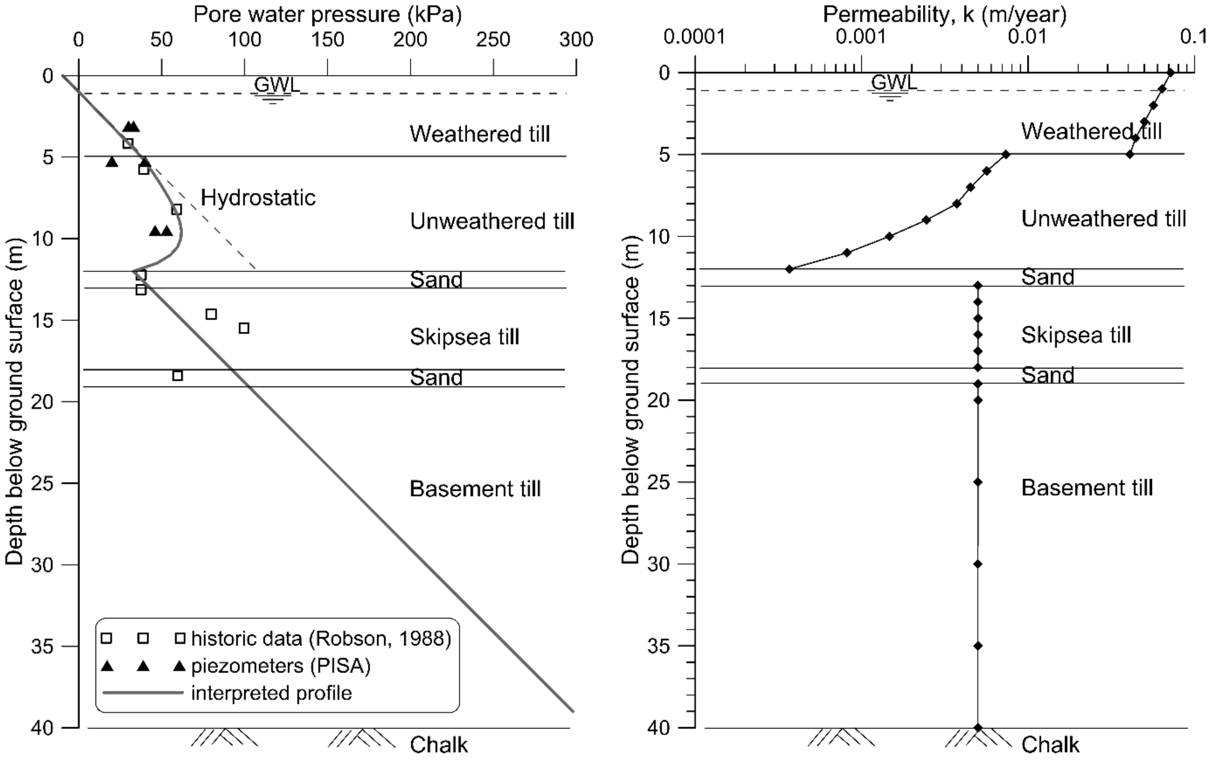


(a) (b)

Figure 3: Cowden ground profile: (a) pore water pressure and (b) permeability profiles

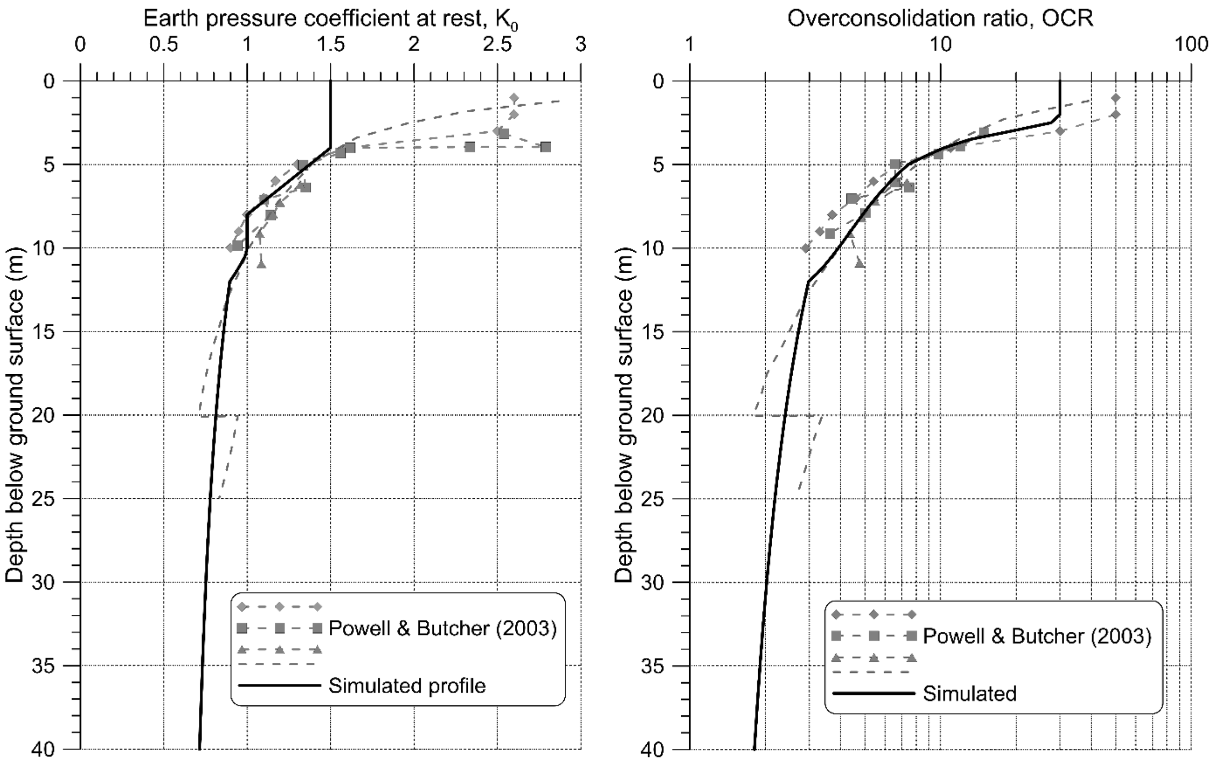


(a) (b)

Figure 4: Measured and simulated: (a) $K_0$ profile and (b) $OCR$ profiles at Cowden test site

## 2.3 Interpretation of soil behaviour and selection of a constitutive model

Given that optimised monopile design needed to produce accurate monopile response at operational (low-level vibrations) and at ultimate conditions (storm load, high overturning moments), the requirement for the soil constitutive model was the ability to capture accurately both the small strain soil response and the response at failure. The former is characterised by the small strain shear and bulk stiffness that are functions of both stress and strain levels in the soil, while the latter is characterised by the soil's drained and undrained strength.

### *2.3.1 Drained shear strength*

Apart from undrained triaxial tests in compression (TXC) and extension (TXE), no other laboratory experiments were available to characterise the strength of Cowden till. Specifically, strength anisotropy due to rotation of principal stresses was unknown, leading to the selection of an isotropic constitutive model for the monopile analyses.

Undrained effective stress paths in triaxial compression, normalised as shown in Figure 5, from overconsolidated Cowden till samples taken at various depths (Ushev, 2018), indicated a critical state-type behaviour, plotting on the dry side of critical state and with stress paths smoothly reaching critical state conditions. Consequently, in terms of the constitutive framework, the isotropic critical state-based modified Cam clay (MCC) model (Roscoe & Burland, 1968) was considered appropriate for representing the strength of Cowden till, albeit with some necessary extensions (as detailed in Zdravković et al., 2019b). It is clear from Figure 5 that the deviatoric yield stress dry of critical was significantly smaller than what would be predicted by the original MCC ellipse, the size of which, $p_0'$, is estimated from the samples' initial stresses and previous stress history. As a result, the *first extension* of the MCC model was to introduce a Hvorslev surface on the dry side, for accurate representation of the Cowden till strength. ICFEP employs a non-linear Hvorslev surface, as developed in Tsiampousi et al. (2013), with the equation of the complete yield surface, in generalised $p' - J - \theta$ space, becoming:

$$F(\boldsymbol{\sigma}', p_0') = F(p', J, \theta, p_0') = \begin{cases} \dfrac{J}{p' g(\theta)} - \dfrac{\alpha}{g(\theta)} - \left(1 - \dfrac{\alpha}{g(\theta)}\right)\left(\dfrac{p_0'}{2p'}\right)^n = 0, & p' < \dfrac{p_0'}{2} = p_{cs}' \\ \left(\dfrac{J}{p' g(\theta)}\right)^2 - \left(\dfrac{p_0'}{p'} - 1\right) = 0, & p' \geq \dfrac{p_0'}{2} = p_{cs}' \end{cases} \qquad (1)$$

where $p'$ is the mean effective stress, $J$ is the generalised deviatoric stress, $\theta$ is the Lode's angle and $p_0'$ is the hardening parameter, representing the size of the yield surface. Parameters $\alpha$ and $n$ control the shape of the Hvorslev surface and are evaluated as $\alpha = 0.25$ and $n = 0.40$ (Zdravković et al., 2019b), reproducing the shape shown in Figure 5 which agrees well with test data. The second part of the equation is the shape of the usual MCC elliptical surface, which applies on the wet side. The inclination of the Critical State Line (CSL), denoted as $g(\theta)$, depends on the Lode's angle, $\theta$, in the deviatoric plane and on the value of the angle of shearing resistance, $\phi_\theta'$, at a given Lode's angle.

Interpreted critical stress states, at axial strains of around 30% in undrained TXC and 15% in undrained TXE, are shown in Figure 6, demonstrating good agreement between historic and PISA triaxial test results. The figure also reveals different ultimate stress ratios ($q/p'$) in compression, $M_{cs}^c = 1.07$, and in extension, $M_{cs}^e = 0.90$, which convert to the respective values of the angle of shearing resistance of $\phi_{TXC}' = 27^\circ$ (at $\theta = -30^\circ$) and $\phi_{TXE}' = 32^\circ$ (at $\theta = +30^\circ$). Considering that the boundary value problem under investigation (i.e. a laterally loaded pile) is three-dimensional, this experimental evidence implies that $\phi'$ in the deviatoric plane should be allowed to vary accordingly with respect to the magnitude of the Lode's angle, $\theta$ (representing the effect of the intermediate principal stress). The original MCC circular shape of the yield surface in the deviatoric plane allows different values of $\phi'$ to be mobilised with respect to $\theta$, however this variation is unrealistic, as shown in Figure 7. If a circle in the deviatoric plane is fitted to $\phi'_{TXC} = 27^{\mathrm{o}}$, the magnitude of $\phi'_{TXE}$ reaches about $41^{\mathrm{o}}$, which, at $9^{\mathrm{o}}$ higher than measured, is clearly unconservative for design. On the other hand, the Mohr-Coulomb shape of the yield surface in the deviatoric plane assumes a constant value of $\phi'$, thus under-predicting the available strength of the soil. As a result, a more accurate definition of soil strength in the deviatoric plane was needed, which comprised the *second extension* of the MCC model. The generalised Van Eekelen (1980) surface given by Equation (2), was introduced to replace the circular shape:

$$g(\theta) = \frac{X}{(1 + Y \sin 3\theta)^Z} \tag{2}$$

where $X$, $Y$ and $Z$ are model parameters and their values have to satisfy a number of constraints to ensure the convexity of the surface. This function can reproduce, with the appropriate choice of parameters, the experimentally derived shapes of Lade & Duncan (1975), or Matsuoka & Nakai (1974) surfaces. The variation of $\phi'$ in the deviatoric plane for Cowden till is also shown in Figure 7, with $Z = 0.1$, $X = 0.548$ and $Y = 0.698$ fitted to achieve a maximum variation of up to $6^{\mathrm{o}}$ between triaxial compression and plane strain loading ($\theta \sim 0^{\mathrm{o}}$), as measured for most soils (e.g. Bishop, 1966; Gens, 1982).

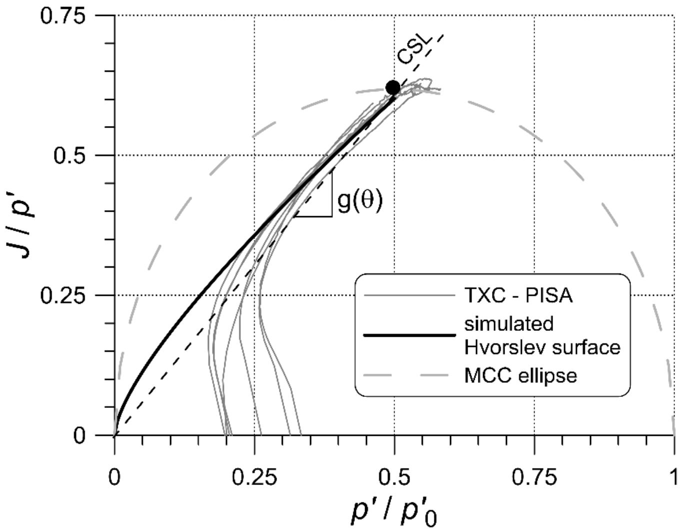


Figure 5: Hvorslev surface in the extended modified Cam clay (MCC) model for Cowden till

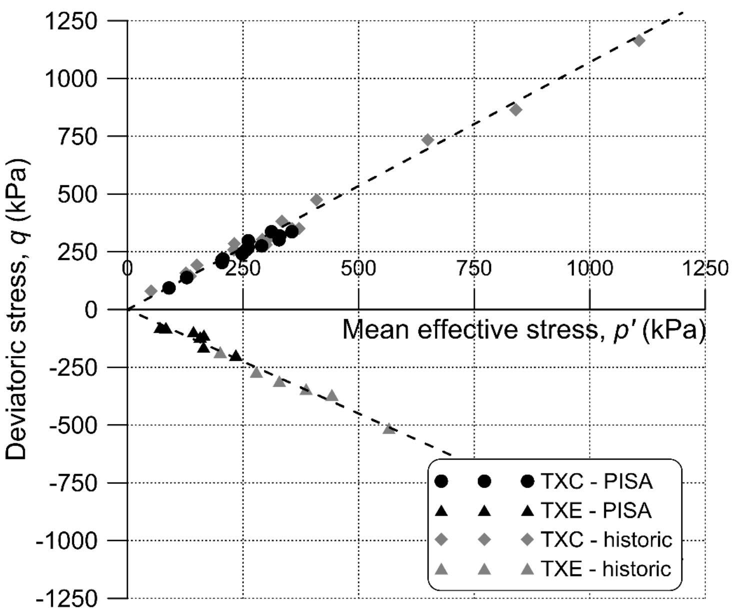


Figure 6: Interpretation of Cowden till effective stress shear strengths

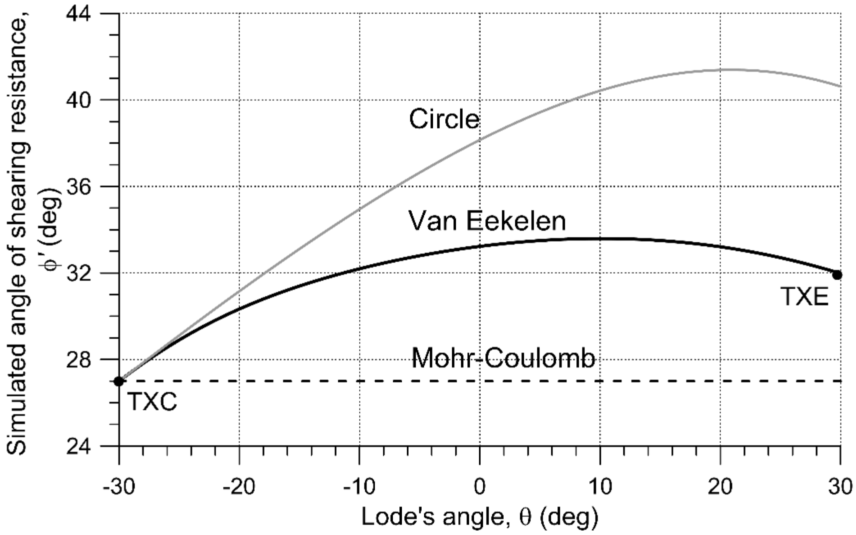


Figure 7: Variation of $\phi'$ in deviatoric plane for different shapes of the yield surface

*2.3.2 Undrained shear strength*

As it was decided that the pile analyses would be performed under undrained conditions, it was necessary to also characterise the undrained shear strength of Cowden till. Figure 8 shows a summary of the historic and new PISA test data from which the undrained strength in triaxial compression, $S_{u,TXC}$, was derived. The historic data (Powell & Butcher, 2003), derived predominantly from samples obtained by pushed-in thin-walled tube sampling, showed a fair scatter and no data in the top 2 m. Powell & Butcher (2003) put the scatter down to site variability, as the tested area was much larger than the PISA site, as well as to some sampling-induced disturbance. The new TXC tests on samples obtained by Geobore-S rotary coring produced consistent data, with very good agreement of undrained strengths derived from 38 mm and 100 mm samples, indicating that the strength was dominated by the soil matrix, rather than by stone inclusions. The undrained strength in the top 2 m of the deposit, which is essential in providing soil resistance to a laterally loaded pile, was also well-characterised by the new PISA triaxial testing and by additional results of the field shear vane testing. As a final check, the $S_u$ profile derived from the average CPT cone resistance (applying a cone factor $N_{kt} = 16$; Powell & Quarterman, 1988), showed a generally good agreement between the laboratory and field interpretations of undrained strength.

Conveniently, the adopted MCC model has an analytical solution for the undrained shear strength (Potts & Zdravković, 1999):

$$S_u = OCR \cdot \sigma'_{v0} \cdot g(\theta) \cdot \cos(\theta) \cdot \frac{1 + 2K_0^{NC}}{6} \cdot (1 + B^2) \cdot \left[\frac{2 \cdot \left(1 + 2K_0^{OC}\right)}{(1 + 2K_0^{NC}) \cdot OCR \cdot (1 + B^2)}\right]^{\frac{\kappa}{\lambda}} \tag{3}$$

where:

$$B = \frac{\sqrt{3} \cdot (1 - K_0^{NC})}{g(-30°) \cdot (1 + 2K_0^{NC})} \tag{4}$$

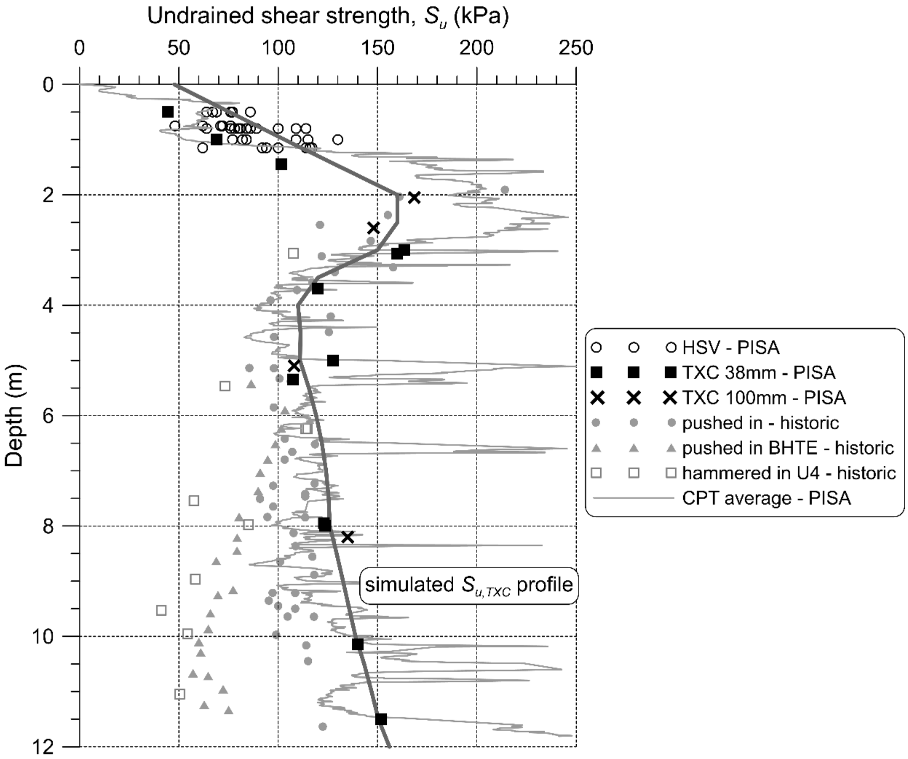


Figure 8: Experimental evidence of laboratory and field data for undrained shear strength of Cowden till, and adopted profile of $S_{u,TXC}$ consistent with the extended MCC model

In Equation (4), $K_0^{OC}$ is the current value of the coefficient of earth pressure at rest, as depicted in Figure 4a, while $K_0^{NC}$ is the value associated with normal consolidation and is taken as $(1 - \sin\phi'_{TXC})$. $OCR$ is defined as the ratio of the maximum previous vertical effective stress, $\sigma'_{v,max}$, and the initial vertical effective stress, $\sigma'_{v0}$. Lacking isotropic compression and swelling tests, parameters $\lambda$ ($= 0.115$, compressibility) and $\kappa$ ($0.021$, swelling) were derived from the constant rate of strain (CSR) oedometer tests on samples from different depths (see Zdravković et al., 2019a, 2019b). Fitting the Equation (3) to the interpreted $S_{u,TXC}$ profile in Figure 8 allowed the distribution of $OCR$ to be evaluated, as shown in Figure 4b. The excellent agreement of the $OCR$ profile with the historic data demonstrates a high level of consistency between the derived model parameters and interpreted ground conditions.

*2.3.3 Stiffness*

To predict the soil response at operational loads, further assessment of experimental data requires characterisation of both the elastic shear modulus, $G_0$, and shear stiffness degradation with increasing deviatoric strain. The interpretation of the experimental evidence on $G_0$ is summarised in Figure 9(a), comprising dynamic and static testing conducted for PISA. The former tests depict two seismic cone (SCPT) profiles which are consistent with the laboratory bender element (BE) measurements of $G_0$ on intact samples. Such an agreement indicates little disturbance induced by sampling. Another observation is that the horizontal ($G_{hh}$) shear modulus is generally larger than the vertical ($G_{vh}$), but not as distinctly as measured in stiff plastic clays (e.g. Gasparre et al., 2007; Brosse et al., 2017). The historic in-situ geophysics down-hole profile ($G_{vh}$) was in reasonable agreement with the new dynamic tests, but the cross-hole ($G_{hh}$) data showed a much bigger difference, which could be attributed to larger variability across the historic testing area at Cowden. The $G_0$ profiles derived from the local gauges in static triaxial compression and extension tests were distinctly smaller compared to the dynamic profiles, which is not uncommon in laboratory testing and could be attributed to insufficient resolution of the transducers at very small strains (considering a very good agreement seen between laboratory and field dynamic measurements). With no other evidence available at the time of the PISA numerical modelling, in particular to support strongly the existence of stiffness anisotropy, the elastic shear stiffness of Cowden till was represented as isotropic and the maximum shear modulus profile in Figure 9(a) was estimated as $G_0 = 1100 \cdot p'$, fitted through the dynamically-measured profiles, but ignoring the historic cross-hole measurement.

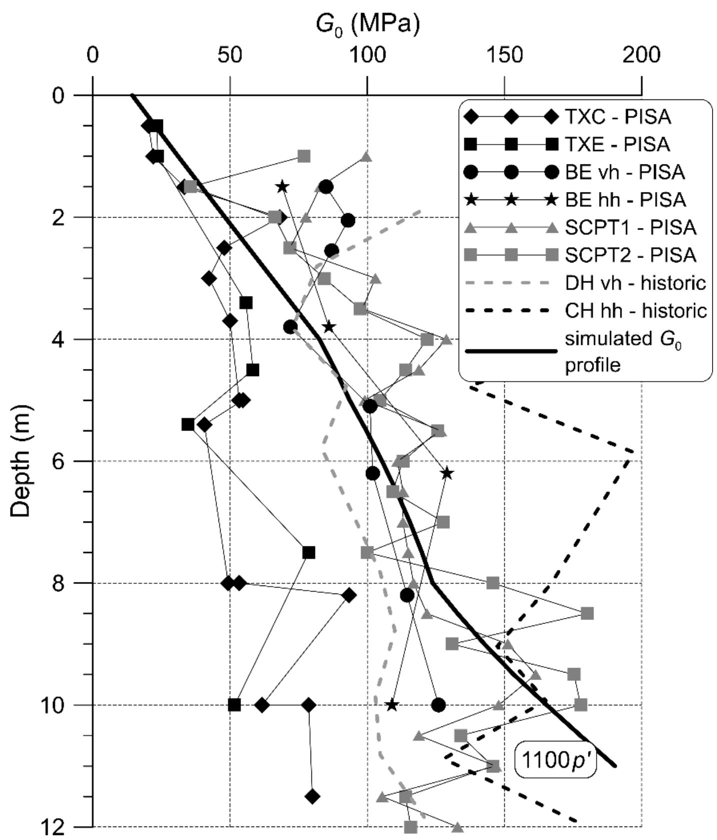


Figure 9 (a): Stiffness of Cowden till: measured and interpreted $G_0$ profile

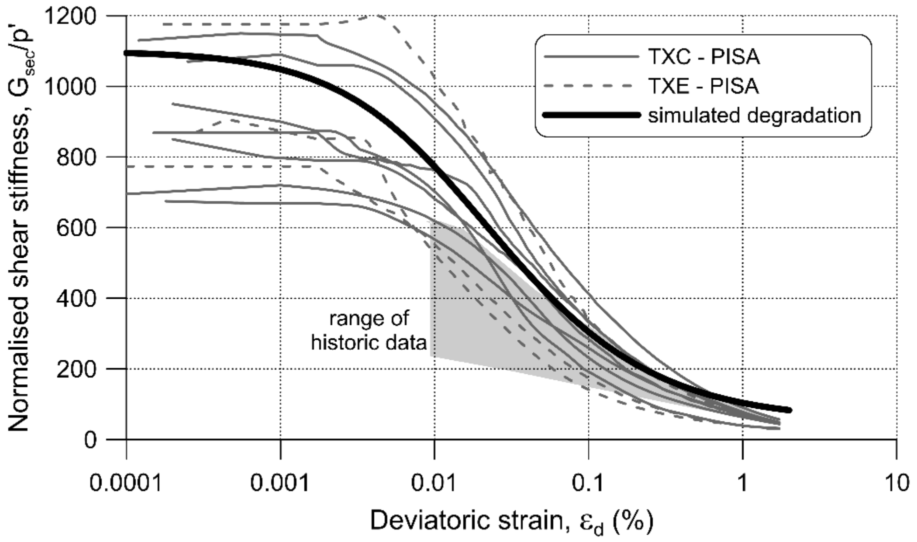


Figure 9 (b): Stiffness of Cowden till: measured and interpreted stiffness degradation with strain level

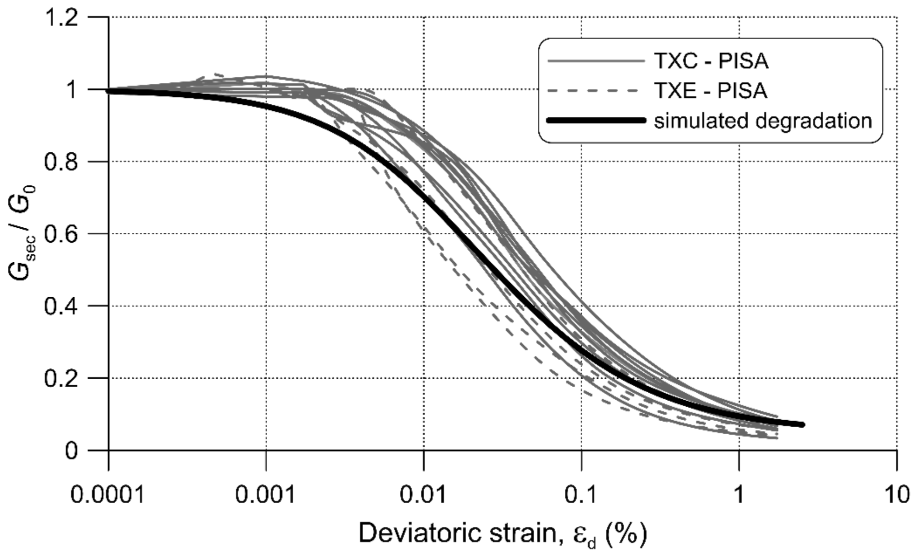


Figure 9 (c): Stiffness of Cowden till: normalised shear stiffness degradation

The degradation of normalised secant shear stiffness, $G_{sec}/p'$, with increasing deviatoric strain, $\varepsilon_d$, is shown in Figure 9(b) from several triaxial undrained shearing tests. Inspecting this evidence, there is no clear distinction between stiffness degradation in TXC and TXE in the small strain range, nor any other data to support stiffness anisotropy in this range. As such, the simulated shear stiffness degradation in the small strain range was assumed isotropic, as depicted in Figure 9(b). It is clear that a number of tests have a maximum stiffness below the adopted $G_0 = 1100 \cdot p'$, consequently the degradation part was calibrated to be significantly sharper than observed in these experiments, so that at medium strains the simulated response would be closer to some average stiffness of all the triaxial tests. The effect of this decision is shown in the normalised $G_{sec}/G_0$ degradation in Figure 9(c), emphasising the need to consider globally the stiffness calibration instead of producing in isolation the maximum stiffness and its degradation. The range of data marked as historic in Figure 9(b) indicates the poor resolution of the pre-1990s measurements.

Based on this evidence, the *third extension* of the MCC model was to replace its pre-yield elasticity with a non-linear small strain overlay, for the purpose of capturing the soil behaviour at operational loads. The ICG3S non-linear model (Taborda & Zdravkovic, 2012; Taborda et al., 2016) introduced the isotropic tangent shear and bulk moduli that are stress, strain and void ratio dependent:

$$G_{tan} = G_0^* \cdot f_G(e) \cdot \left(\frac{p'}{p'_{ref}}\right)^{m_G} \cdot \left(R_{G,min} + \frac{1 - R_{G,min}}{1 + \left(\frac{\varepsilon_d}{a}\right)^b}\right) \tag{5}$$

$$K_{tan} = K_0^* \cdot f_K(e) \cdot \left(\frac{p'}{p'_{ref}}\right)^{m_K} \cdot \left(R_{K,min} + \frac{1 - R_{K,min}}{1 + \left(\frac{|\varepsilon_{vol}|}{r}\right)^s}\right) \tag{6}$$

The effect of void ratio was ignored in the shear stiffness calibration in Equation (5) (i.e. $f_G(e) = 1$), with other model parameters ($a$, $b$, $R_{G,min}$) evaluated to produce the shear stiffness shown in Figures 9(b) and 9(c).

Calibration of the tangent bulk stiffness required further care as elasticity in the original MCC formulation, which assumes the swelling parameter $\kappa$ to be constant, implies that $K_{tan} = (v \cdot p')/\kappa$. This is inconsistent with the non-linear model in Equation (6), raising a problem with the evaluation of the undrained strength profile, $S_u$, in Equation (3), which requires a constant value of $\kappa$. For the model to reproduce swelling lines of constant gradient, the void ratio function was adopted as $f_K(e) = 1 + e$ and parameters $m_K$ and $R_{K,min}$ were set to 1.0, rendering values of $s$ and $r$ irrelevant.

Input parameters for the extended MCC model, calibrated from the available historic and new laboratory and field data on Cowden till, are summarised in Table 1.

### 2.4 Boundary value problem – laterally loaded pile at Cowden

Sections 2.2 and 2.3 demonstrated the process of developing and ensuring the consistency between the ground and soil characterisation and the selected constitutive framework, as well as the necessity for a very good understanding of the constitutive model formulation and what it entails. The evolution of the constitutive model, from its original formulation, was presented in conjunction with the experimental information available for the soil, and it enabled the model to capture more accurately the governing facets of the soil behaviour for the given boundary value problem of undrained lateral loading of monopile foundations.

The main purpose of the study was to develop a 3D FE model to, first, design the PISA test piles at Cowden from the predicted responses of the 3D FE model, and, second, to validate the 3D FE model by comparing these predictions with the field test results obtained subsequently. Two pile diameters ($D = 0.762$ m and $D = 2.0$ m) and three length-to-diameter ratios ($L/D = 3$, $5.25$ and $10$) were used for field testing, with a monotonic horizontal load applied at the top of a 10 m high steel tubular extension mounted on the pile heads (see Byrne et al., 2019a). The problem was discretised into the FE mesh shown in Figure 10. The soil was simulated as a single Cowden till layer (due to the lack of experimental evidence to distinguish between different levels of weathering with depth), ignoring the presence of the two sand layers and adopting the initial stresses and the pore water pressure profile as described in Section 2.2. The steel tubular pile was discretised with shell elements (Schroeder et al., 2007) and modelled as elastic, with a Young's modulus of 200 GPa and a Poisson ratio of 0.3. As horizontal pile loading could create a gap on the active side of the pile, zero-thickness interface elements (Day & Potts, 1994) were placed on the outside of the pile to allow this to happen if the soil tensile strength (set to zero) was mobilised during loading (see Zdravkovic et al. 2019b for details of the numerical model).

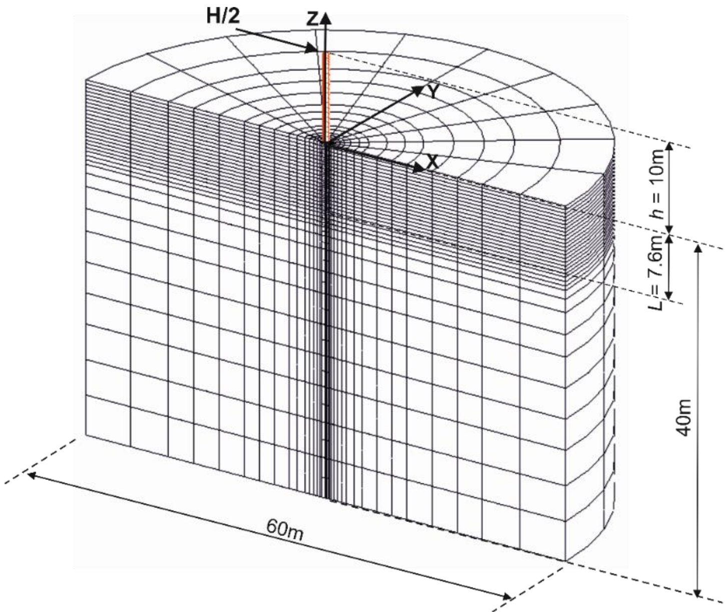


Figure 10: Representative finite element mesh for PISA test piles at Cowden

For brevity, Figure 11 compares the predicted and measured horizontal force, $H$, versus the horizontal ground-level displacement, $v_G$, for only two test piles of different diameter and length. The field tests were performed with a minimum displacement rate that ensured the completion of each test over a period of 8 hours. The applied stages of loading indicate the existence of rate effects at the beginning of each stage, while holding periods ensured that negligible strain rates were reached after each loading. Consequently, the predicted load-displacement curves, which were obtained from analyses that were not developed to simulate a rate-dependent response, are compared with the end points of each holding stage, as these points represent the rate-independent backbone curve. The agreement between the measured and predicted curves is excellent, both at operational loads, when $v_G = 0.01D$ (Figure 11(b) & (d)), and at nominal ultimate loads, when $v_G = 0.1D$ (Figure 11(a) & (c)). The predicted embedded response of the piles, in terms of deflected shapes and bending moments, was also shown to be in very good agreement with measurements, as well as the occurrence of gapping around the piles, as detailed in Zdravkovic et al. (2019b).

This level of agreement between 'blind' Class A predictions and subsequent field test measurements was crucial to convincing the PISA Industry Partners and the Independent Technical Review Panel (ITRP) of the ability of advanced numerical analysis, as developed for PISA using the ICFEP modelling platform, to predict accurately the monopile response under lateral loading. Following this, further ICFEP 3D FE analyses of full scale monopiles ($D = 5 \text{ to } 10$ m and $L/D = 2 \text{ to } 6$) in similar ground conditions, but adjusted to an offshore environment, were performed and results used as direct input into the formulation of a new simplified, Winkler-type, PISA design method for laterally loaded monopiles in clays (see Byrne et al. 2019b).

## 2.5 Considerations for stiff plastic clays

In the previous discussion the soil was an overconsolidated stiff low-plasticity clay till, with its mechanical behaviour shown to follow critical state principles. Shearing in compression of clay till samples was shown to mobilise ductile stress paths to critical states, while their shear stiffness was reasonably well interpreted as isotropic. This section considers some implications for numerical modelling of the same undrained problem (laterally loaded monopiles) in the case of the soil being a stiff, overconsolidated marine plastic clay, such as London clay with $PI{\sim}35-50$, which exhibits non-critical state ultimate conditions. Compared to the above Cowden till characterisation, the two principal aspects of the mechanical behaviour of such clays are a markedly anisotropic shear stiffness, with $G_{hh} > G_{vh}$, (e.g. Gaspare et al., 2007; Brosse et al., 2017) and a brittle behaviour resulting in a reduction of strength from peak to residual over a certain strain interval (e.g. Kovacevic et al., 2007; Hosseini Kamal et al., 2014).

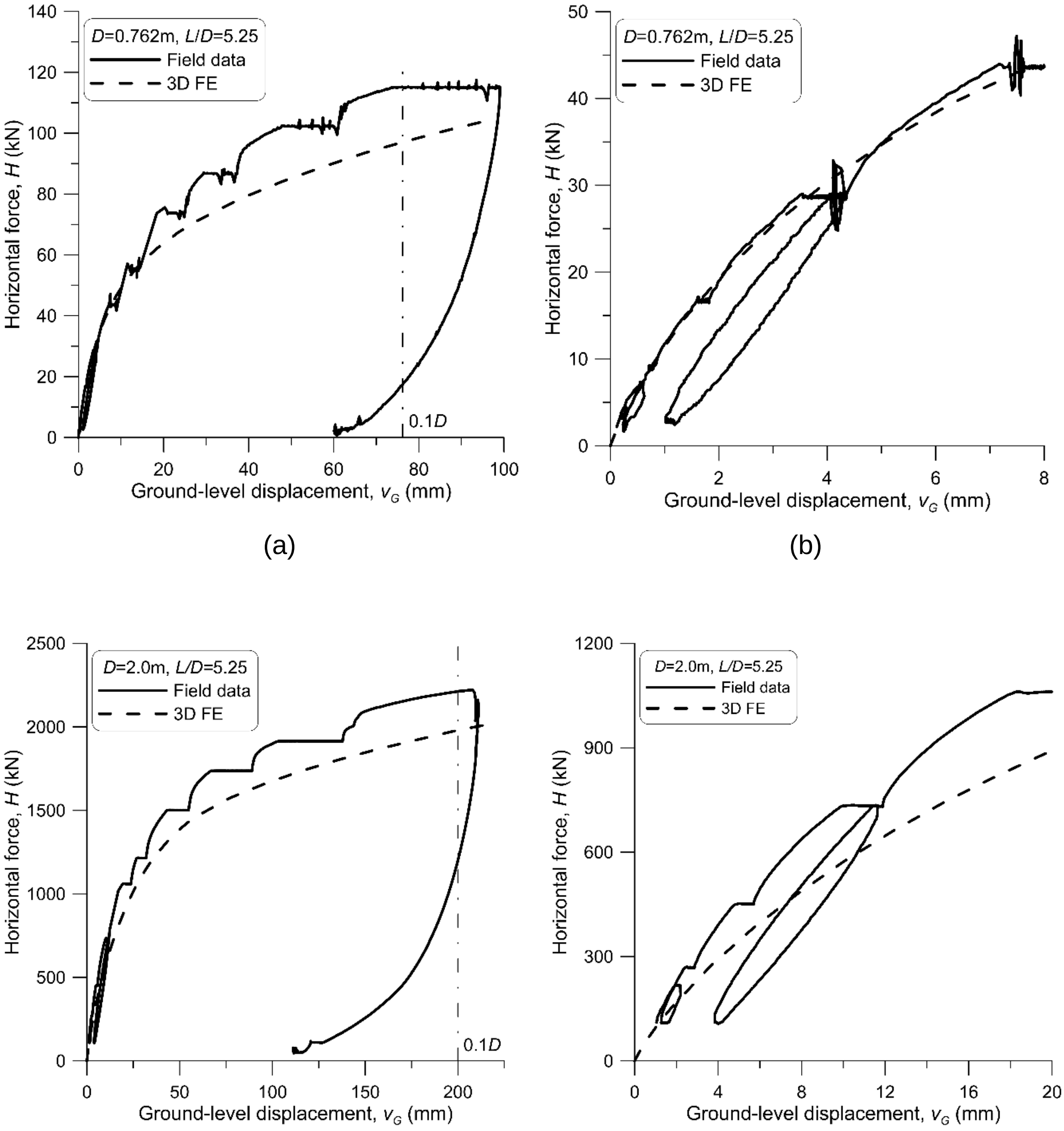


Figure 11: Predicted vs. measured response for Cowden test pile: medium diameter, $D = 0.762$ m, (a) up to nominal failure at $v_G = 0.1D$ and (b) at early loading, $v_G = 0.01D$; large diameter, $D = 2.0$ m, (c) up to nominal failure at $v_G = 0.1D$ and (d) at early loading, up to $v_G = 0.01D$

The implication of these two features of stiff plastic clays is that the modelling framework developed above for Cowden till would be unable to reproduce them and would therefore require further extensions of the MCC model. With respect to strength brittleness, Taborda et al. (2020) investigated its effect on an undrained response of laterally loaded monopiles in London clay using a strain-softening Mohr-Coulomb model (Potts & Zdravković, 1999), coupled with the same isotropic ICG3S nonlinear small strain model (Taborda et al., 2016) introduced in Section 2.3. The results, not repeated here for brevity, showed a marginal effect of strain-softening – visible only at intermediate ground-level displacements – on the monopile response compared to a non-softening analysis, principally due to the lack of a distinct shear surface developing in an undrained failure mechanism of the monopile. The effect of the anisotropic shear stiffness, however, is more significant and is discussed below.

*2.5.1 Effect of anisotropic shear stiffness*

As an example, Figure 12 presents normalised undrained effective stress paths (ESPs) in triaxial compression, where $p_0'$ is the mean effective stress at the start of shearing, applied to samples of London clay taken from a site at Hyde Park, as part of the Crossrail research project conducted at Imperial College (Wan et al., 2017; Avgerinos et al., 2017). Compared to the Cowden till ESPs in Figure 5, it is evident that London clay ESPs are markedly inclined (to the left) as a result of stiffness anisotropy, as well as that their ultimate stress states plot in the vicinity of the initial stress states in terms of $p'$ (i.e. the ESPs do not rise to critical state like the Cowden till's ESPs in Figure 5).

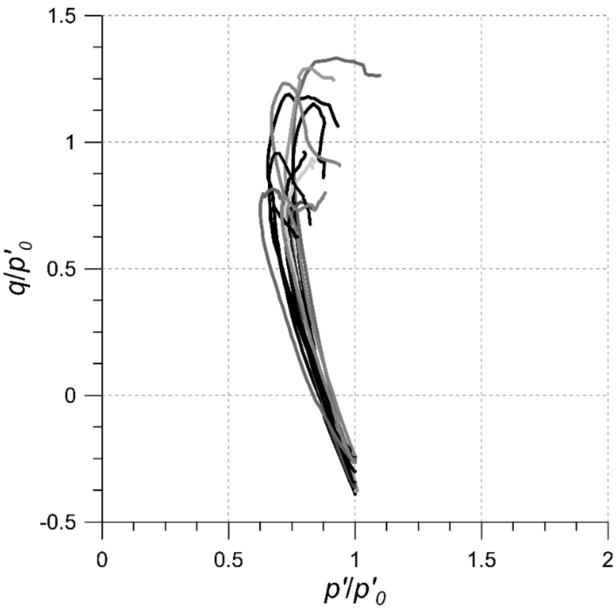


Figure 12: Normalised undrained effective stress paths of London clay

Dynamic measurements of the elastic shear stiffness of London clay, from field geophysics and from laboratory bender element (BE) and resonant column (RC) tests (Hight et al., 2003; Gasparre et al., 2007) are collated in Figure 13. The data is taken from various projects (T5 in the legend being Heathrow Terminal 5) and sites across the London basin. The vertical axis is marked as 'Depth below the top of London clay', as the London clay deposit had experienced up to 200 m of erosion in its geological history, followed by deposition of Thames gravel on top of the clay in the last geological age. The thickness of this top cover varies and at some sites the London clay formation appears at the ground surface (i.e. no top cover). The normalised shear moduli in Figure 13(a) reveal that the elastic vertical shear stiffness components could be interpreted as equal ($G_{vh,0} = G_{hv,0}$) and that $G_{vh,0}/p' \sim 370$. Data for the horizontal modulus are more scattered but could be approximated with a ratio $G_{hh,0}/p' \sim 740$, indicating $G_{hh,0}/G_{vh,0} \sim 2$. These ratios agree very well with the un-normalised data in Figures 13(b) and 13(c).

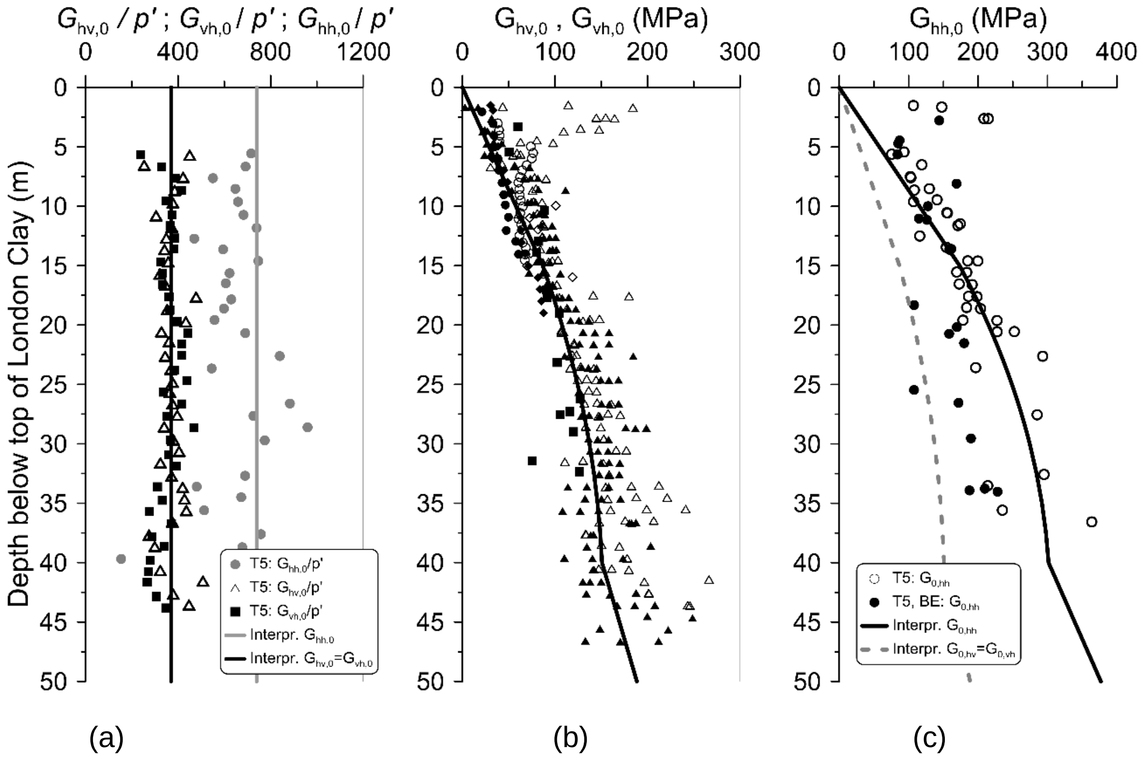


Figure 13: Elastic shear stiffness components of London clay

The degradation of the two shear stiffness components is more problematic, in particular that of $G_{hh}$, which is not readily measured in standard site investigations. Equally, the non-linear small strain ICG3S model (Taborda et al., 2016), used in the modelling framework of Cowden till, needs to be extended to account for stiffness anisotropy. A suitable extension has been outlined by Franzius et al. (2005), using a different small strain model and incorporating the three-parameter anisotropic model of Graham & Houlsby (1983). The three parameters are the vertical shear stiffness component, $G_{vh}$, the horizontal Poisson's ratio, $\mu_{hh}$, and the parameter of stiffness anisotropy, $\alpha$, which gives $G_{hh} = \alpha \cdot G_{vh}$. The vertical Young's modulus is then calculated as $E_v = 2G_{vh}(1 + \mu_{hh})/\alpha$, from which the horizontal Young's modulus becomes $E_h = \alpha^2 E_v$. With such an extension, Equation (5) of the ICG3S model represents the anisotropic shear stiffness component $G_{vh}$. Interpreting the triaxial data in terms of shear stiffness enables the model to be calibrated for the $G_{vh}$ component and its degradation with the deviatoric strain, $\varepsilon_d$, as shown in Figure 14, with $G_{vh,sec}/p' = 370$ at very small strains. The degradation of the $G_{hh}$ stiffness component is then 'scaled' with respect to $G_{vh}$, as shown in Figure 14, using the stiffness anisotropy parameter, $\alpha$. The magnitude of $\alpha = 2$ clearly applies to very small strains, as interpreted earlier, but it is uncertain whether it remains constant with stiffness degradation or reduces to 1 at larger strains (i.e. $G_{hh} = G_{vh}$). This is examined on a selection of London clay ESPs in Figure 15, from samples denoted as T5, T11 and T17, which were re-consolidated to their initial stress states before undrained shearing (note that $K_0 > 1$ for London clay results in the negative initial deviatoric stress, $q$, for these samples). Adopting a constant value of $\alpha = 2$ in the simulations of these tests demonstrates that the predicted ESPs (T-5 A, T-11 A, T-17 A) reproduce correctly the initial inclination of the measured ESPs, but this inclination remains practically constant with further straining, thus deviating from the measured paths. However, adopting a variable parameter $\alpha$ (reducing from 2 to 1, as outlined in Franzius et al., 2005) enables the non-linearity of the stress paths to be reproduced, leading to more realistic final stress states (T-5 Av, T-11 Av, T-17 Av). If isotropic non-linear shear stiffness was adopted, as for Cowden till, the predicted ESPs would simply rise vertically to ultimate stress states from their initial stresses, thus being unrepresentative of real London clay behaviour.

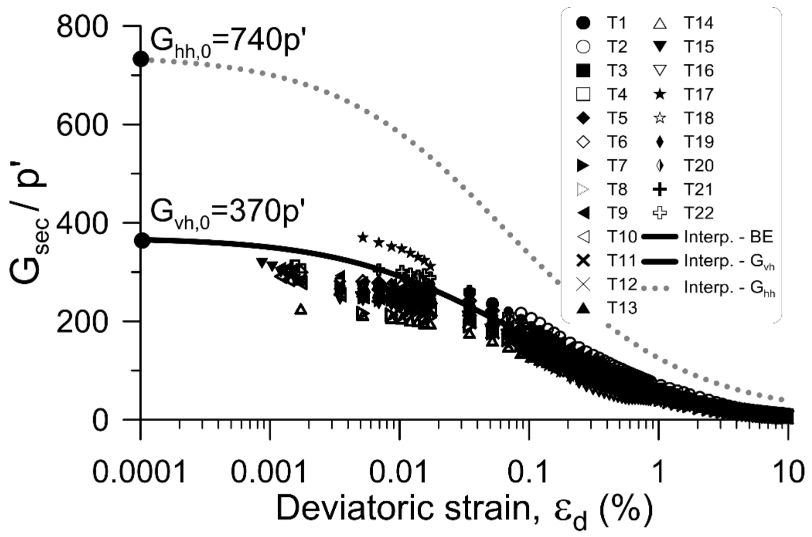


Figure 14: Anisotropic shear stiffness of London clay (data after Standing, 2018)

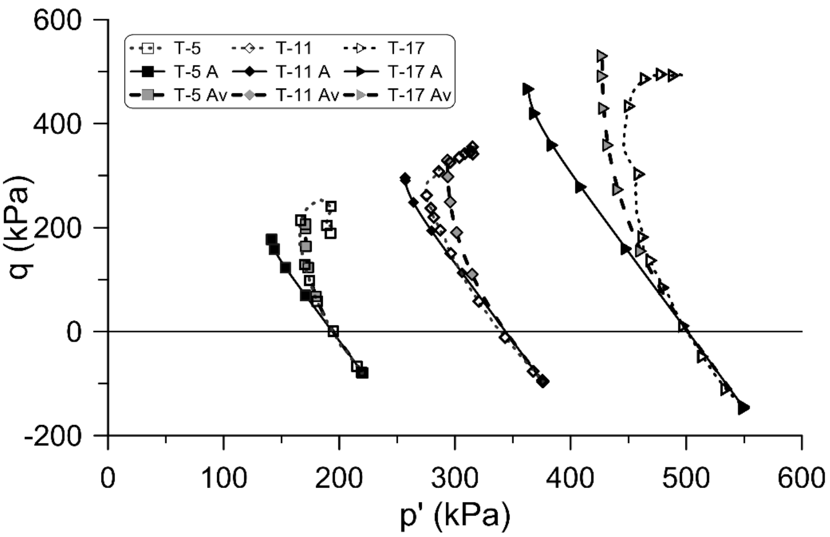


Figure 15: Representative undrained effective stress paths for London clay

*2.5.2 Modelling framework of stiff plastic clays for undrained lateral loading of monopiles*

As the brittle strength of stiff plastic clays was shown to have a negligible effect on the load-displacement response of wind-turbine monopiles under undrained lateral loading, it was possible to adopt the same modelling framework developed above for clay tills, but extended further with the inclusion of an anisotropic non-linear small strain stiffness overlay, as discussed in Section 2.5.1. The characterisation of the London clay behaviour and derivation of model parameters (see Taborda et al., 2020) followed similar steps applied to the Cowden till study, the principal difference being that the plastic potential associated with the Hvorslev surface on the dry side was chosen not to permit plastic volumetric straining when the stress states reached the Hvorslev surface. In effect, having reached the Hvorslev surface, the model becomes perfectly-plastic and suppresses any strain-softening characteristic of London clay, as well as any ductile hardening that would be otherwise predicted by the critical state framework (as was the case for Cowden till). The calibrated model parameters are summarised in Table 2.

Using this modelling framework three analyses were performed of a large-scale monopile in London clay, adopting $D = 10$ m, $L = 20$ m and $h = 50$ m (one of the geometries analysed in the PISA study). One analysis simulated the non-linear small strain shear stiffness anisotropy interpreted in Figure

14, adopting a variable parameter $\alpha$, while the remaining two analyses adopted isotropic small strain stiffness represented by either the $G_{vh}$ or the $G_{hh}$ degradation in Figure 14. The resulting load-displacement curves demonstrate significant implications of the anisotropic small strain stiffness in predicting the monopile response at operational loads (Figure 16a), but negligible effects at ultimate conditions (Figure 16b).

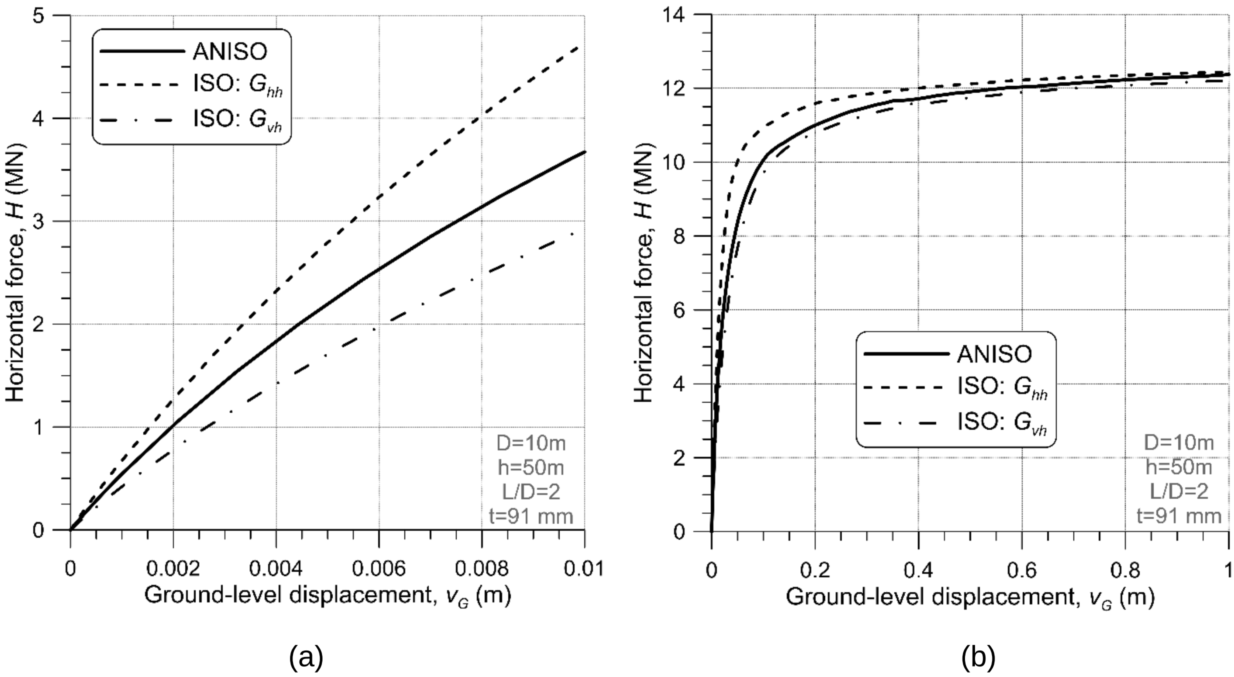


Figure 16: Effect of non-linear small strain stiffness anisotropy: $H - v_G$ at (a) operational and (b) ultimate loads

**3. Transient problems in stiff plastic clays**

3.1 Background

The offshore monopile foundations in stiff clays, discussed in the previous section, may be considered to predominantly operate under undrained conditions due to the low permeability of such soils. This is true at operational loads, where low-level vibrations result from the rotating mechanism, waves and wind, as well as at ultimate loads, where a storm can cause foundation failure. On the example of the Cowden study, the key design parameter for the former was demonstrated to be the small strain shear stiffness of the clay, while the latter depended on the accurate characterisation of the clay's shear strength. There are, however, other geotechnical problems, such as cut slopes in stiff plastic clays, where transient soil behaviour is critical for their stability and serviceability. The analysis of such problems has to be hydro-mechanically coupled, to account for transient changes in pore water pressure and effective stresses in the ground.

3.2 Stability of cut slopes

An excavation of a slope in a stiff plastic clay may be initially undrained, causing a depression of the initial phreatic surface (i.e. initial ground water table, GWT) and creating negative pore water pressures above it. If such a slope is initially stable, the numerical studies conducted in the 1990s, using ICFEP to analyse cuttings in London clay (Kovacevic, 1994; Potts et al., 1990, 1997), demonstrated that the slope may fail some time post-excavation, as a result of pore water pressure equilibration with time, in conjunction with the brittle nature of stiff plastic clays. Figure 17, after Potts et al. (1997), shows (a) vectors of ground movements and (b) contours of plastic shear strains, $\varepsilon_d^p$, in a slope at failure, predicted to happen 14.5 years after excavation. The London clay was modelled with a non-linear strain-softening Mohr-Coulomb model (mentioned in Section 2.5 above), and the inset in Figure 17 shows that the strength of the clay reduced from its peak value at $\varepsilon_d^p = 5\%$ to its residual value at $\varepsilon_d^p = 20\%$. Considering that the brittle behaviour of the clay was a dominant design concern for slope stability, it was deemed appropriate to employ a constitutive model capable of reproducing such a behaviour, even if this is a simpler model compared to the modified Cam Clay model employed in the Cowden study. The latter model would have needed further extension to account for strain softening post-peak. Moreover, the strain-softening Mohr-Coulomb model was enhanced with a small strain overlay model for accurate representation of the shear and bulk stiffness of London clay.

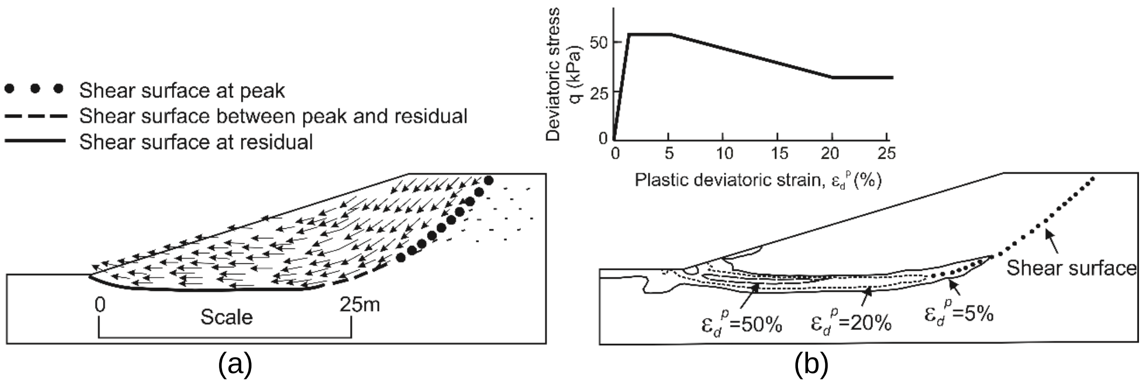


Figure 17: (a) Vectors of ground movement and (b) Contours of plastic shear strains at failure, mobilised in the slope 14.5 years after its excavation (after Potts et al., 1990)

The failure mechanism in Figure 17 clearly demonstrates the non-uniform mobilisation of the soil's strength along the shear surface, which has reached a residual value along some distance from the toe, and is below peak near the crest of the slope, in the last stable increment of the analysis that is represented in the figure. Those studies explained and quantified for the first time the importance of the brittle behaviour of stiff clays in the transient development of progressive failure in cut slopes. The stability was further shown to depend also on the slope's inclination and depth, initial stresses in the ground ($K_0$ in particular) and hydraulic boundary conditions applied along the excavated surface of the slope. It was established from the numerical study that cut infrastructure slopes in London clay would typically be stable in the long term if they were up to 10 m deep, with mostly 1:3 (vertical to horizontal) inclination and with 10 kPa suction along the slope surface (estimated as an average annual hydraulic boundary condition from measurements collated in Vaughan, 1994). These findings assisted the subsequent development of new infrastructure slopes in London clay, as well as the redesign of existing cuttings in conjunction with the widening of motorways.

A recent numerical study conducted by the authors, in conjunction with the intended development of a high speed rail line in the UK, applied the same modelling approach to add to the investigation the effect of the small strain stiffness on the stability and serviceability of cut slopes in London clay. As the slope excavation is likely to be undrained (with respect to the clay's permeability and rate of excavation), the magnitudes of ground movements in this phase are likely to depend on the mobilised shear stiffness in the soil. On the other hand, the long-term post-excavation movements, involving volumetric swelling, will mostly depend on the soil's bulk stiffness and permeability. While the measurement of the shear stiffness of soils has received significant attention in the past twenty years and is now readily available from both research and commercial experimental campaigns, the bulk stiffness is rarely measured and interpreted. Consequently, for modelling purposes, it is usually calculated from the prescribed shear stiffness and Poisson's ratio. The permeability is also a difficult parameter to establish, especially in stiff plastic clays that suffer from weathering and fissuring, which leads to vastly different magnitudes of permeability that may be measured in the field and in the laboratory.

Figure 18 shows an example finite element mesh used in this study for 2D plane strain slope analyses, in which the shaded area represents the excavation, the initial GWT is at 1.0 m below the ground surface and the long-term hydraulic boundary condition post-excavation is that of a pore fluid pressure $p_{fb} = -10$ kPa (i.e. 10 kPa of suction). This numerical study also made use of the nonlocal strain regularisation algorithm (Summersgill et al., 2017), as a means of removing mesh objectivity in the solution of boundary value problems which have a strain-softening material behaviour.

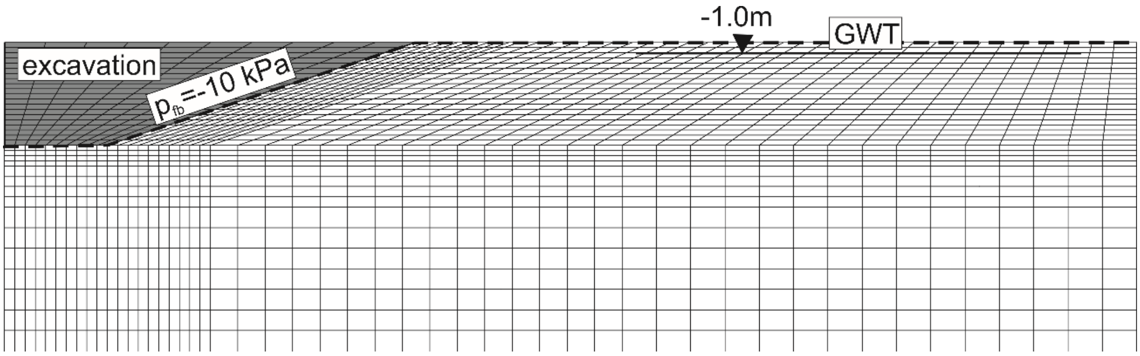


Figure 18: Part of a finite element mesh for cut slope analyses

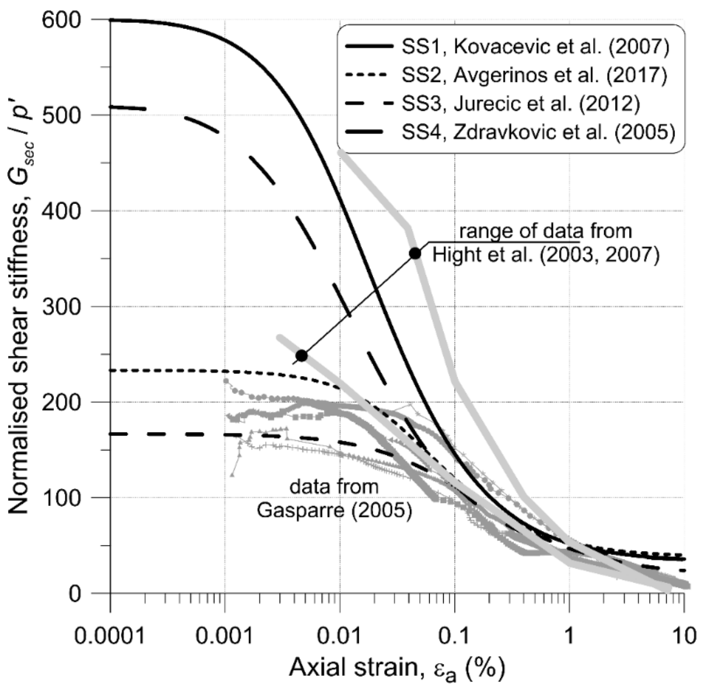


Figure 19: Small strain shear stiffness of London clay

Figure 19 summarises interpretations of the isotropic shear stiffness of London clay from several sites in London associated with recent engineering projects: Crossrail station box at Moorhouse (Zdravkovic et al., 2005); Heathrow Terminal 5 expansion (Kovacevic et al., 2007); Jubilee Line Extension (JLE) tunnelling at St James's Park (Jurecic et al., 2012) and Crossrail tunnelling at Hyde Park (Avgerinos et al., 2017). The experimental data was sourced from Hight et al. (2003, 2007) and

Gasparre (2005), while the ICG3S non-linear model (Taborda et al., 2016) described in Section 2.3 was fitted to the data. The associated small strain bulk stiffness for each of the shear stiffness curves was simulated with the same ICG3S model, with model parameters summarised in Table 3. These sets of small strain stiffness data are marked as SS1 to SS4 in Figure 19. The strength parameters of London clay, as input to the strain-softening Mohr-Coulomb model, were adopted from the analyses of temporary cut slopes at Heathrow Terminal 5 (Kovacevic et al., 2007) and comprised a peak angle of shearing resistance, $\phi'_{peak} = 25^{\text{o}}$, mobilised at a plastic shear strain $\varepsilon^{p}_{d,peak} = 2.0\%$, reducing linearly towards its residual value of $\phi'_{res} = 13^{\text{o}}$, reached at $\varepsilon^{p}_{d,res} = 15\%$. Considering that a high speed rail may require up to 20 m deep cuttings, which may also be excavated in geologically older (and therefore more brittle) plastic clays (e.g. Oxford clay), the study additionally examined the effects of the rate of softening from peak to residual and of depth of excavation on slope stability.

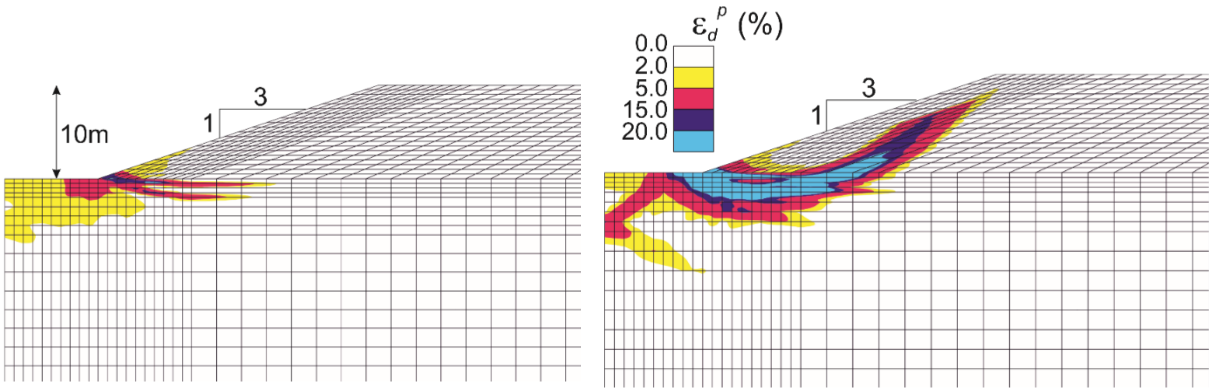


Figure 20: Contours of plastic shear strains in a stiff clay slope: (a) at 120 years post-excavation, London clay softening rate; (b) at 21 years post-excavation, Oxford clay softening rate

Figure 20(a) shows contours of plastic shear strains at 120 years post-excavation, predicted from the analysis of a 10 m deep slope at 1:3 inclination, which adopts the Kovacevic et al. (2007) strength and stiffness parameters (small strain data set SS1) of London clay as input for the non-linear strain-softening Mohr-Coulomb model. The shear surface developed from the toe until about 10 years after excavation, but then remained stable until the full 120 years of the assumed slope's design life, which is consistent with the findings of the 1990s numerical studies discussed above. The same analysis with a steeper, 1:2.5 slope, predicted failure 30 years after excavation. With respect to older clays, recent experimental research on stiff clays from the southern UK, reported in Hosseini Kamal et al. (2014), involved testing of Oxford clay which, in comparison to London clay, showed a significantly higher rate of softening from peak to residual (i.e. over a smaller strain range). Figure 20(b) presents contours of plastic shear strains from the analysis that adopted the same model input as the previous analysis, but halved the plastic shear strain at residual strength, approximating the softening rate of Oxford clay. The same slope was predicted to fail 21 years post-excavation. Contrary to the undrained lateral loading of monopiles in brittle plastic clays, which experienced marginal effects of strain-softening on monopile response, this aspect of the mechanical behaviour of plastic clays is crucial for the transient stability of slopes excavated in such clays.

The remaining analyses adopted the London clay rate of softening and focused on the slope depth and inclination, varying the small strain stiffness properties (SS1 to SS4) as introduced above. Figure 21 summarises the predicted stability of the analysed slopes, showing a clear position of the design line, which is in agreement with the 1990s numerical studies. The small strain stiffness properties were shown not to affect the stability of up to 10 m deep and up to 1:3 inclined slopes, which all developed some shear surface post-excavation, but it remained stable in the long term. While some transition between stable and unstable slopes is indicated in Figure 21 for gentler (1:4) 15 m deep slopes, the steeper and deeper slopes are predicted to fail mostly within 10 years post-excavation.

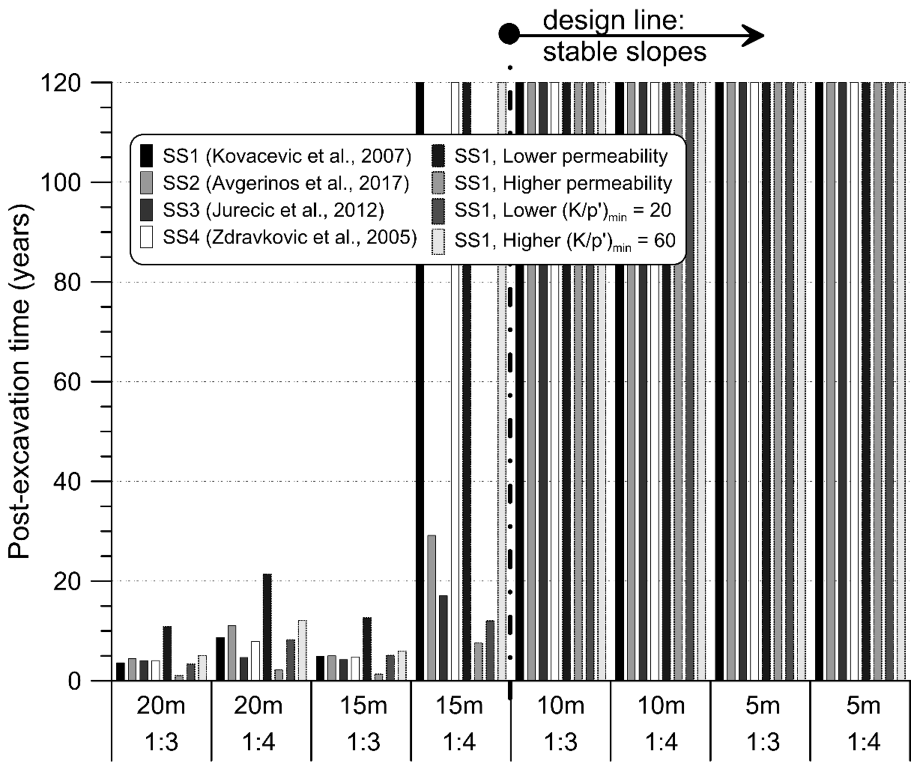


Figure 21: Summary of the predicted long-term stability of cut slopes in London clay

3.3 Serviceability of cut slopes

The additional concern for the high speed rail line has been the magnitude of the long-term base heave, due to the intended type of track to be placed, which was a less critical design constraint in past road and rail developments. As discussed above, the post-excavation transient behaviour of the soil, which involves significant heave, would be predominantly governed by its small strain bulk stiffness and permeability. In all of the above analyses of this cut slope study the permeability was modelled as dependent on the magnitude of mean effective stress, $p'$, in the ground:

$$k = k_0 \cdot \mathrm{e}^{b \cdot p'} \tag{7}$$

where $k_0$ is a reference permeability, $\mathrm{e}$ is Euler's number and $b$ is a model parameter. With respect to the field data summarised in Hight et al. (2003), these parameters were derived as $k_0 = 2 \times 10^{-9}$ m/s and $b = 0.007$, representing an average permeability profile (solid line) in Figure 22.

The effect of the bulk stiffness on the magnitude of base heave is examined first, adopting the geometry of a stable slope (as per Figure 21), that is 10 m deep and at 1:3 inclination. The adopted small strain behaviour is associated with the analysis of temporary cut slopes at Heathrow Terminal 5 (SS1 data in Table 3, Kovacevic et al., 2007), while the average permeability profile is adopted, as in Figure 22, associated with $k_0 = 2 \times 10^{-9}$ m/s. The experimental data for the bulk stiffness, shown in Figure 23, were obtained from the recompression paths of triaxial samples tested by Gasparre (2005). The data shows a sizable scatter and the non-linear part of the adopted bulk stiffness curve (up to around 0.1% volumetric strain) is perhaps an upper boundary to the measurements. Due to the nature of the problem, this non-linear part of the curve is likely to be mobilised by swelling reasonably early post-excavation, while the magnitude of the remaining long-term heave is likely to be controlled by the interpreted minimum (tail-end) value of $K/p'$, which is around 40 in Figure 23. To demonstrate the controlling influence of this tail-end value of $K/p'$ on the long-term heave, the same non-linear bulk stiffness of Kovacevic et al. (2007) was adopted up to around 0.1% volumetric strain, then extended with two additional tail-end minimum values of $K/p'$ of 20 and 60, both of which seem reasonable derivations from the data (see Figure 23).

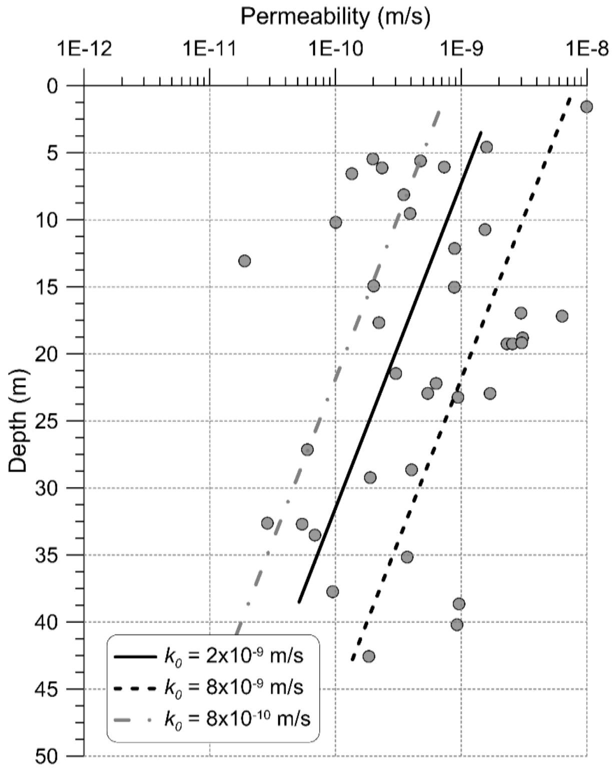


Figure 22: Derived permeability profiles of London clay (data after Hight et al., 2003)

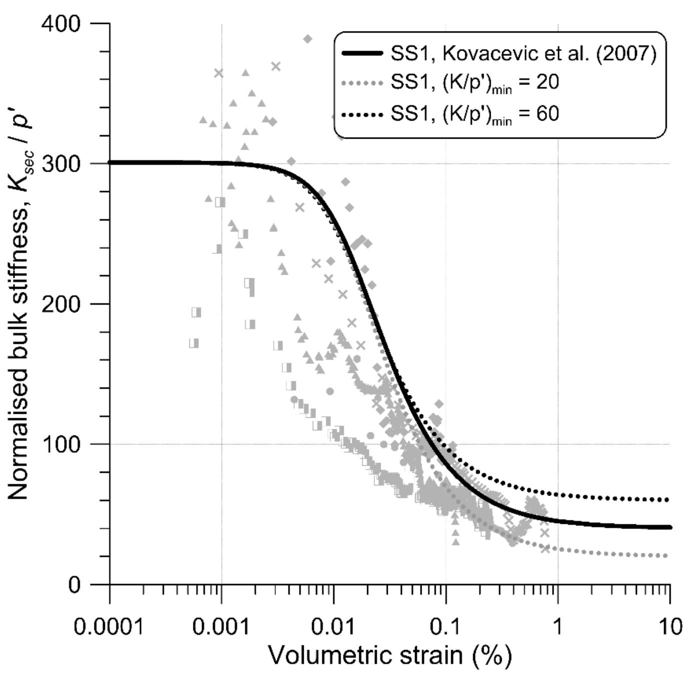


Figure 23: Bulk stiffness of London clay (data after Gasparre, 2005)

The results of the above three analyses are plotted in Figure 24, as an evolution of the post-excavation base heave (in the centre of the base, see inset) with time. Analyses accounted for 120 years post-excavation, considered to be the slope's design life. The results show similar magnitudes of heave developing within the first year, indicating this to have developed mostly from the mobilisation of the non-linear part of the bulk stiffness curve in Figure 23, which is the same in all three analyses. The magnitudes of heave clearly start to differ in the long-term, as does the time to mobilising full heave (marked in years on each curve), with higher values of $(K/p')_{min}$ reducing both quantities. The design envisages the rail track to be placed one year after excavation, with the intention of allowing most of the swelling to develop and hence reduce the magnitude of the remaining heave during the subsequent operation of the track. However, this is unlikely to be the case from the predictions in Figure 24, as the operational heave is still significant (52 to 138 mm) and clearly dependent on the interpretation of the bulk stiffness.

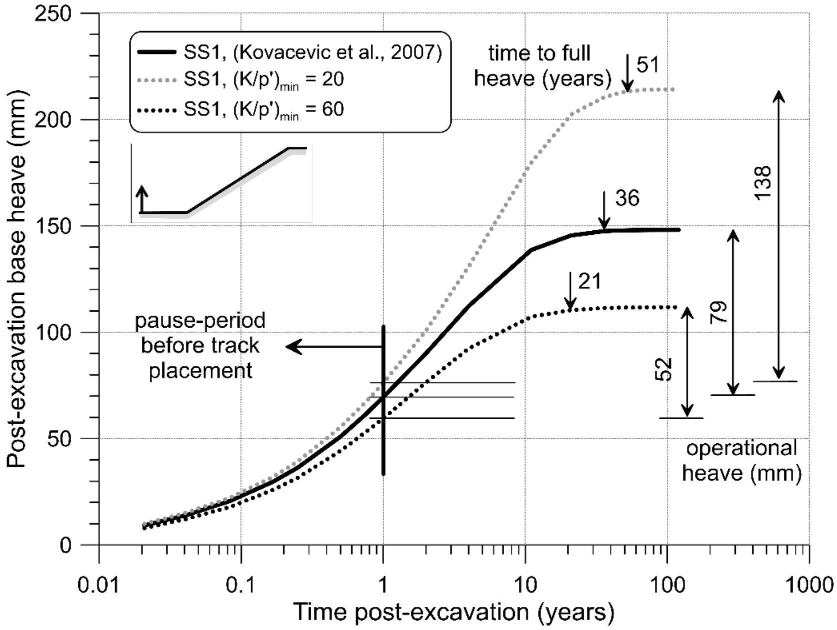


Figure 24: Effect of the minimum bulk stiffness on the predicted magnitude of transient heave

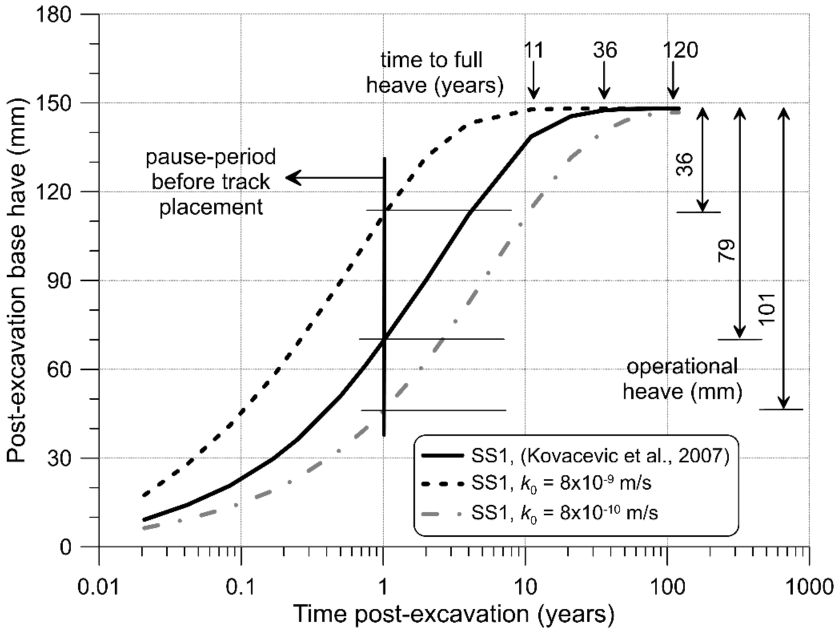


Figure 25: Effect of permeability on the predicted evolution of transient heave

The effect of permeability was investigated next, deriving two additional profiles from the same data in Figure 22, using Equation (7). One profile assumes higher permeability, with $k_0 = 8 \times 10^{-9}$ m/s and $b = 0.007$, while the other is approximately a lower boundary to permeability, with $k_0 = 8 \times 10^{-10}$ m/s and $b = 0.007$. The strength and small strain model parameters are again associated with the Heathrow Terminal 5 study of Kovacevic at al. (2007). The results in Figure 25, of the three analyses with different permeability profiles, show the evolution of the post-excavation base heave (also in the centre of the excavation base) with time. The curve resulting from the Kovacevic et al. (2007) model input is the same as in Figure 24. While the magnitude of the total heave is the same from all three analyses, being determined by the same adopted bulk stiffness, the evolution of heave differs significantly. The time to full heave is the shortest (11 years) with a profile of higher permeability in the ground, as would be expected, while with a lower permeability profile heave develops practically over the whole design life of the slope (120 years). Applying the same assumption of track placement one year after the slope excavation, the operational heave is still large (36 to 100 mm) and clearly dependent on the soil permeability.

3.4. Discussion

Four additional analysis with derived variations of permeability and small strain bulk stiffness, as discussed in Section 3.3, were conducted for each of the slope geometries summarised in Figure 21. As expected, these aspects of soil behaviour did not alter design recommendations in terms of slope stability, with long-term stability confirmed for up to 10 m deep and up to 1:3 inclined slopes. Some transition is again observed for 15 m deep and 1:4 inclined slopes, while failure is predicted predominantly within 10 years post-excavation for the remaining deeper and steeper slopes.

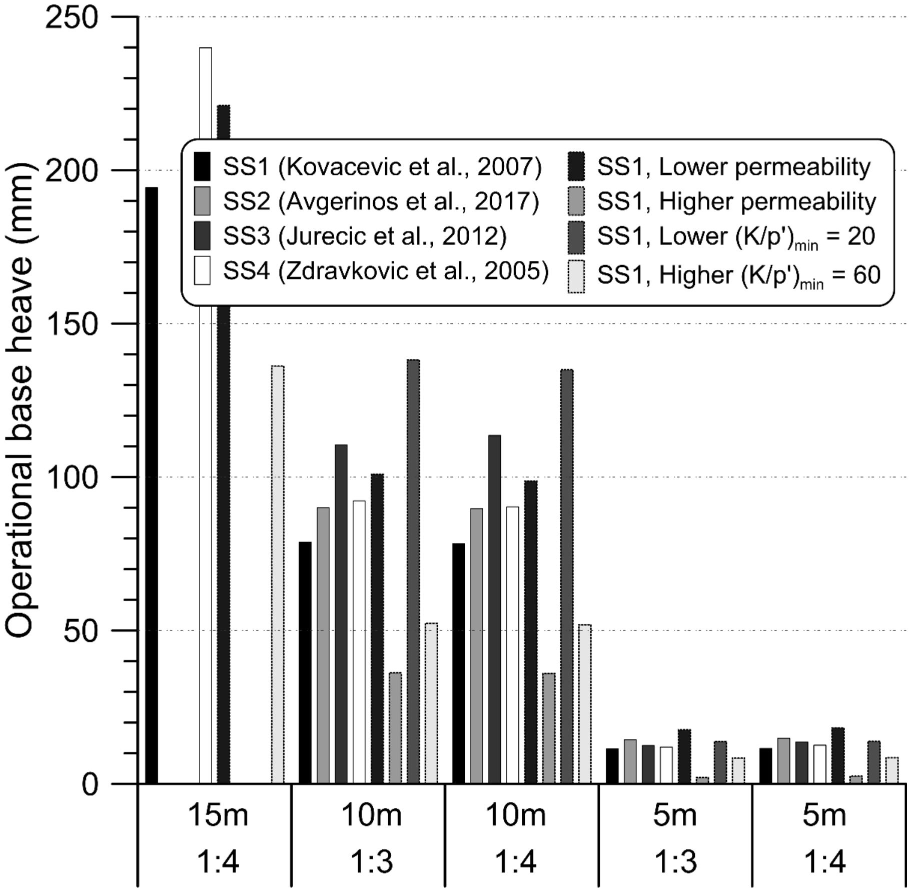


Figure 26: Summary of the predicted long-term operational base heave of cut slopes in London clay

In a similar manner, Figure 26 summarises magnitudes of operational heave (i.e. from one year post-excavation) from all analyses in which slopes remained stable in the long-term. Initial design requirements for the high speed rail indicated about 15 to 20 mm maximum operational base heave to be acceptable over the slope's design life. As shown in Figure 26, unless the depth of the slope is small, this requirement is unlikely to be satisfied by the majority of slope geometries. The implication of the serviceability study is that, unless ground investigation enables more accurate interpretation of the soil's permeability and small strain bulk stiffness that may predict smaller base heave, the envisaged cuttings for the high speed rail line would need to implement significant mitigation measures to reduce the base heave to design requirements.

## 4. Conclusions

Using a number of practical examples, this lecture outlines the process involved in the interpretation of soil behaviour and site conditions in conjunction with the selection of appropriate material modelling and application in advanced numerical analyses that may be conducted as part of the design of geotechnical structures.
It is emphasised that establishing a realistic ground model is challenging and requires careful integration of both field and laboratory data obtained from experimental campaigns. Checking new experimental evidence against historic data, where possible, is equally vital and necessary to fill any gaps in the understanding of soil behaviour.

It is further emphasised that the selection of a constitutive model with which to simulate the soil is a function of the available data and of the nature of the geotechnical problem. It is also important to ensure that any simplifications adopted in a constitutive model retain consistency between the overall model performance and the experimental data.

All these processes require significant engineering judgement when deriving the numerical input, which in turn relies on an equal understanding of the numerical tools and of the real soil behaviour.

The lecture also demonstrates the use of numerical analysis to identify the governing parameters of soil behaviour and their effect in a given geotechnical problem, and to therefore guide the necessary site investigation.

Table 1: Model parameters for Cowden Till: extended MCC model

| Component | Parameters |
|---|---|
| Strength | $\varphi_{TX,C} = 27°, \varphi_{TX,E} = 32°$ |
| (Van Eekelen, 1980), Eq. (3) | $X = 0.548, Y = 0.698, Z = 0.100$ |
| Nonlinear Hvorslev surface – shape (Tsiampousi et al., 2013), Eq. (1) | $\alpha = 0.25, n = 0.40$ |
| Nonlinear Hvorslev surface – plastic potential (Tsiampousi et al., 2013), Eq. (2) | $\beta = 0.20, m = 1.00$ |
| Virgin consolidation line | $\nu_1 = 2.20, \lambda = 0.115$ |
| Nonlinear elasticity – swelling behaviour | $\kappa = 0.021$ |
| Nonlinear elasticity – small-strain shear modulus (Taborda et al., 2016), Eq. (4) | $G_0^* = 110\ MPa, p'_{ref} = 100.0\ kPa$ |
| Nonlinear elasticity – shear stiffness degradation (Taborda et al., 2016), Eq. (4) | $a = 9.78 \times 10^{-5}$, $b = 0.987$, $R_{G,min} = 0.05$ |

Table 2: Model parameters for London clay: extended MCC model

| Component | Parameters |
|---|---|
| Strength | $\varphi_{TX,C} = 24°, \varphi_{TX,E} = 20°$ |
| (Van Eekelen, 1980), Eq. (3) | $X = 0.406, Y = 0.659, Z = 0.270$ |
| Nonlinear Hvorslev surface – shape (Tsiampousi et al., 2013), Eq. (1) | $\alpha = 0.35, n = 0.40$ |
| Nonlinear Hvorslev surface – plastic potential (Tsiampousi et al., 2013), Eq. (2) | $\beta = 0.0, m = 0.0$ |
| Virgin consolidation line | $\nu_1 = 2.433, \lambda = 0.111$ |
| Nonlinear elasticity – swelling behaviour | $\kappa = 0.066$ |
| Nonlinear elasticity – small-strain shear modulus (Taborda et al., 2016), Eq. (4) | $G^*_{\mathrm{hv0}} = 37\ MPa,\ G^*_{\mathrm{hh0}} = 74\ MPa,$ $p'_{ref} = 100.0\ kPa$ |
| Nonlinear elasticity – shear stiffness degradation (Taborda et al., 2016), Eq. (4) | $a = 2.8 \times 10^{-4}$, $b = 0.7$, $R_{G,min} = 0.01$ |
| Stiffness anisotropy | $\alpha_{max} = G^*_{\mathrm{hh0}}/G^*_{\mathrm{hv0}} = 2.0,\quad E_{d,min} = 0.08$ $\alpha_{min} = 1,\quad E_{d,max} = 2.0$ |

Table 3: Isotropic small strain stiffness parameters for London clay: ICG3S model

| Components | Kovacevic et al. (2007) – SS1 | Avgerinos et al. (2017) – SS2 | Jurecic et al. (2012) – SS3 | Zdravkovic et al. (2005) – SS4 |
|---|---|---|---|---|
| $G_0$ | 60376.2 | 23321.1 | 16670.1 | 51743.5 |
| $K_0$ | 30079.5 | 30011.2 | 21400.7 | 26692.7 |
| $G_{min}\ (kPa)$ | 3333.3 | 2000 | 2667 | 2667 |
| $K_{min}\ (kPa)$ | 4000 | 2500 | 5000 | 5000 |
| $m_G\ \&\ m_K$ | 1.0 | 1.0 | 1.0 | 1.0 |
| $a_0$ | 8.25E-05 | 2.96E-04 | 7.20E-04 | 5.60E-05 |
| $b_0$ | 1.09 | 1.26 | 1.03 | 0.99 |
| $R_{G,min}$ | 5.53E-02 | 1.63E-01 | 1.13E-01 | 6.45E-02 |
| $R_{K,min}$ | 1.34E-01 | 1.23E-01 | 1.35E-01 | 1.33E-01 |
| $r_0$ | 1.23E-04 | 6.06E-05 | 1.23E-04 | 1.23E-04 |
| $s_0$ | 2.05 | 1.04 | 2.05 | 2.04 |
| $p'_{ref}\ (kPa)$ | 100 | 100 | 100 | 100 |

## REFERENCES


Aghakouchak, A. (2015) *Advanced laboratory studies to explore the axial cyclic behaviour of driven piles*. PhD thesis, Imperial College London, London.

API (2010). *RP 2A-WSD - Recommended Practice for Planning, Designing and Constructing Fixed Offshore Platforms*. Washington: Amaerican Petroleum Institute.

Avgerinos, V., Potts, D.M. and Standing, J.R. (2017). Numerical investigation of the effects of tunnelling on existing tunnels. *Géotechnique* 67 (9): 808-822.

Baldi, G., Bellotti, R., Ghionna, V., Jamiolkowski, M., Marchetti, S. & Pasquelini, E. (1986). Flat dilatometer tests in calibration chambers. *Geotechnical Special Publication, ASCE*, 6: 431–446.

Been, K. & Jefferies, M.G. (1985). A state parameter for sands. *Géotechnique*, 35(2), pp.99–112.

Brosse, A., Kamal, R.H., Jardine, R.J. & Coop, M.R. (2017) The shear stiffness characteristics of four Eocene-to-Jurassic UK stiff clays. *Géotechnique*, 67 (3): 242–259.

Burd, H.J., Beuckelaers, W.J.A.P., Byrne, B.W., Gavin, K., Houlsby, G.T., Igoe, D., Jardine, R.J., Martin, C.M., McAdam, R.A., Muir Wood, A., Potts, D.M., Skov Gretlund, J., Taborda, D.M.G. and Zdravković, L. (2019a). New data analysis methods for instrumented medium scale monopile field tests. *Géotechnique*, doi.org/10.1680/jgeot.18.pisa.002

Burd, H.J., Taborda, D.M.G. Zdravković, L. Abadie, C.N., Byrne, B.W., Houlsby, G.T., Gavin, K.G, Igoe, D., Jardine, R.J., Martin, C.M., McAdam, R.A., Pedro, A.M.G. and Potts, D.M. (2019b). PISA design model for monopiles for offshore wind turbines: application to a marine sand *Géotechnique*, doi.org/10.1680/jgeot.18.p.277

Byrne, B.W., McAdam, R.A., Burd, H.J., Beuckelaers, W.J.A.P., Gavin, K., Houlsby, G.T., Igoe, D., Jardine, R.J., Martin, C.M., Muir Wood, A., Potts, D.M., Skov Gretlund, J., Taborda, D.M.G. and Zdravković, L. (2019a). Monotonic laterally loaded pile testing in a stiff glacial clay till at Cowden. *Géotechnique*, doi.org/10.1680/jgeot.18.pisa.003

Byrne, B.W., Houlsby, G.T., Burd, H.J., Gavin, K.G, Igoe, D., Jardine, R.J., Martin, C.M., McAdam, R.A., Potts, D.M., Taborda, D.M.G. and Zdravković, L. (2019b). PISA design model for monopiles for offshore wind turbines: application to a stiff glacial clay till. *Géotechnique*, doi.org/10.1680/jgeot.18.p.255

Chow, F. (1997). *Investigations into the behaviour of displacement piles for offshore foundations*. PhD thesis; Imperial College of Science, Technology and Medicine, University of London, London.

Day, R.A. and Potts, D.M. (1994). Zero thickness interface elements - numerical stability and application. *Int. Jnl. Num. Analy. Meth. Geomech.* **18**: 689-708.

DNV-GL (2016). *DNVGL-ST-0126 – Support structure for wind turbines.* Oslo: Det Norske Veritas.

Franzius, J.N., Potts, D.M. & Burland, J.B. (2005). The influence of soil anisotropy and $K0$ on ground surface movements resulting from tunnel excavation. *Géotechnique*, 55 (3): 189-199.

Gasparre, A. (2005). *Advanced laboratory characterisation of London clay*. PhD thesis. Imperial College of London, London.

Gasparre, A., Nishimura, S., Minh, N. A., Coop, M.R. & Jardine, R.J. (2007). The stiffness of natural London clay. *Géotechnique*, 57 (1): 33–47.

Graham, J. & Houlsby, G. (1983). Anisotropic elasticity of a natural clay. Géotechnique, 33 (2): 165-180.

Hardin, B.O. (1978) The nature of stress-strain behaviour for soils. In *Proceedings of the ASCE Geotechnical Engineering Division Specialty Center*. pp. 3–90.

Hight, D., Gasparre, A., Nishimura, S., Minh, N. A., Jardine, R. J. & Coop, M. R. (2007). Characteristics of the London Clay from the Terminal 5 site at Heathrow Airport. *Géotechnique*, 57 (1): 3-18.

Hight, D. W., McMillan, F., Powell, J. J. M., Jardine, R. J. & Allenou, C. P. (2003). Some characteristics of London Clay. In *Proceedings of the Conf. Characterisation and Engineering*, National University Singapore. Balkema, Vol. 2: 851-907.

Hosseini Kamal, R., Coop, M.R., Jardine, R.J. and Brosse, A. (2014). The post-yield behaviour of four Eocene-to-Jurassic UK stiff clays. *Géotechnique* 64 (8): 620-634.

Jurečič, N., Zdravković, L. & Jovičić, V. (2012). Predicting ground movements in London Clay. Proc. ICE – Geotechnical Engineering 166 (5): 466-482.

Kovacevic, N. (1994). *Numerical analysis of rockfill dams, cut slopes and road embankments*. PhD thesis, Imperial College, University of London.

Kovacevic, N., Hight, D.W. & Potts, D.M. (2007). Predicting the stand-up time of temporary London Clay slopes at Terminal 5, Heathrow Airport. *Géotechnique* 47 (5): 953-982.

Kulhawy, F.H. & Mayne, P.W. (1990). *Manual on estimating soil properties for foundation design*, Electric Power Research Inst., Palo Alto, CA (USA); Cornell Univ., Ithaca, NY (USA). Geotechnical Engineering Group.

Kuwano, R. (1999). *The Stiffness and Yielding Anisotropy of Sand*. PhD thesis; Imperial College of Science, Technology and Medicine, University of London, London.

Lade, P.V. & Duncan, J.M. (1975). Elasto-plastic stress-strain theory for cohesionless soil. *ASCE Jnl. Geotech. Eng. Div*. 101 (10): 1037-1053.

Lambe, T.W. (1973). Predictions in soil engineering. *Geotechnique*, 23 (2): 149–202.

Li, X. S. & Wang, Y. (1998) Linear representation of steady-state line for sand. *Journal of Geotechnical and Geoenvironmental Engineering*, 124 (12): 1215-1217.

Liu, T.F. (2018). *Advanced laboratory testing for offshore pile foundations under monotonic and cyclic loading*. PhD thesis, Imperial College London, London.

Lunne, T. & Christofferson, H.P. (1983). Cone penetrometer interpretation for offshore sands. In *Proceedings of the Offshore Technology Conference,* Houston, OTC4464: 181–192.

Manzari, M.T. & Dafalias, Y.F. (1997). A critical state two-surface plasticity model for sands. *Géotechnique*, 47 (2): 255–272.

Masing, G. (1926) Eigenspannungen Und Verfestigung Beim Messing. *Proceedings of the 2nd International Conference of Applied Mechanics*, Zurich, Switzerland. pp. 332-335.

Matsuoka, H. & Nakai, T. (1974). Stress-deformation and strength characteristics of soil under three different principal stresses. *Proc. Japanese Soc. Civ. Eng*., Vol. 232: 59-70.

McAdam, R.A., Byrne, B.W., Houlsby, G.T., Beuckelaers, W.J.A.P., Burd, H.J., Gavin, K., Igoe, D., Jardine, R.J., Martin, C.M., Muir Wood, A., Potts, D.M., Skov Gretlund, J., Taborda, D.M.G. and Zdravković, L. (2019). Monotonic laterally loaded pile testing in a dense marine sand at Dunkirk. *Géotechnique*, doi.org/10.1680/jgeot.18.pisa.004

Pedro, A. M. G., Zdravković, L., Potts, D. M. and Almeida e Sousa, J. (2017). Derivation of model parameters for numerical analysis of the Ivens shaft excavation. *Engineering Geology,* 217: 49-60

Potts, D.M., Dounias, G.T., & Vaughan, P.R. 1990. Finite element analysis of progressive failure of Carsington embankment. *Géotechnique* 40 (1): 79-101.

Potts, D.M., Kovacevic, N., & Vaughan, P.R. 1997. Delayed collapse of cut slopes in stiff clay. *Géotechnique* 47 (5): 953-982.

Potts, D.M. and Zdravkovic, L. (1999). *Finite element analysis in geotechnical engineering: theory.* London, Thomas Telford.

Potts, D.M. and Zdravkovic, L. (2001). *Finite element analysis in geotechnical engineering: application.* London, Thomas Telford.

Powell, J.J.M. & Butcher, A.P. (2003). Characterisation of a glacial till at Cowden, Humberside. In T. S. Tan et al., eds. *Characterisation and Engineering Properties of Natural Soils*. Lisse: Swets & Zeitlinger, pp. 983–1020.

Powell, J.J.M. & Quarterman, R.S.T. (1988). The interpretation of cone penetration tests in clays, with particular reference to rate effects. *Penetration Testing 1988*, 2, pp.903–909.

Powell, J.J.M., Marsland, A. and Alkhafagi, A.N. (1983). Pressuremeter testing of glacial clay till. *Proc. Symp. on In Situ Testing*, vol. 2: 373-378.

Ramberg, W. & Osgood, W. R. (1943) *Description of Stress-Strain Curves by Three Parameters*. National Advisory Committee for Aeronautics. Technical Note No. 902.

Reese, L.C., Cox, W.R. & Koop, F.D. (1974). Analysis of laterally loaded piles in sand. *Offshore Technology Conference*, Dallas, Texas. OTC 2080.

Reese, L.C., Cox, W.R. & Koop, F.D. (1975). Field testing and analysis of laterally load piles in stiff clay. *Offshore Technology Conference*, Dallas, Texas. OTC 2312.

Roscoe, K.H. & Burland, J.B. (1968). On the generalized stress-strain behavior of wet clay. In J. Heyman & F. A. Leckie, eds. *Engineering Plasticity.* Cambridge University Press, pp. 535–609.

Schroeder, F.C., Day, R.A., Potts, D.M. & Addenbrooke, T. I. (2007). An 8-node isoparametric shear deformable shell element. *Int. Jnl of Geomechanics* **7** (1): 44-52.

Summersgill, F.C., Kontoe S. & Potts, D.M. (2017). On the use of nonlocal regularisation in slope stability problems. *Computers and Geotechnics* 82: 187-200.

Taborda, D.M.G. & Zdravkovic, L. (2012). Application of a Hill-Climbing technique to the formulation of a new cyclic nonlinear elastic constitutive model. *Computers and Geotechnics*, 43: 80–91.

Taborda, D.M.G., Potts, D.M. & Zdravkovic, L. (2016). On the assessment of energy dissipated through hysteresis in finite element analysis. *Computers and Geotechnics*, 71: 180–194.

Taborda, D. M. G., Zdravković, L., Kontoe, S. & Potts, D. M. (2014) Computational Study on the Modification of a Bounding Surface Plasticity Model for Sands. *Computers and Geotechnics*, 59: 145-160.

Taborda, D.M.G., Pedro, A.M.G., Zdravković, L, Potts D.M., Jardine R.J., Abadie, C,N., Burd, H.J., Byrne, B.W., Houlsby, G.T., Martin, C.M., McAdam, R.A. and Pacheco Andrade, M. (2020). A unified modelling framework for wind turbine monopiles in stiff and soft clays. *Géotechnique* (under review).

Taborda, D.M.G., Zdravković, L., Potts. D.M., Burd, H.J., Byrne, B.W., Gavin, K.G, Houlsby, G.T., Jardine, R.J., Liu, T., Martin, C.M. and McAdam, R.A. (2019). Finite element modelling of laterally loaded piles in a dense marine sand at Dunkirk. *Géotechnique*, doi.org/10.1680/jgeot.18.pisa.006.

Tatsuoka, F. & Shibuya, S. (1991) Deformation characteristics of soils and rocks from field and laboratory tests. *Proceedings of the 9th Asian Regional Conference on Soil Mechanics and Foundation Engineering,* Bangkok, 2: 101-170.

Tedd, P., Powell, J.J.M., Charles, J.A. and Uglow, I.M. (1989). In situ measurement of earth pressures using push-in spade-shaped pressure cells: ten years experience. *Proc. Conf. on Instrumentation In Geotech. Eng.*, Nottingham, pp: 701-715.

Tsiampousi, A., Zdravković, L. & Potts, D.M. (2013). A new Hvorslev surface for critical state type unsaturated and saturated constitutive models. *Computers and Geotechnics*, 48: 156–166.

Ushev, E. (2018). *Laboratory investigation of the mechanical properties of Cowden till under static and cyclic conditions*. PhD thesis, Imperial College London, London.

Van Eekelen, H. A. M. (1980). Isotropic yield surfaces in three dimensions for use in soil mechanics. *Int. J. Numer. Analyt.Methods Geomech*. 4, (1): 89–101.

Vaughan, P.R., 1994. Assumption, prediction and reality in geotechnical engineering. *Géotechnique*, 44 (4): 573-609.

Wan, M.S.P., Standing, J.R., Potts, D.M. & Burland, J.B. (2017). Measured short-term subsurface ground displacements from EPBM tunnelling in London Clay. *Géotechnique*, 67 (9): 748-779.

Zdravkovic, L., Potts, D.M. & St John, H.D. (2005). Modelling of a 3D excavation in finite element analysis. *Géotechnique*, 55 (7): 497-513.

Zdravković, L., Jardine, R.J., Taborda D.M.G., Abadias, D., Burd, H.J., Byrne, B.W., Gavin, K., Houlsby, G.T., Igoe, D., Liu, T, Martin, C.M., McAdam, R.A., Muir Wood, A., Potts, D.M., Skov Gretlund, J. and Ushev, E. (2019a). Ground characterisation for PISA pile testing and analysis. *Géotechnique*, doi.org/10.1680/jgeot.18.pisa.001

Zdravković, L., Taborda, D.M.G., Potts, D.M., Abadias, D., Burd, H.J., Byrne, B.W., Gavin, K., Houlsby, G.T., Jardine, R.J., Martin, C.M., McAdam, R.A. and Ushev, E. (2019b). Finite element modelling of laterally loaded piles in a stiff glacial clay till at Cowden. *Géotechnique*, doi.org/10.1680/jgeot.18.pisa.005

# *Response of Soil Sites During Earthquakes, A 60-Year Perspective*

The 2019 Terzaghi Lecture

By Dr. Ed Idriss

***THE 55TH TERZAGHI LECTURE***

# *RESPONSE OF SOIL SITES DURING EARTHQUAKES A 60-YEAR PERSPECTIVE*

*by*

*Izzat M. Idriss, Professor Emeritus, Univ. of California at Davis*
*Consulting Geotechnical Engineer, Santa Fe, NM*
*e-mail: imidriss@aol.com*

*First Presented at the 2019 GEO-CONGRESS in Philadelphia, PA, on March 26, 2019*

*Presented again at Texas A & M*
*November 6, 2020*

1

## *KARL VON TERZAGHI (1883 –1963)*

*Father of Soil Mechanics*

2

## *TOPICS FOR TODAY*

1. *Why site response*
2. *Recorded earthquake ground motion data*
3. *Comparison with empirical earthquake ground motion models (GMMs) & need for analytical approaches*
4. *Historical perspective*
5. *Currently available analytical procedures*
6. *Concluding Remarks/Recommendations*

3

## *TOPIC 1*

## *WHY SITE RESPONSE*

4

*The New East Span of the San Francisco Oakland Bay Bridge*

5


*Nuclear Plant in California*

6

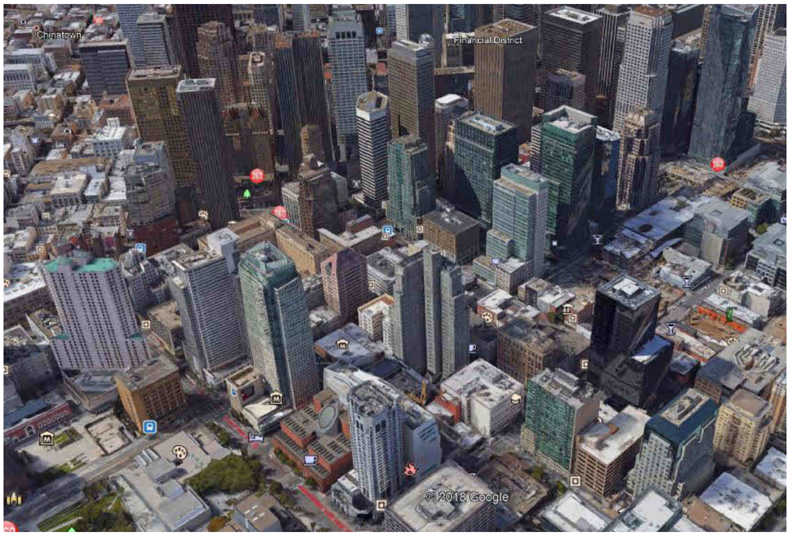


***Portion of Downtown San Francisco***

7

***C***

***half-space***

***Idealized outcrop***

***"C" corresponds to earthquake ground motion recorded on a rock outcrop***

8

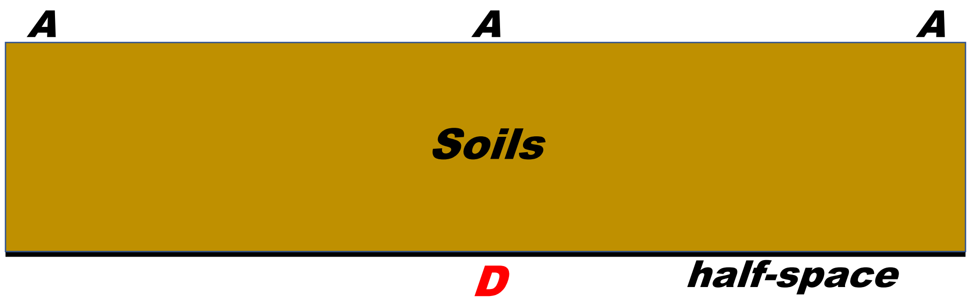


*Idealized soil profile to represent free field conditions*

*"D" corresponds to the earthquake ground motion needed as the "within" rock motion to use in a dynamic response analysis*

9

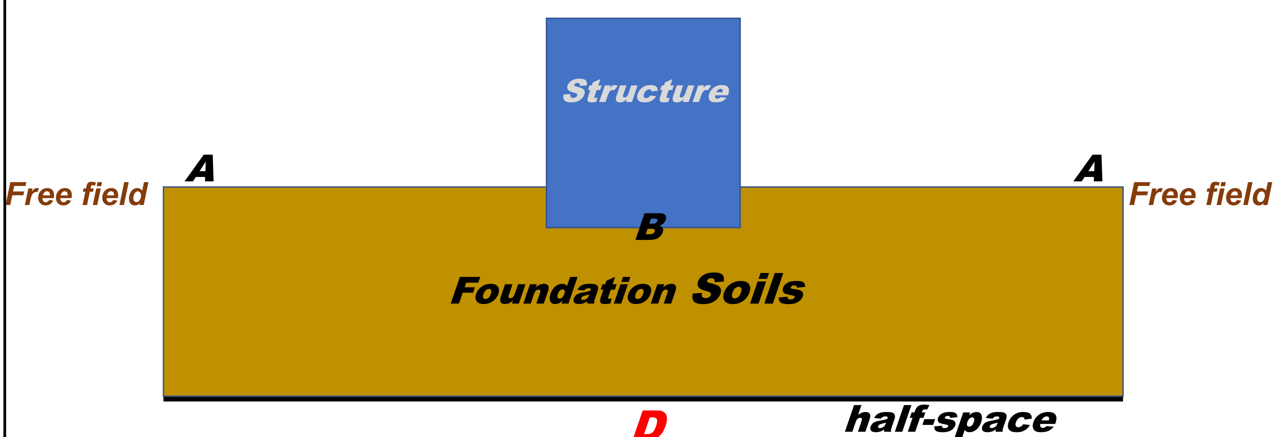


*Idealized soil-foundation-structure (SFS) system*

10

***Embankment Dam***

11

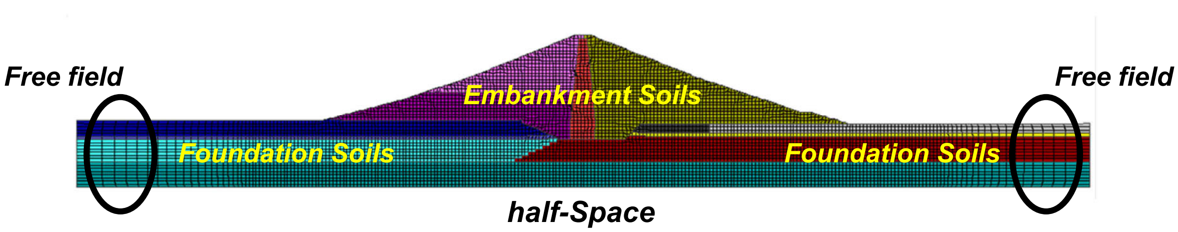


*Finite difference mesh courtesy of Dr. Michael Beaty*

12

### ***Why Site Response***

***A ground response analysis provides a means to check the results in the free field of dynamic analyses that incorporate SSI or SFSI … etc.***

***Therefore, it is important to have in our "Computation–Tool Bucket" procedures and computer programs that we can rely on to provide us with reasonably reliable estimates that correlate well with measured values and are physically meaningful.***

13

## ***TOPIC 2***

## ***RECORDED EARTHQUAKE GROUND MOTION DATA***

14

## *Recorded Earthquake Ground Motion Data*

*The New Generation Attenuation (NGA) Project was initiated in 2004 and resulted in accumulating, checking, organizing and disseminating tens of thousands of motions recorded during earthquakes as follows:*

- *Shallow crustal earthquakes in active tectonic regions (such as California); designated NGA West2.*
- *Shallow crustal earthquakes in stable continental tectonic regions (such as Central and East North America); designated NGA East.*
- *Subduction zone earthquakes; designated NGA Subduction.*

15

## *RECORDED EARTHQUAKE GROUND MOTION DATA*

### *NGA West2*

- *Total Number of Recordings* 21,540
- *Usable FF Number of Recordings* 19,572

*Range of Data:* $M$ = 3 to 7.9
$R_{rup}$ = 0.1 to 1,500 km
$V_{S30}$ = 89 to 2,100 m/sec

16

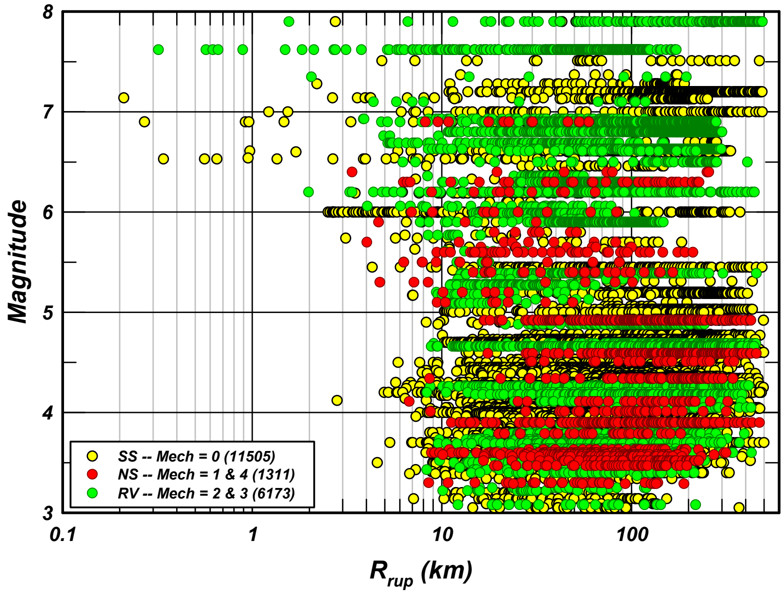


***Magnitude – $R_{rup}$ plot of Recordings obtained during crustal earthquakes***
***$R_{rup} \leq 500$ km; $M \geq 3$***

17

## ***RECORDED EARTHQUAKE GROUND MOTION DATA***

***NGA East***

- ***Total Number of Recordings 9,382***
- ***Usable FF Number of Recordings 8,918; 59 events***

***Range of Data:*** ***$M$ = 3.1 to 5.85***
***$R_{rup}$ = 4.2 to 3,510 km***
***$V_{S30}$ = 144 to 2,000 m/sec***

***Plus one recording – $M$ = 6.8 at 5.5 km; $V_{S30}$ = 300 m/sec***
***& three recordings – $M$ 6.76 at 4.9 to 9.6 km; $V_{S30}$ = 1700 m/sec***

18

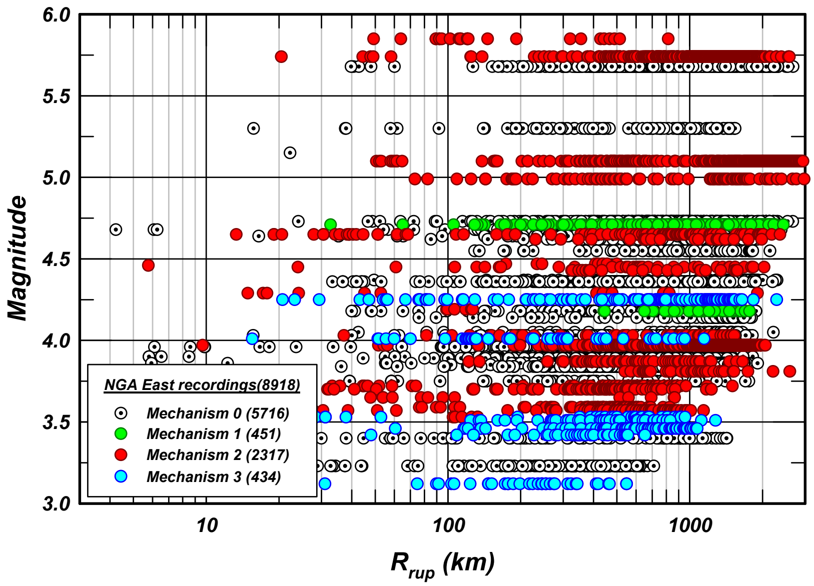


**Magnitude – $R_{rup}$ plot of Recordings obtained during earthquakes in CENA***
**$R_{rup} \leq 3000$ km; $M \geq 3$**

* Central and East North America

19

## RECORDED EARTHQUAKE GROUND MOTION DATA

### NGA Subduction

- *Total Number of Recordings:* 71,343
- *Usable FF Number of Recordings:* 49,259; 736 events

*Range of Data:*

*Interface:* $M$ = 4 to 9.1
$R_{rup}$ = 8 to 6,500 km
$V_{S30}$ = 53 to 2,230 m/sec

*Intraslab:* $M$ = 3.3 to 8.4
$R_{rup}$ = 17 to 5,400 km
$V_{S30}$ = 88 to 2,100 m/sec

20

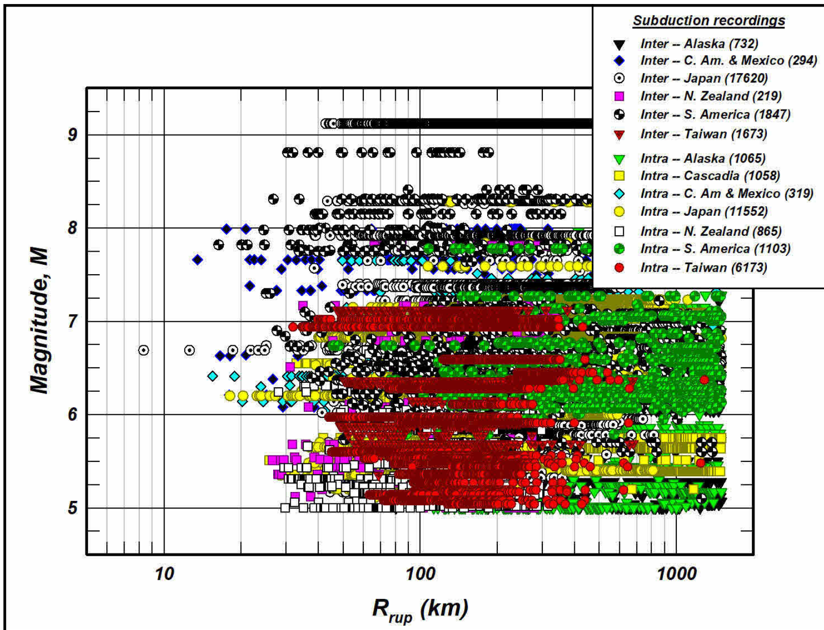


***Magnitude – $R_{rup}$ plot of Recordings obtained during subduction earthquakes $R_{rup} \leq 1500$ km; $M \geq 5$***

21

***WHAT WE CAN GLEAN FROM RECORDED EARTHQUAKE GROUND MOTION DATA***

22

## *LEARNING FROM RECORDED DATA*

***Will examine spectra, in terms of spectral shapes***

***Spectral shape is the ratio of the spectral acceleration, PSA, at period, T, divided by the spectral acceleration at T = 0.01 sec, which typically corresponds to the maximum acceleration of the record, i.e., PGA.***

***Key metrics to examine are:***

- ***Plot of PSA/PGA versus T***
- ***The maximum ratio PSA/PGA***
- ***The period, $T_{@max}$. at which this maximum occurs***

23

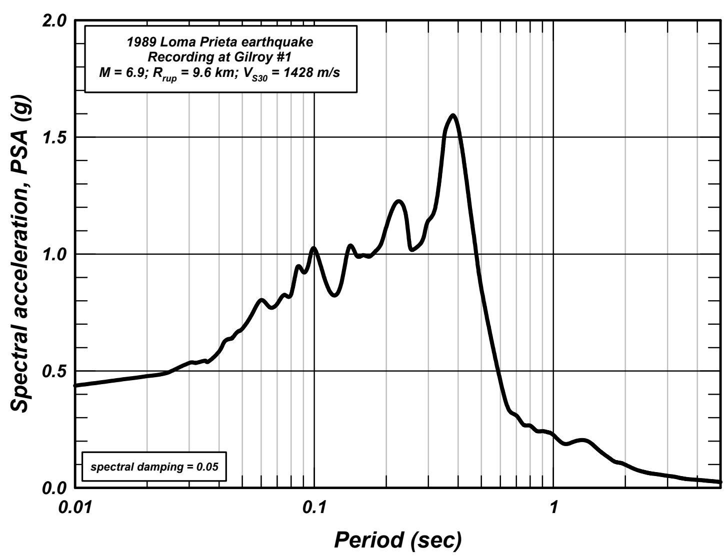


***Plot of spectral acceleration versus period***

24

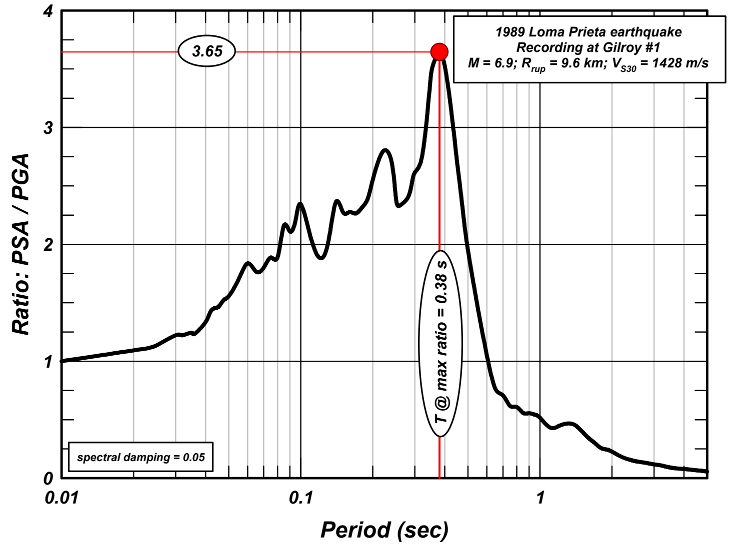


*Spectral Shape*

25

**_EXAMINATION OF THE PERIOD, $T_{@max}$, AT WHICH THE MAXIMUM RATIO OF PSA/PGA OCCURS_**

26

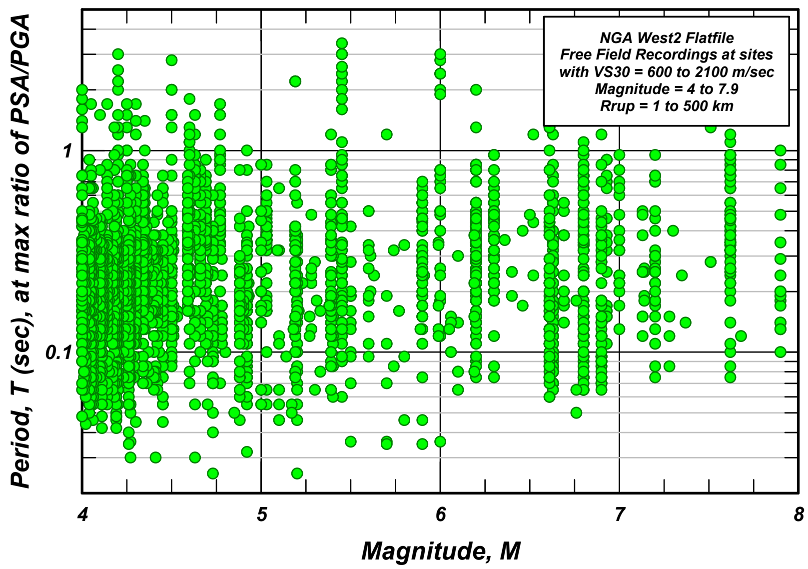


*Rock sites – Plot of T at max ratio of PSA/PGA versus M*

27

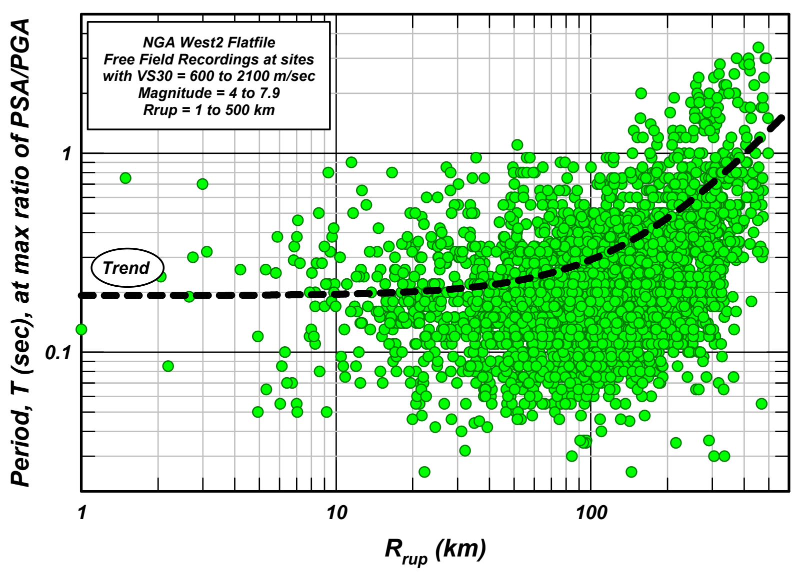


*Rock sites – Plot of T at max ratio of PSA/PGA versus $R_{rup}$*

28

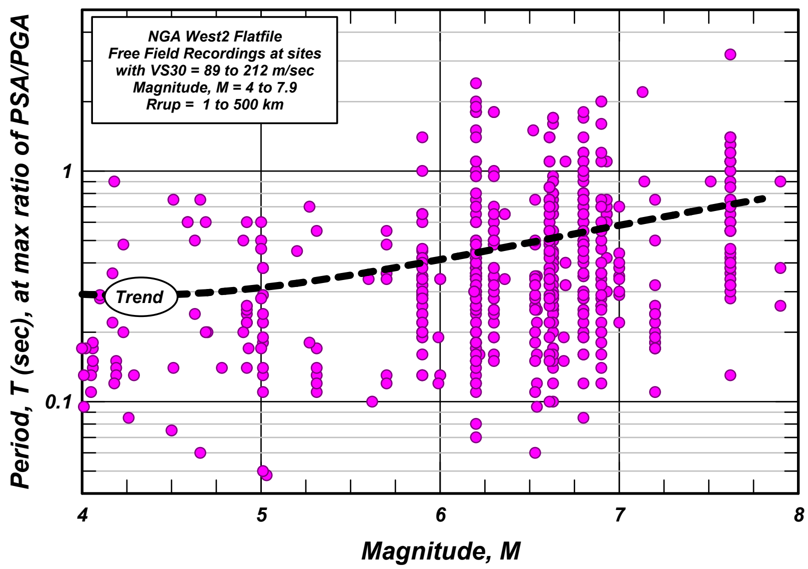


***Soft Soil sites – Plot of T at max ratio of PSA/PGA versus M***

29

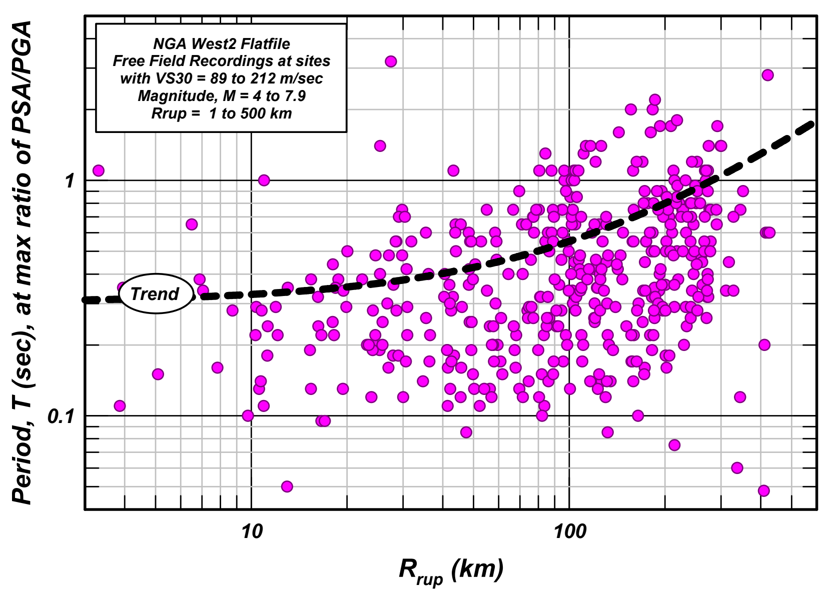


***Soft Soil sites – Plot of T at max ratio of PSA/PGA versus $R_{rup}$***

30

## *LEARNING FROM RECORDED DATA*

***Conclusions regrading the period, $T_{@max}$, at which the max ratio of PSA/PGA occurs can be summarized as follows:***

1. ***Rock Sites [$V_{S30} \geq 600$ m/sec]***
   - ***$T_{@max}$ is essentially independent of magnitude, M, and $V_{S30}$.***
   - ***$T_{@max}$ increases with $R_{rup}$.***

2. ***Soft Soil Sites [$V_{S30} \leq 212$ m/sec]***
   - ***$T_{@max}$ is essentially independent $V_{S30}$.***
   - ***$T_{@max}$ increases with of magnitude, M, and $R_{rup}$.***

31

## *EXAMINATION OF THE MAXIMUM RATIO OF PSA/PGA*

32

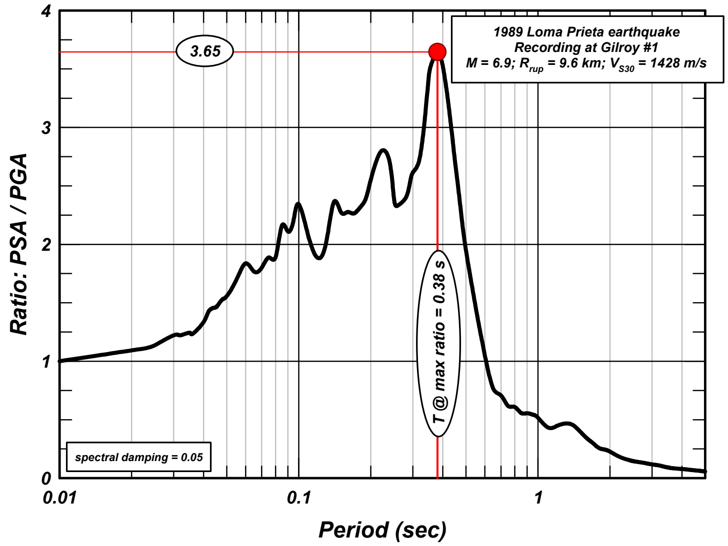


***Spectral Shape***

33

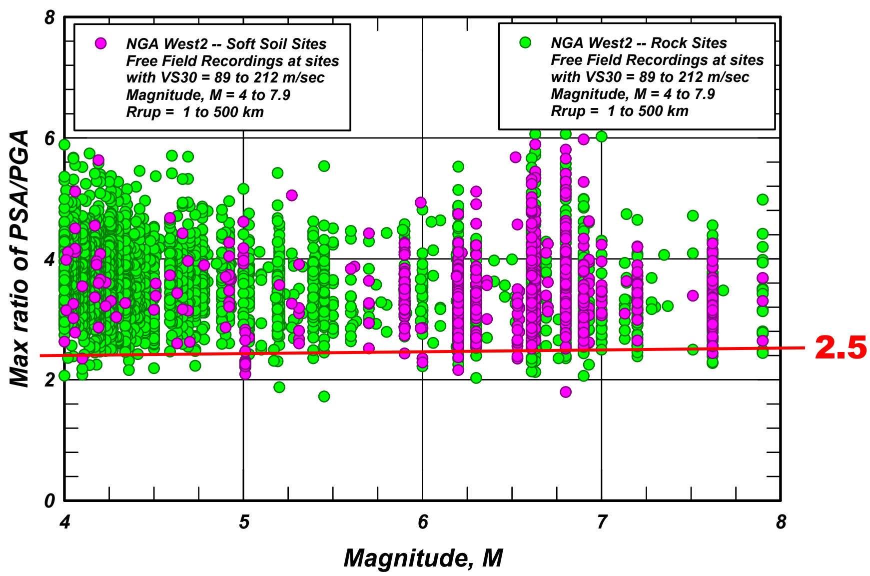


***Rock and Soft Soil sites – Plot of the max ratio of PSA/PGA versus M***

34

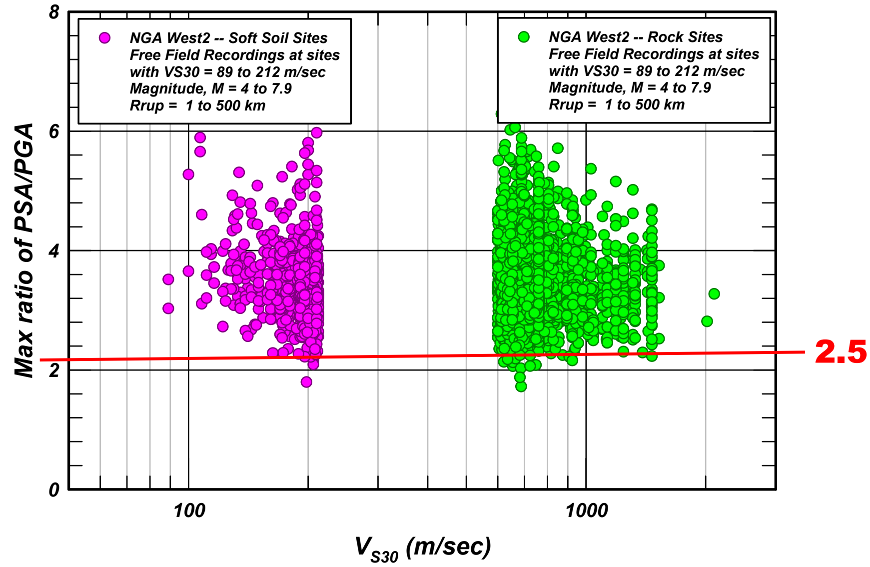


*Rock and Soft Soil sites – Plot of the max ratio of PSA/PGA versus $V_{S30}$*

35

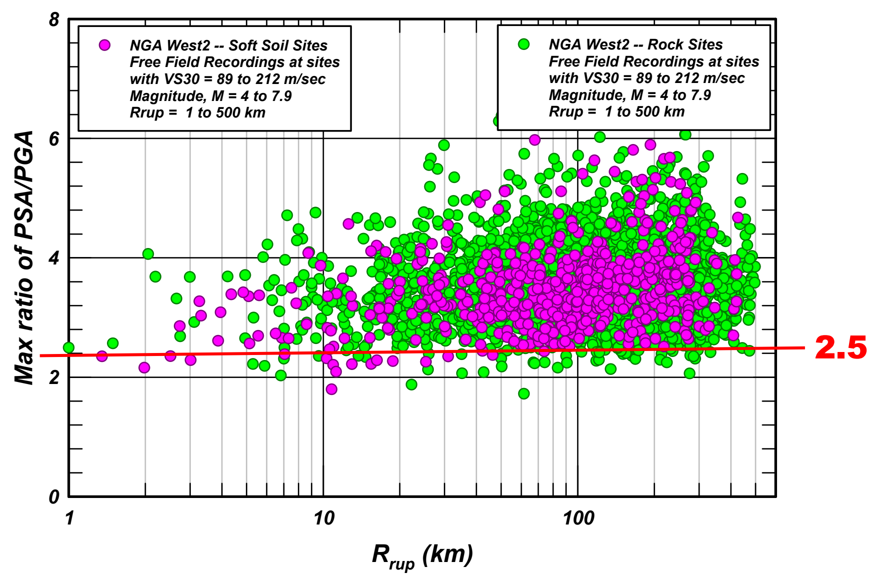


*Rock and Soft Soil sites – Plot of the max ratio of PSA/PGA versus $R_{rup}$*

36

## *LEARNING FROM RECORDED DATA*

***Conclusions regarding the max ratio of PSA/PGA can be summarized as follows:***

***The max ratio of PSA/PGA appears to be essentially independent of magnitude, M, or $V_{S30}$.  There is an apparent hint that this metric may increase with $R_{rup}$.***

***The range of this ratio is from 2 to about 6.  This ratio exceeds 2.5 for about 97% of the recordings.***

***These conclusions apply at rock as well as at soft soil sites.***

37

## *TOPIC 3*

## *EMPIRICAL EARTHQUAKE GROUND MOTION MODELS*

38

## *EMPIRICAL EARTHQUAKE GROUND MOTION MODELS*

***Conclusions regarding the use of empirical earthquake ground motion models (GMMs) can be summarized as follows:***

- ***The spectral shapes obtained for a rock site [$V_{S30}$ = 760 m/sec] using the NGA West2 GMM are generally consistent with the recorded data.***
- ***However, those obtained for a soft soil site are not as well constrained.***

39

## *EMPIRICAL EARTHQUAKE GROUND MOTION MODELS*

***Differing results were obtained for the soft soil site [$V_{S30}$ = 180 m/sec] using the other three NGA West2 GMMs. The conclusion stated above, however, applied to each.***

***Accordingly, it is appropriate to use the empirically-derived earthquake ground motion models (GMMs) to estimate spectral values at a rock site, which becomes the "rock outcrop" for a specific application.***

***Such spectra can then be used to represent the target spectrum at a rock outcrop in a seismic analysis.***

40

***TOPIC 4***

***HISTORICAL PERSPECTIVE***

41

## *The 1906 San Francisco Earthquake*

***The performance of various sites during the 1906 San Francisco earthquake highlighted the importance of site response during earthquakes and, as noted by Lawson (1908), emphasized the effects of local site conditions.***

***Although some attempts were made to explain these effects using wave propagation theories, it was not possible, at that time, to go beyond qualitative explanations.***

42

## *Professor Kanai's Contributions*

***In 1952 – 1956 Professor Kanai proposed the use of the continuous solution to the wave equation to study site effects on earthquake ground motions.***

***Professor C. Martin Duke brought Kanai's work to attention of US researchers & practitioners in 1958.***

***This was met with strong resistance from structural engineers in the USA.***

43

## *Activities in the 1960s*

***The late Professor Seed presented a paper at the WCEE advancing the concerns with the behavior of soils during earthquakes and the potential effects of local site conditions on earthquake ground motions -- 1960.***

***Donald Hudson (Caltech) proposed the use of values of damping that are dependent on the level of deformation in structural elements – 1963.***

***Penzien, Parmelee & Seed developed a bilinear procedure & wrote a computer program to calculate the response of soft soil sites – 1963.***

44

## Activities in the 1960s (Cont'd)

***G. R. Martin suggested the need to incorporate the influence of the level of shaking in calculating response of earth dams – 1965.***

***Idriss examined the laboratory test results by Thiers & Seed and suggested the use of strain-compatible modulus & damping values in site response calculations – 1966***

***Idriss & Seed used the bilinear solution to show that strain-compatible modulus & damping values can be used in a linear program to produce comparable results; i.e. <u>Equivalent Linear Solution</u> -- 1968***

45

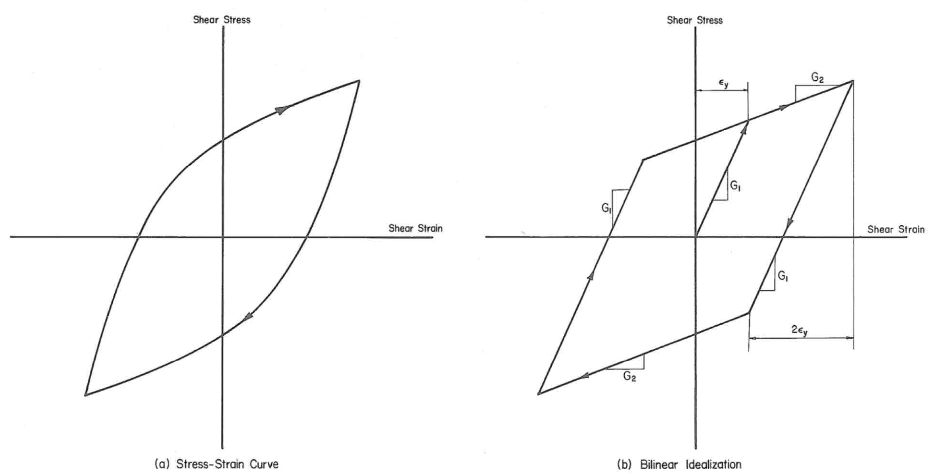


FIG. 15 STRESS-STRAIN CHARACTERISTICS OF SOIL

46

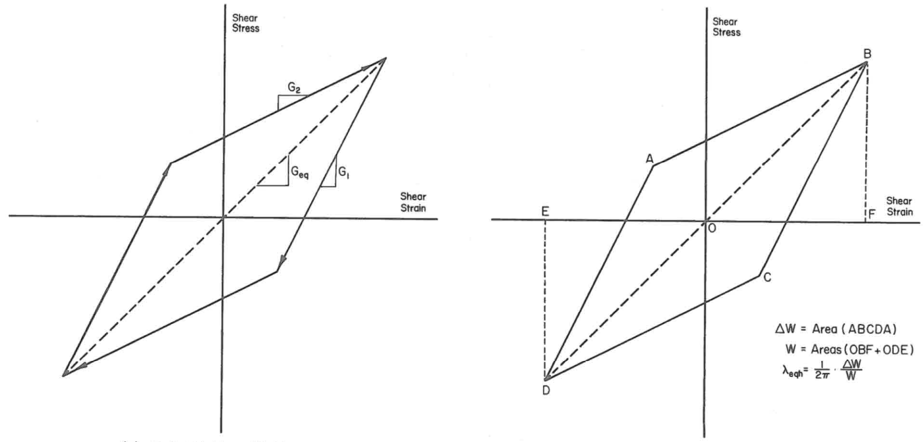


(a) Equivalent Linear Modulus

(b) Equivalent Viscous Damping Ratio

FIG. 20 EVALUATION OF EQUIVALENT LINEAR PARAMETERS FROM BILINEAR HYSTERETIC STRESS-STRAIN CYCLE.

47

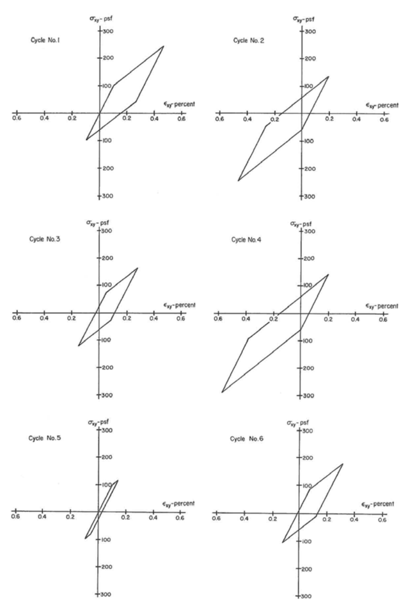


FIG.19 HYSTERETIC CYCLES DEVELOPED AT MIDHEIGHT OF LAYER WITH BILINEAR STRESS-STRAIN CHARACTERISTICS.

48

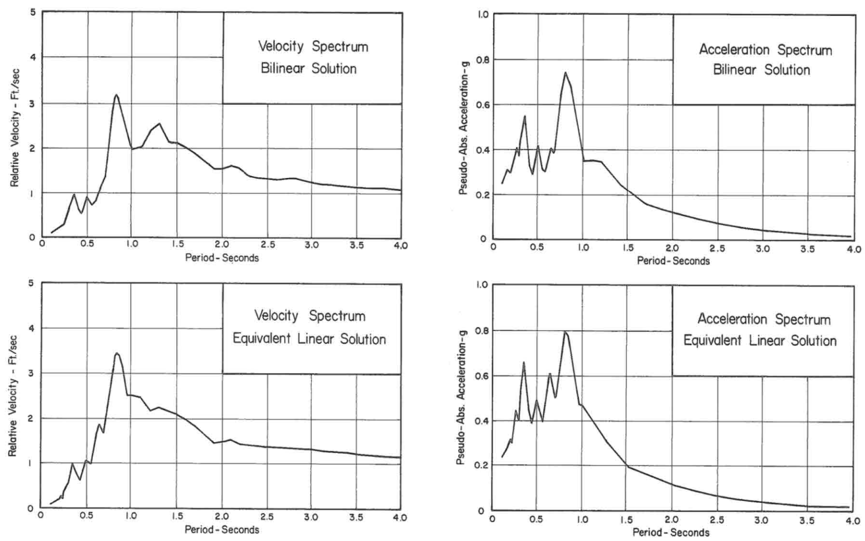


FIG. 21 RESPONSE SPECTRA FOR BILINEAR AND EQUIVALENT LINEAR SOLUTIONS.

49

## *Activities in the 1960s*

***Researchers at the University of Michigan (under the leadership of Professor Richart) carried out a comprehensive testing program to measure modulus & damping values. They showed dependence of these values on amplitude of vibration – this work was initiated beginning in the early 1960s.***

***The late Professor Seed and I began to compile the dynamic laboratory tests on sands, which included free vibration and resonant column tests. This effort began in 1968 and culminated in the preparation of the Report summarizing these results and introducing the concept of using $G/G_{max}$. This Report was published by EERC in 1970.***

50

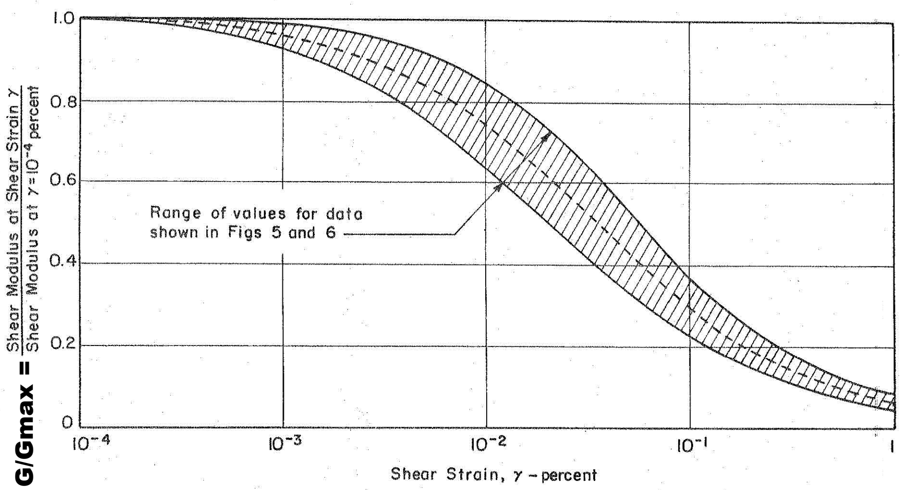


Fig. 7 VARIATION OF SHEAR MODULUS WITH SHEAR STRAIN FOR SANDS.

***From Seed and Idriss (1970)***

51

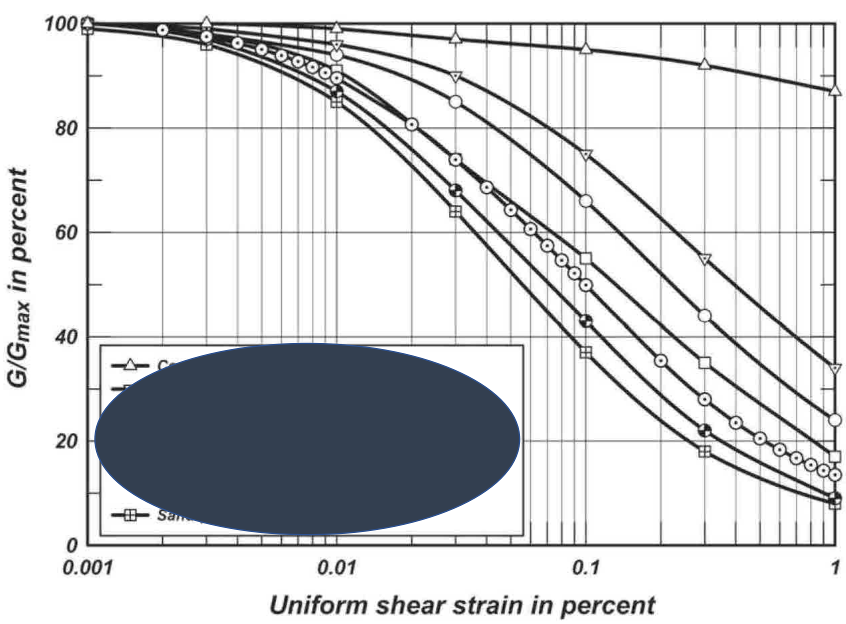


***Examples of G/Gmax Curves published over the years***

52

## Link Between Field and Lab:

### Estimating the Field G – log $\gamma$ Relationship (Soil)

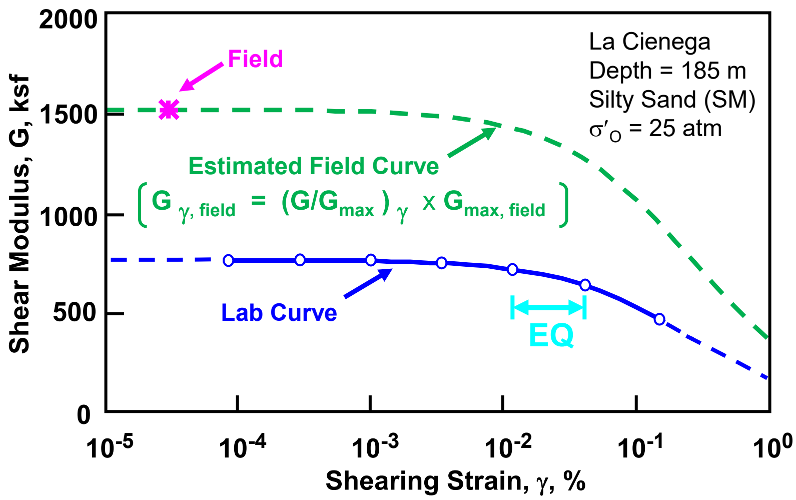


***Courtesy of Professor K. Stokoe***

53

### *Activities in late 1960s and early 1970s*

***Analyses of shaking table tests on earth slopes suggested the need to have the ability to use different damping values in various parts of the slope & to the development of a variable damping FE program – 1969, which was later named QUAD4.***

***Schnabel started his research using the FE program developed in 1969 and initiating comparisons using a continuous solution to check accuracy – 1970.***

***Both approaches (the time-domain FE and the frequency-domain continuous formulations) introduce high damping. When Schnabel and I discussed this issue with Professor Lysmer, who had up to that time concentrated on working on foundation vibration issues, he suggested a novel approach to overcome this issue.***

54

## *Activities in the1970*

***Professor Lysmer suggested that the viscosity coefficient in the complex modulus expression be replaced by the damping ratio; thus making the damping ratio frequency-independent – 1971.***

***These developments & using Cooley & Tukey fast Fourier transform made it possible to have an efficient continuous solution that can be programmed to provide for incorporating strain-compatible modulus & damping values – 1972***

***Thus, the birth of the Computer Program SHAKE.***

***Professor Lysmer "converted" to geotechnical earthquake engineering and introduced the Computer Programs LUSH, FLUSH culminating in the Program SASSI, which has been widely used in evaluating SSI for nuclear plant structures since its introduction some 40 years ago.***

55

## ***TOPIC 5***

## ***SITE RESPONSE ANALYSES***

56

## *Site Response Calculations*

***A large number of recordings were obtained at many sites during the 1989 Loma Prieta earthquake (M = 6.9). Many of these sites were in the San Francisco Bay Area, including the site at Treasure Island.***

***Calculation of the response of the Treasure Island site will be covered as follows:***

1. ***Loma Prieta – equiv. linear analyses (EQL)***
2. ***Downhole Array -- Comparison with other programs (EQL)***
3. ***Loma Prieta – Comparison with other programs (EQL & NL)***

57

***TREASURE ISLAND SITE***

1. ***Loma Prieta – equiv. linear analyses (EQL)***
2. ***Downhole Array -- Comparison with other programs (EQL)***
3. ***Loma Prieta – Comparison with other programs (EQL & NL)***

58


San Rafael
San Quentin
Richmond
Kentfield
Larkspur
Corte Madera
Mill Valley
Paradise Cay
El Cerrito
Lafayette
Orinda
Albany
Tiburon
Sausalito
Belvedere
Berkeley
San Francisco Bay
Piedmont
Oakland
Alameda
San Francisco
Daly City
San Bruno Mountain
Metropolitan Oakland International Airport
South San Francisco
San Lorenzo
Pacific Manor
Pacifica
Edgemar
San Francisco International Airport
San Bruno
Millbrae
Burlingame
Hillsborough
San Mateo
Foster City
Montara
Belmont
Moss Beach
El Vallejo Beach
San Carlos
Granada
Francis Beach
Redwood City
North Fair Oaks
Half Moon Bay
Woodside
Menlo Park
Sierra Morena
Stanford
Perimeter Rd
Treasure Island
Avenue M
Avenue N
13th St
11th St
9th St
5th St
4th St
3rd St
Avenue B
Avenue of the Palms
San Francisco
North Gate Rd
Macalla Rd
Yerba Buena Island
Coast Guard Reservation
80
© 2000 Microsoft Corp. and/or its suppliers. All rights reserved.



59

59


Bird Island
Albany
Silva Island
Belvedere Island
Angel Island
Point Blunt Rock
Alcatraz Island
Treasure Island
Yerba Buena Island
Piedmont
Oakland
Fort Point Rock
Helmet Rock
Pyramid Rock
Seal Rocks
San Francisco
San Francisco, CA
Coast Guard Island
Alameda
Bay Farm Island
Google
Strong motion recording stations
Treasure Island
Yerba Buena Island
Other "rock" sites

60

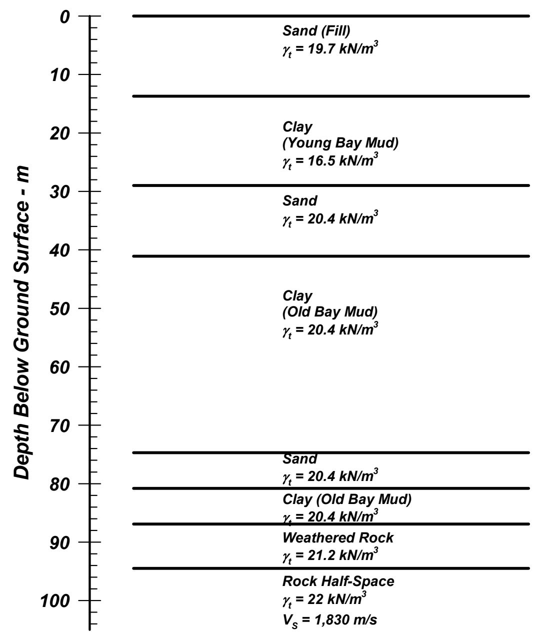


***Subsurface layers at the Treasure Island site***

61

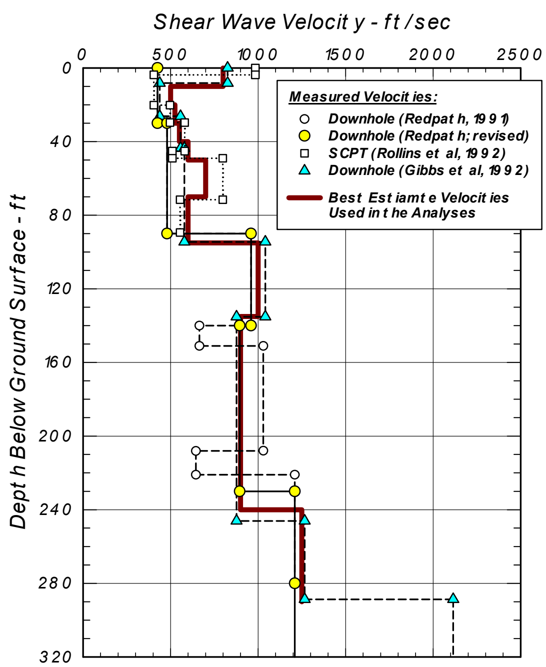


***Range of shear wave velocities Measured at the Treasure Island site***

62

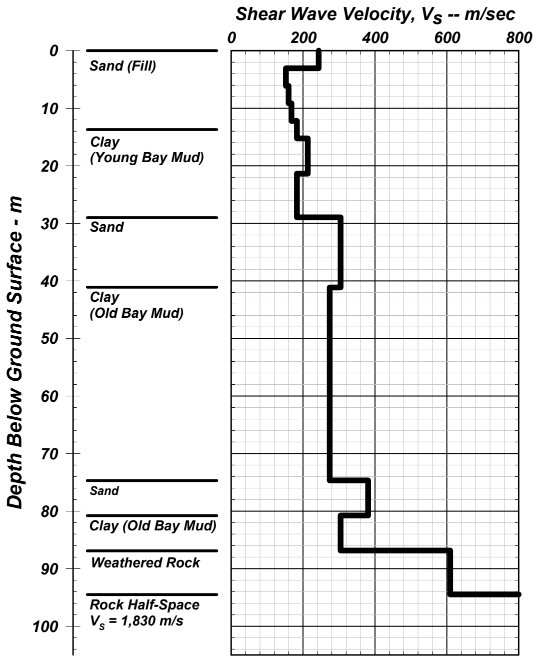


***Best estimate***
***Shear wave velocity profile at the Treasure Island site***

63

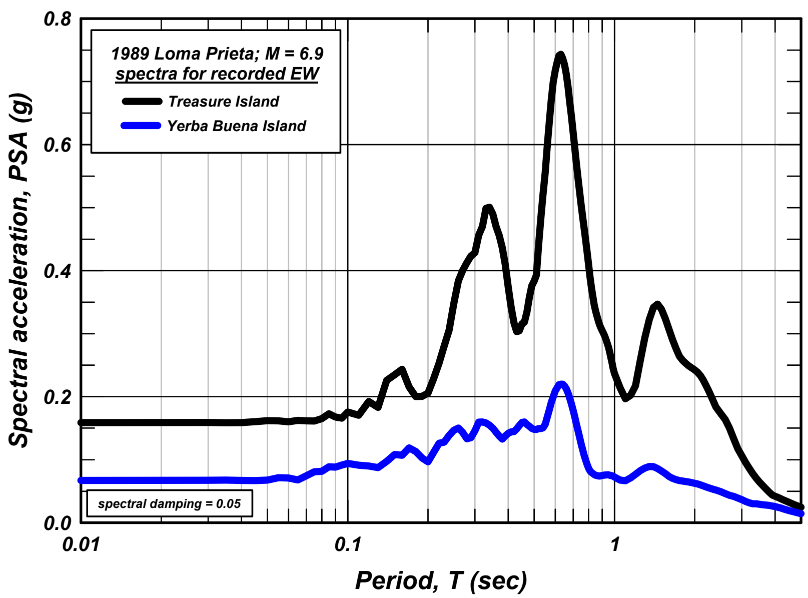


64

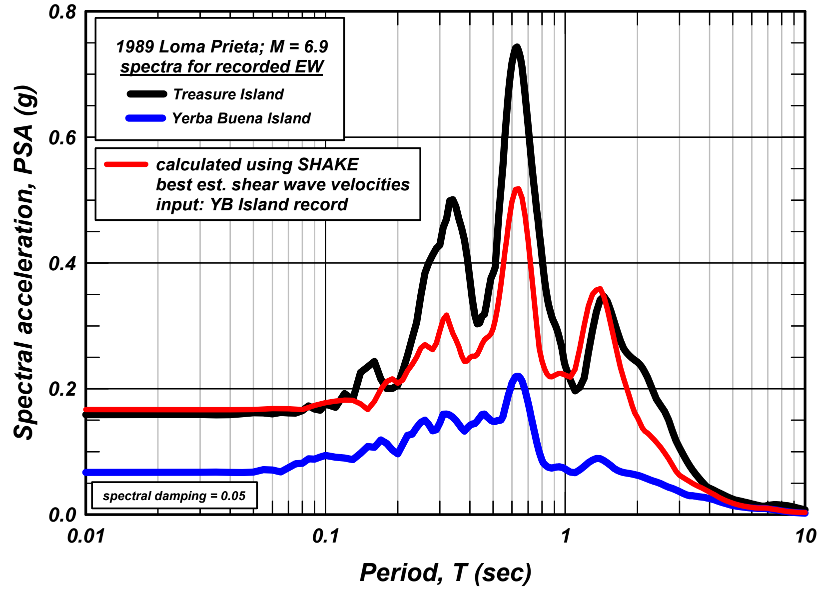


65

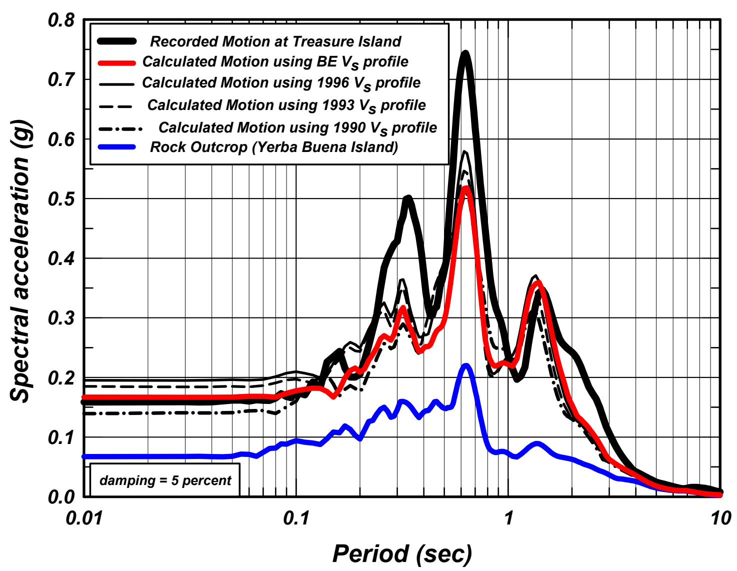


***Effects of varying dynamic soil Properties On calculated surface Response – Treasure Island site***

66

Bird Island
Silva Island
Albany
Belvedere Island
Angel Island
Point Blunt Rock
Needles
Alcatraz Island
Piedmont
Helmet Rock
Oakland
Pyramid Rock
Seal Rocks
San Francisco
San Francisco, CA
Coast Guard Island
Alameda
Strong motion recording stations
Treasure Island
Yerba Buena Island
Other "rock" sites
© 2007 Europa Technologies
Image NASA
Image © 2008 TerraMetrics
Image © 2008 Sanborn
Google


67

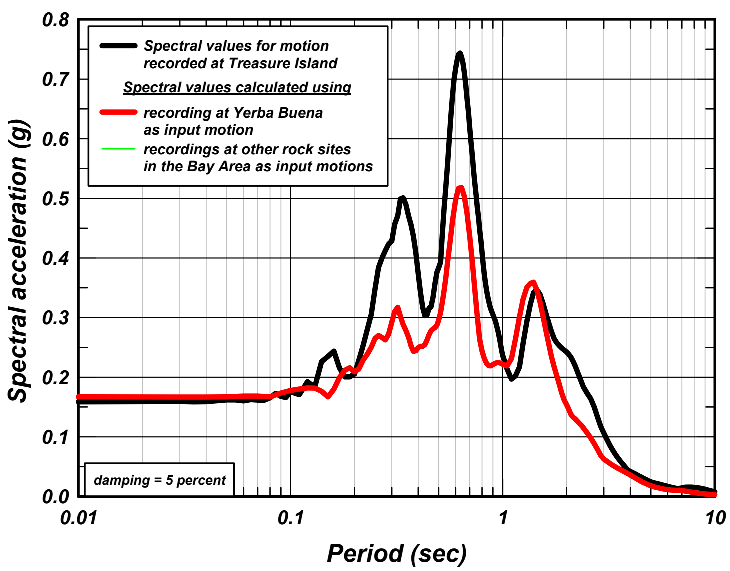

Spectral acceleration (g)
0.8
0.7
0.6
0.5
0.4
0.3
0.2
0.1
0.0
Spectral values for motion recorded at Treasure Island
Spectral values calculated using
recording at Yerba Buena as input motion
recordings at other rock sites in the Bay Area as input motions
damping = 5 percent
0.01
0.1
1
10
Period (sec)


68

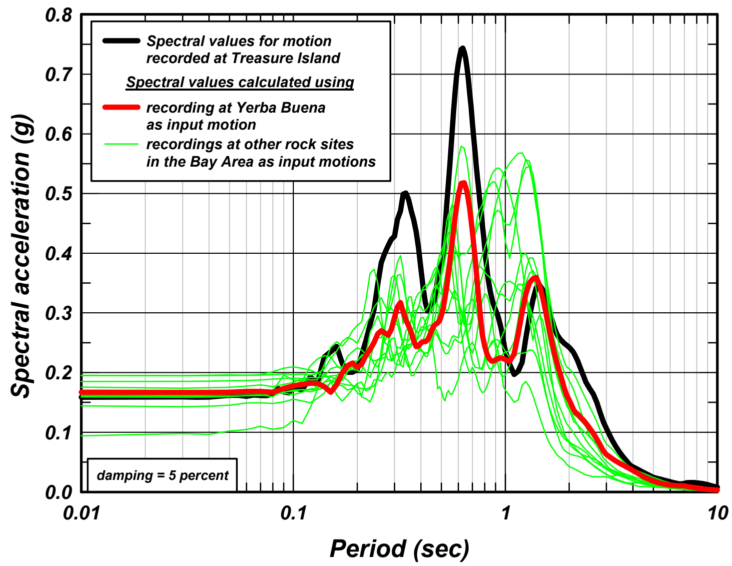


***Effects of varying input motion on calculated surface response Treasure Island site***

69

## ***TREASURE ISLAND SITE***

1. ***Loma Prieta – equiv. linear analyses (EQL)***
2. ***Downhole Array -- Comparison with other programs (EQL)***
3. ***Loma Prieta – Comparison with other programs (EQL & NL)***

70

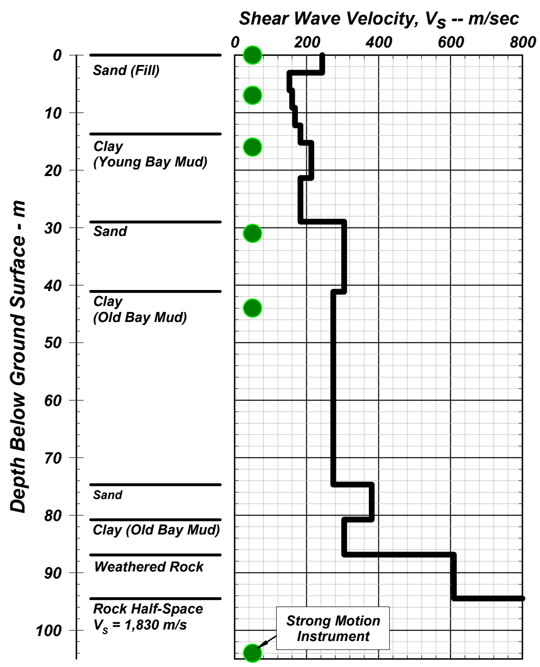


***Vertical Array at the Treasure Island site***

71

***<u>TREASURE ISLAND SITE</u>***

1. ***Loma Prieta – equiv. linear analyses (EQL)***
2. ***Downhole Array -- Comparison with other programs (EQL)***
3. ***Loma Prieta – Comparison with other programs (EQL & NL)***

72

## Loma Prieta – Comparison with DeepSoil (EQL)

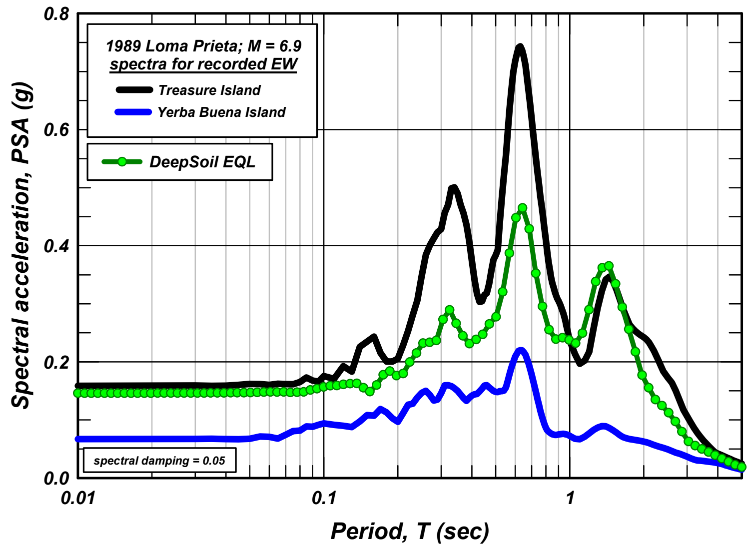


73

## Loma Prieta – Comparison with DeepSoil & SHAKE (EQL)

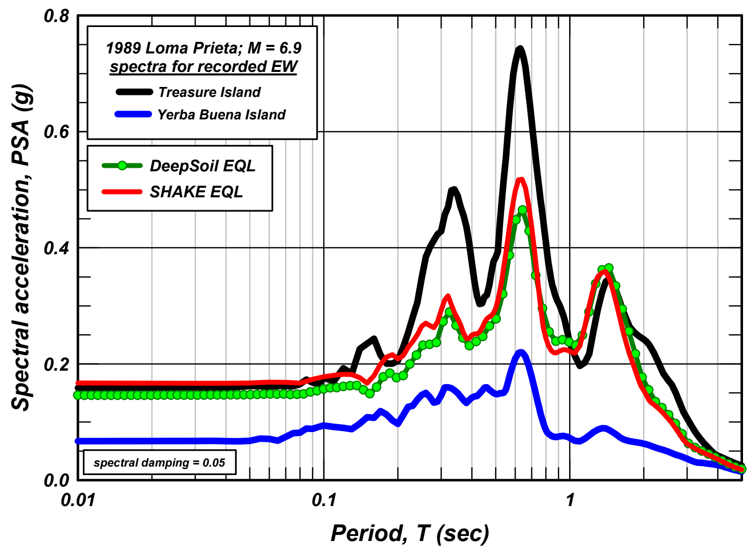


74

## Loma Prieta – Comparison with DeepSoil (NL)

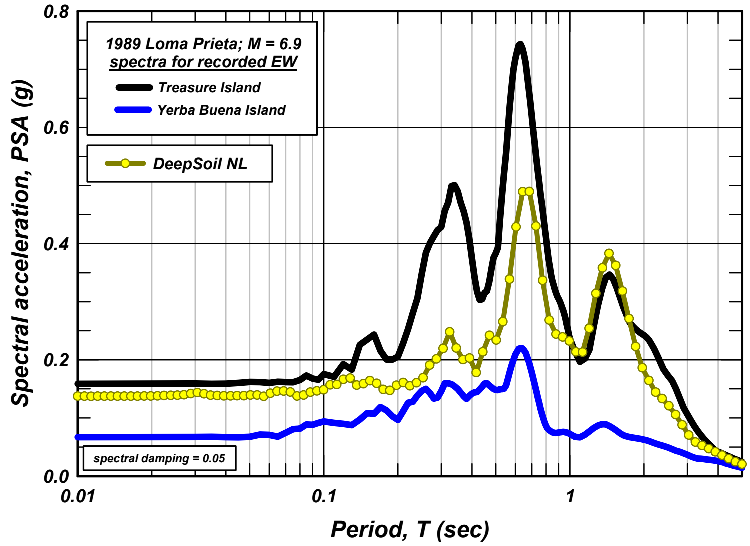


75

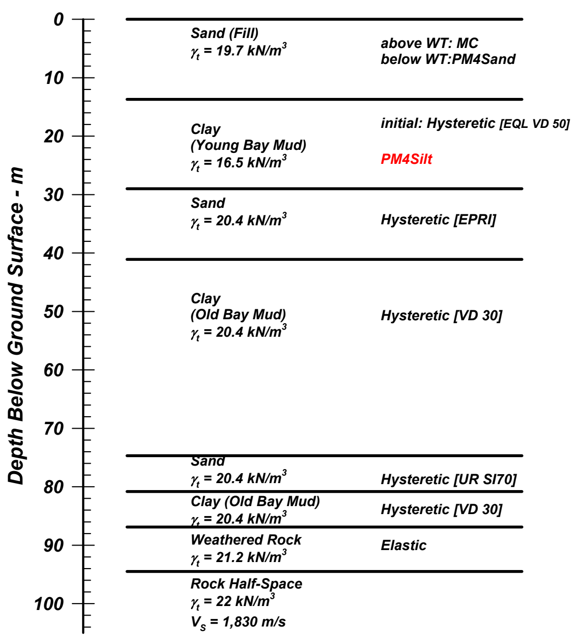


*Subsurface layers at the Treasure Island site & Const. Models assigned for FLAC Analyses*

76

## Loma Prieta – Comparison with FLAC Hysteretic Model for YBM

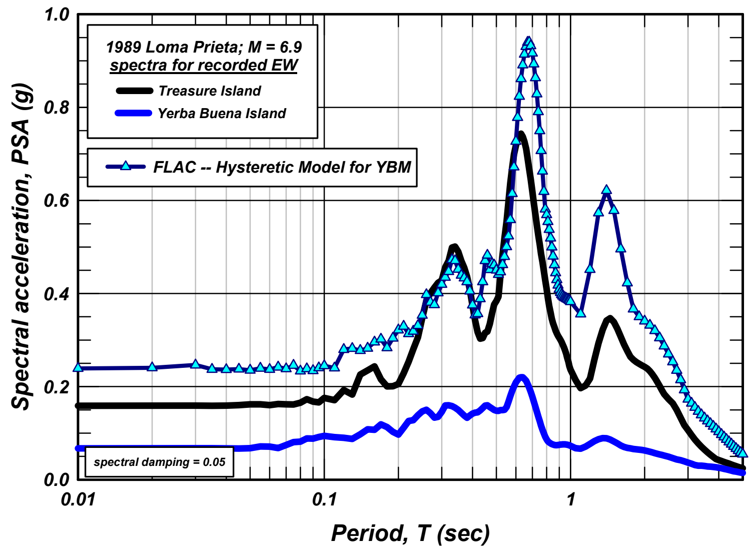


77

## Loma Prieta – Comparison with FLAC using PM4Silt for YBM

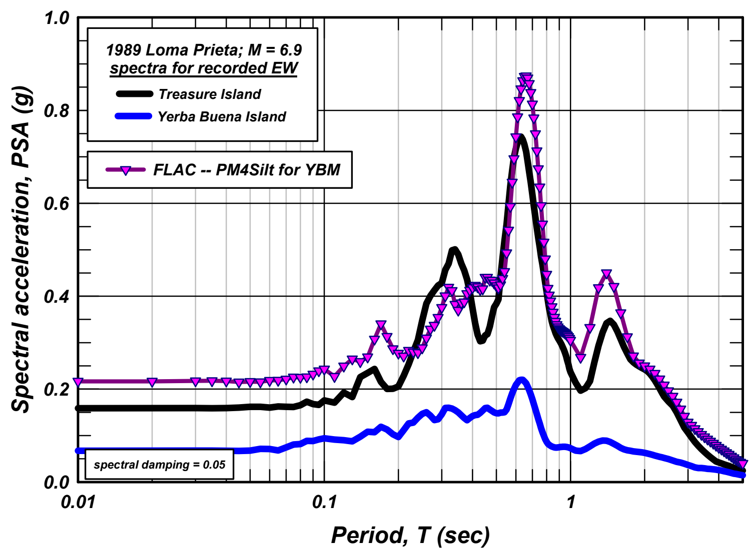


78

Spectral Shapes

79

## Spectral Shape – Recorded Motion at TI

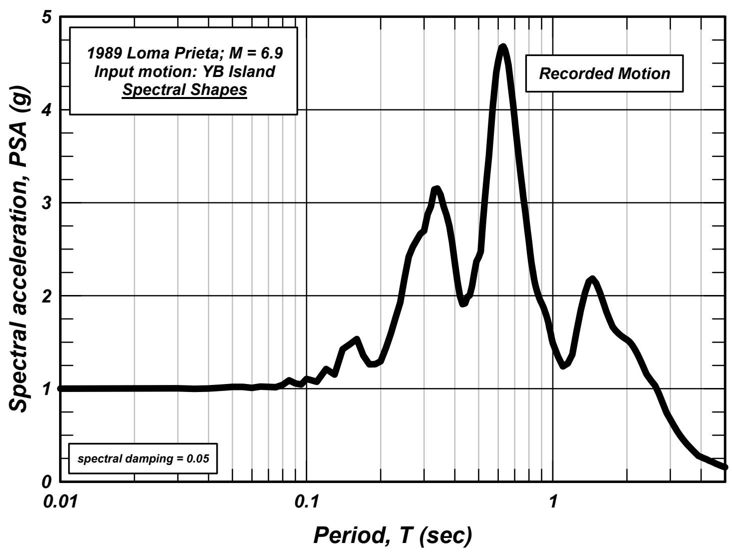


80

## Spectral Shapes – FLAC Analyses

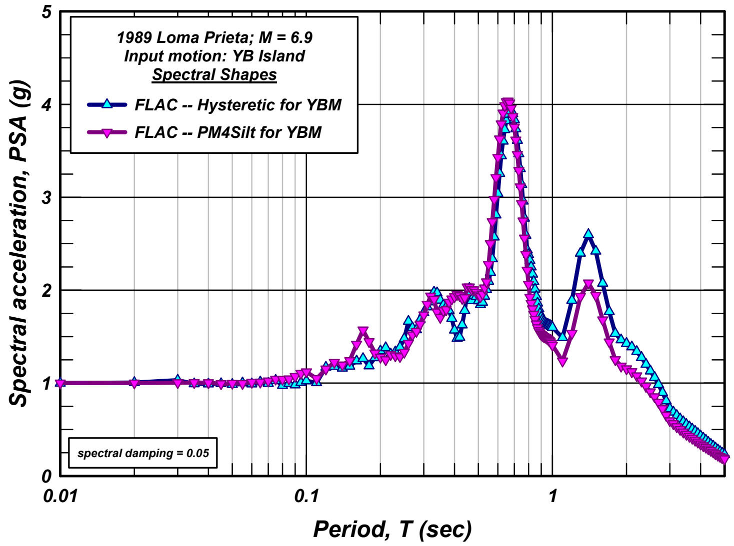


81

## Spectral Shapes – FLAC Analyses and DeepSoil NL

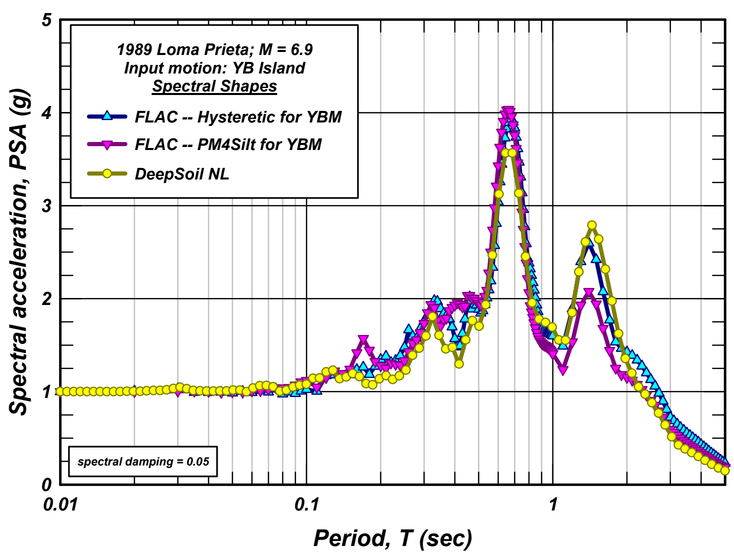


82

## Spectral Shapes – NL and EQL Analyses

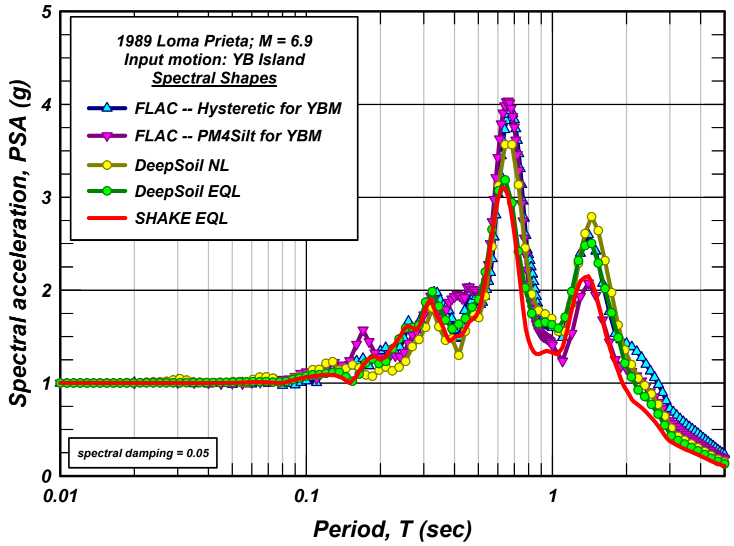


83

## Spectral Shapes – Recorded Motion and NL & EQL Analyses

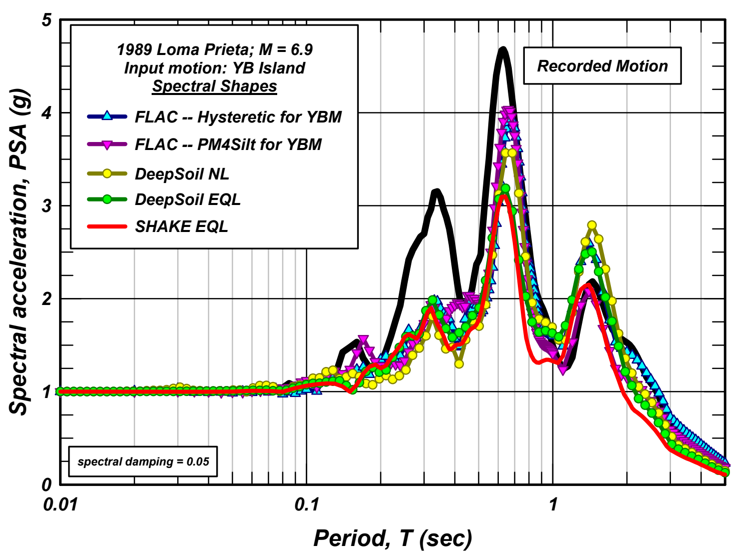


84

## FLAC ANALYSES – DEVELOPMENT OF EXCESS PWP

85

## FLAC Analyses – Excess PWP Induced during Shaking

The use of PM4Sand for the sand layers and PM4Silt for the Young Bay Mud layers provides the means to calculate the excess pore water pressure (PWP) induced in these layers during shaking, as illustrated at a depth of 10.5 m within the upper sand layer and a depth of 20.5 m within the YBM layer.

86

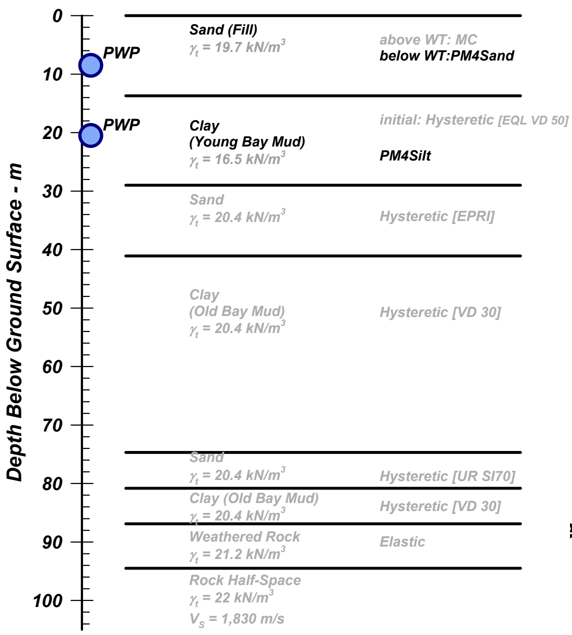


***Treasure Island Site***

***FLAC Analysis -- depths at which PWP generation/dissipation are shown in next figures***

87

## ***FLAC Analyses – Excess PWP Induced during Shaking***

***Sand Fill – Depth = 8.5 m***

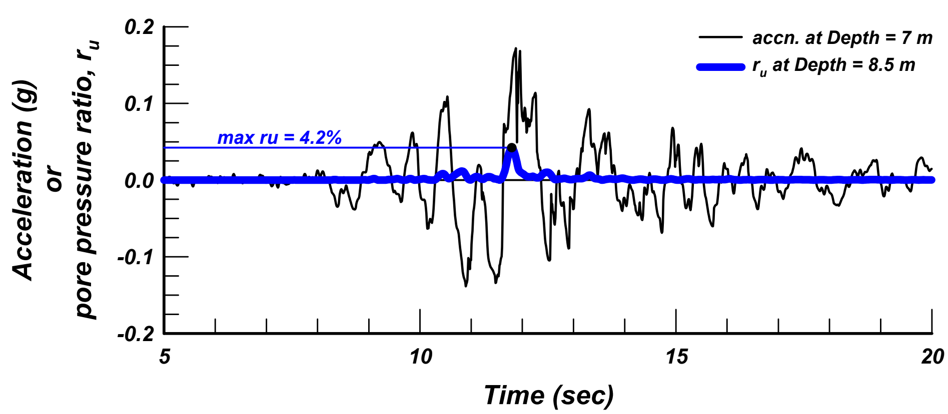


88

## FLAC Analyses – Excess PWP Induced during Shaking

### Young Bay Mud – Depth = 20.5 m

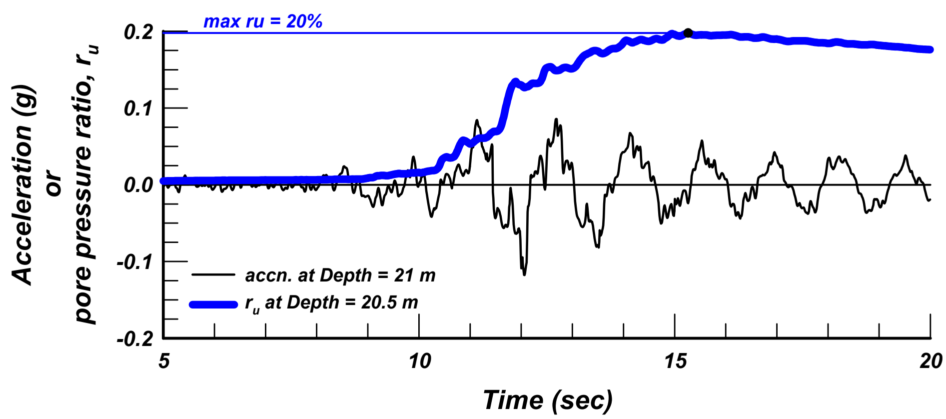


89

## CONCLUDING REMARKS

***The equivalent linear procedure has been & continues to be widely used procedure in practice for calculating site response & for developing site specific earthquake ground motions and design parameters.***

***It has also been widely used for evaluating existing and new earth structures and for assessing SSI aspects.***

90

## *CONCLUDING REMARKS*

***Advances in nonlinear analyses are encouraging and the results presented today highlight the values of using such analyses.***

***Care must be exercised in selecting appropriate constitutive models for the various soil layers comprising the profile under considerations.***

***Calibration of the selected constitutive model with relevant test data and empirical correlations is essential. Professor Hashash and his collaborators have done that for the model built into DeepSoil. Professors Boulanger and Ziotopoulou and their collaborators have done that extensively for PM4Sand and are continually adding to that effort for PM4Silt.***

***The results for the Treasure Island site, using PM4Silt for the Young Bay Mud layer, highlight the importance of accounting for pwp generation and cyclic softening during shaking.***

91

## *CONCLUDING REMARKS*

***The key factors that affect a site response calculation are:***

1. ***The <u>input motion</u> can have a profound influence on calculated site response, as evidenced from the results shown earlier for the Treasure Island site.***
2. ***The <u>soil profile</u> also will influence the calculated site response.***
3. ***The <u>soil properties</u> also influence the calculated site response, but to a lesser degree than input motion or soil profile.***
4. ***The <u>method of analysis</u> will influence the results, depending on the level of shaking and the selection of parameters. For the Treasure Island site, the effect was minimal for the level of shaking experienced in the Loma Prieta earthquake.***

92

## *A FEW RECOMMENDATIONS*

1. ***PLEASE** limit the use of the equivalent linear procedure to those in which the calculated **effective strain** is less than about **0.6%**, which corresponds to a **maximum strain < 1%**.*

2. ***For a "deconvolution" analysis, I have found it useful to get the strain-compatible properties by completing the analysis with a low cuff-off frequency (say 5± Hz, depending on the level of shaking), then using the resulting strain-compatible modulus and damping values for one iteration and the desired cuff-off frequency (typically 20 to 30± Hz).***



## *A FEW RECOMMENDATIONS*

3. ***Allow for variations in shear wave velocities and in modulus reduction and damping curve within physically meaningful ranges.***

4. ***When using a randomizing process to allow for variations in these properties, be sure to check that any realization is physically meaningful.***

5. ***Casagrande, in his Terzaghi Lecture (No. 2), emphasized the need to select a "probable range of pertinent soil properties guided by judgement and experience". This is a valuable and timeless advice. We should all heed it.***

## *PARTING THOUGHTS*

***Confucius said***

***"Life is really simple, but we insist on making it complicated"***

***Einstein said***

***"Everything should be made as simple as possible, but no simpler"***

95

# *Acknowledgments*

**I am most grateful to My Family for continuing love, support and tolerance.**

**I am eternally grateful to numerous very talented friends and colleagues**
**Let me just mention a few**

**Colleagues and clients on various projects over the past 30 + years**

**And finally, to ASCE & G-I for this great honor – I appreciate it.**

96

***THANK YOU***
***very much***

97

Texas A&M Foundation

# Spencer J. Buchanan '26 Chair in Civil Engineering

| PLEDGE INFORMATION | | | | | | |
|---|---|---|---|---|---|---|
| My personal pledge: | $ | Payment Schedule | | | | |
| My matching gift company will contribute:<br>Name of company: | $ | Year 1 | $ | Year 4 | $ |
| | | Year 2 | $ | Year 5 | $ |
| Total Commitment: | $ | Year 3 | $ | | |

| DONOR INFORMATION (Please Print) | |
|---|---|
| **Name** | **Class Year** |
| **Address** | |
| **Email** | **Phone** |

| PAYMENT INFORMATION | | |
|---|---|---|
| Enclosed Contribution:<br>$ | Please make checks payable to **TEXAS A&M UNIVERSITY**.<br>On the memo line, indicate: Buchanan Chair (074227) | Return to: Texas A&M Foundation<br>401 George Bush Drive<br>College Station, TX 77840-2811 |
| | Contact: Jay Roberts '05<br>Phone 979-845-5113 Fax: 979-862-8572<br>Email: jay-roberts@tamu.edu | |